2010

REMOTE CONTROLLED HYDROGEL NANOCOMPOSITES: SYNTHESIS, CHARACTERIZATION, AND APPLICATIONS

Nitin S. Satarkar
University of Kentucky, nitin1109@gmail.com

ABSTRACT OF DISSERTATION

Nitin S. Satarkar

The Graduate School

University of Kentucky

2010

REMOTE CONTROLLED HYDROGEL NANOCOMPOSITES: SYNTHESIS, CHARACTERIZATION, AND APPLICATIONS

ABSTRACT OF DISSERTATION

A dissertation submitted in partial fulfillment of the
requirements for the degree of Doctor of Philosophy in the
College of Engineering
at the University of Kentucky

By
Nitin S. Satarkar

Lexington, Kentucky

Director: Dr. J. Zach Hilt, Assistant Professor of Chemical Engineering

Lexington, Kentucky

2010

ABSTRACT OF DISSERTATION

REMOTE CONTROLLED HYDROGEL NANOCOMPOSITES: SYNTHESIS, CHARACTERIZATION, AND APPLICATIONS

There is significant interest in the development of hydrogels and hydrogel nanocomposites for a variety of biomedical applications including drug delivery, sensors and actuators, and hyperthermia cancer treatment. The incorporation of nanoparticulates into a hydrogel matrix can result in unique material characteristics such as enhanced mechanical properties, swelling response, and capability of remote controlled (RC) actuation. In this dissertation, the development of hydrogel nanocomposites containing magnetic nanoparticles/carbon nanotubes, actuation with remote stimulus, and some of their applications are highlighted.

The primary hydrogel nanocomposite systems were synthesized by incorporation of magnetic nanoparticles into temperature responsive N-isopropylacrylamide (NIPAAm) matrices. Various nanocomposite properties were characterized such as temperature responsive swelling, RC heating with a 300 kHz alternating magnetic field (AMF), and resultant collapse. The nanoparticle loadings and hydrogel composition were tailored to obtain a nanocomposite system that exhibited significant change in its volume when exposed to AMF. The nanocomposites were loaded with model drugs of varying molecular weights, and RC pulsatile release was demonstrated.

A microfluidic device was fabricated using the low temperature co-fired ceramic (LTCC) processing technique. A magnetic nanocomposite of PNIPAAm was placed as a valve in one of the channels. The remote controlled liquid flow with AMF was observed for multiple on-off cycles, and the kinetics of the RC valve were quantified by pressure measurements.

The addition of multi-walled carbon nanotubes (MWCNTs) in NIPAAm matrices was also explored for the possibility of enhancement in mechanical properties and achieving remote heating capabilities. The application of a radiofrequency (RF) field of 13.56 MHz resulted in the remote heating of the nanocomposites. The intensity of the resultant heating was dependent on the MWCNT loadings.

In order to further understand the RC actuation phenomenon, a semi-empirical heat transfer model was developed for heating of a nanocomposite disc in air. The model successfully predicted the temperature rise as well as equilibrium temperatures for different hydrogel dimensions, swelling properties, nanoparticles loadings, and AMF amplitude. COMSOL was used to simulate temperature rise of the hydrogel nanocomposite and the surrounding tissue for hyperthermia cancer treatment application.

KEYWORDS: Hydrogel nanocomposites, magnetic, remote control, drug delivery, microfluidic valves

Nitin S. Satarkar

03/03/2010

REMOTE CONTROLLED HYDROGEL NANOCOMPOSITES: SYNTHESIS, CHARACTERIZATION, AND APPLICATIONS

By

Nitin S. Satarkar

Dr. J. Zach Hilt
Director of Dissertation

Dr. Barbara Knutson
Director of Graduate Studies

Date

RULES FOR THE USE OF DISSERTATIONS

Unpublished dissertations submitted for the Doctor's degree and deposited in the University of Kentucky Library are as a rule open for inspection, but are to be used only with due regard to the rights of the authors. Bibliographical references may be noted, but quotations or summaries of parts may be published only with the permission of the author, and with the usual scholarly acknowledgments.

Extensive copying or publication of the dissertation in whole or in part also requires the consent of the Dean of the Graduate School of the University of Kentucky.

A library that borrows this dissertation for use by its patrons is expected to secure the signature of each user.

Name	Date

DISSERTATION

Nitin S. Satarkar

The Graduate School

University of Kentucky

2010

REMOTE CONTROLLED HYDROGEL NANOCOMPOSITES: SYNTHESIS, CHARACTERIZATION, AND APPLICATIONS

DISSERTATION

A dissertation submitted in partial fulfillment of the
requirements for the degree of Doctor of Philosophy in the
College of Engineering
at the University of Kentucky

By
Nitin S. Satarkar

Lexington, Kentucky

Director: Dr. J. Zach Hilt, Assistant Professor of Chemical Engineering

Lexington, Kentucky

2010

ACKNOWLEDGEMENTS

I wish to express my most sincere gratitude and appreciation to Dr Zach Hilt, my advisor, for support, guidance, and encouragement throughout the course of my PhD. His critical comments on several aspects have immensely helped me in developing an understanding of the subject. I also thank my committee members Professors Dibakar Bhattacharyya, Douglas Kalika, Sylvia Daunert, and Louis Hersh for their time and inputs on the work.

I am grateful to Professors Richard Eitel, Kimberley Anderson, and Todd Hastings for their resourceful insights and discussions. I also thank Jerome Vice, Churn Poh, Mike Spencer, and Dr Brock Marrs for helping me with experimental protocols and setups. I am also grateful to fellow members of Hilt lab including Reynolds Frimpong, Hari Chirra, Dr Dipti Biswal, Ashley Hawkins, and Samantha Meenach for their friendship and unconditional help. I also thank undergraduate research students Lisa He, Don Johnson, and Aaron Hickey for their experimental contributions.

My special thanks to my friends Jivan, Sarita, Abhay, Anjali, Kunal, Paritosh for their warm and fun-filled company. My deepest gratitude goes to my parents and siblings. I could not have completed this dissertation without their love, encouragement, and support.

Finally, I want to thank the National Science Foundation (#ECS-0508254 and CTS-0609117), and the Kentucky Science and Engineering Foundation (#1169-RDE-009) for the financial support to this work.

TABLE OF CONTENTS

LIST OF TABLES

LIST OF FIGURES

CHAPTER 1

INTRODUCTION

The development and application of novel biomaterials have played an important role in improving the treatment of diseases and the quality of health care. The focus of current research in polymeric biomaterials is on creating new materials including those with improved biocompatibility, mechanical properties, and responsiveness (smart materials). Current applications of polymeric biomaterials in medicine include controlled drug delivery systems, coatings of tablets, artificial organs, tissue engineering, polymer-coated stents, dental implants, and sutures.[1, 2] The first step towards the development of novel diagnostic and therapeutic devices is the synthesis of materials with desired properties.

The objective of this dissertation is the synthesis of different polymeric nanocomposites, characterization of their properties, and demonstration of their potential biomedical applications. These nanocomposites consist of nanoparticulate material dispersed in a polymer matrix of particular interest. The nanoparticulate is selected for its unique properties to be combined with the base properties of the polymer system. For example, magnetic nanoparticles and carbon nanotubes have the unique property of heat generation when subjected to specific external stimuli.[3, 4] The polymer matrix is selected based on its property change (i.e. responsiveness) with change in temperature such as swelling, degradation, or glass transition.[5, 6] When the nanocomposite is subjected to remote external stimuli, the nanoparticulates transform external energy into heat leading to changes in the properties of the polymer. This unique phenomenon of remote controlled

(RC) actuation has various potential applications including drug delivery systems, hyperthermia cancer treatment, stent applications, and valves for microfluidic devices. Since the response of the nanocomposite to external stimuli depends on the properties of the polymer and that of the nanoparticles, there is flexibility to tune the response for desired applications.

In particular, hydrogels are a class of polymers that can absorb water or biological fluids and swell several times their dry volume. Hydrogels can have swelling behavior that is dependent on changes in the external environment.[7] Poly (N-isopropylacrylamide) (PNIPAAm), a temperature responsive hydrogel, is the primary focus of this dissertation. PNIPAAm undergoes a reversible volume phase transition around a lower critical solution temperature (LCST) of 34°C.[8] The gel collapses as the temperature is increased above the LCST and swells at temperatures below the LCST. Thus, if magnetic nanoparticles or carbon nanotubes are incorporated in PNIPAAm, application of remote stimuli can generate heat and control swelling properties of the resultant nanocomposite.

A couple examples of the high interest areas of PNIPAAm nanocomposite applications are in RC drug delivery and RC microvalves for microfluidics. Conventional methods of drug delivery typically involve administration of therapeutic agents orally or through injections. The oral route is not suitable for certain drugs like proteins, while the injections lead to increased discomfort and reduced patient compliance. Hence, there is increasing interest in developing drug delivery systems that can be implanted in the body and release drug in controlled manner for long periods of time.

In the area of microfluidic devices, researchers have investigated a wide range of chemical and biological applications.[9] Microfluidic technology promises several

benefits including reduced reagent consumption, short analysis time, portability, low cost, and high sensitivity.[10] However, current microfluidic flow regulation requires extensive off-chip controls. In contrast, hydrogel nanocomposites are easy to fabricate in microchannels and can be controlled by remote stimuli. Hence, they can eliminate the need for integrated electronics, controls, and power source. Hydrogel nanocomposites can thus be an attractive alternative for flow regulation in a variety of microfluidic functions.

The success of the potential applications described above depends on the development of nanocomposites that can address specific biological and medical challenges. Understanding the materials at a fundamental level is the key in making their applications more efficient. For example, controlling the molecular structure of hydrogels can control temperature responsive swelling, diffusive properties, and biocompatibility. On the other hand, properties of nanoparticulates and quality of dispersion can control the nanocomposite properties including mechanical strength and RC collapse. The key research objectives and dissertation contents are described in the following section.

1.1 Dissertation overview

The specific research objectives of this dissertation can be summarized as

- Synthesize nanocomposites of different hydrogel systems and different nanoparticulate materials.
- Characterize dispersion of the nanoparticulate material, temperature responsive swelling of the nanocomposite, and heating response to specific external stimuli.

- Obtain RC collapse of the temperature responsive hydrogel nanocomposites and characterize the effect of hydrogel geometry on the kinetics of collapse and recovery.
- Load a variety of model drug molecules in hydrogel nanocomposites and demonstrate RC drug delivery.
- Incorporate temperature responsive hydrogel nanocomposites as a valve in a microfluidic device and demonstrate flow control with the application of external stimulus.
- Model the effect of different parameters on the RC heating of nanocomposites, and simulate their *in vivo* application for hyperthermia cancer treatment.

Chapter 2 discusses the background on hydrogels, nanoparticulate materials, and hydrogel nanocomposites. The different techniques for synthesis of hydrogel nanocomposites of different sizes (i.e. bulk, particle, core-shell), and their RC actuation are summarized. Additionally, applications of hydrogel nanocomposites in drug delivery, sensors and actuators, and thermal therapy are summarized with emphasis on RC demonstrations. In chapter 3, experimental work on the development of magnetic hydrogel nanocomposites is presented. The nanocomposites in this work were synthesized by incorporation of superparamagnetic Fe_3O_4 particles in negative temperature sensitive PNIPAAm hydrogels. The systems were characterized for temperature responsive swelling and RC heating on application of a 300 kHz alternating magnetic field (AMF). Furthermore, some of the preliminary studies on RC drug release are described.

Chapter 4 describes detailed studies on RC drug release from magnetic PNIPAAm nanocomposites. An AMF was used to heat the nanocomposites, and the resultant collapse was characterized. PNIPAAm nanocomposites were loaded with model drug molecules, and an AMF was used to trigger on demand pulsatile release. RC pulsatile drug release was characterized for different drugs as well as for different ON-OFF durations of the AMF. Chapter 5 presents a demonstration of RC flow regulation in a microfluidic device using a hydrogel nanocomposite valve. A ceramic microfluidic device was fabricated using low temperature co-fired ceramic (LTCC) technology. The magnetic PNIPAAm nanocomposite was incorporated as a valve in one of the channels of the device. An AMF was then applied to the device and ON-OFF control on the flow was achieved. Pressure measurements were conducted at the inlet of the channel to check reproducibility of the valve for multiple AMF ON-OFF cycles.

Chapter 6 discusses experiments with incorporation of multi-walled carbon nanotubes in PNIPAAm hydrogels. The LCST of the nanocomposites was tailored for physiological applications by the addition of varying amounts of acrylamide (AAm). Swelling and mechanical properties of the nanocomposites were studied over a range of temperatures (25-55°C) to characterize the effect of nanotube addition. Furthermore, the RC heating on the application of a 13.56 MHz radiofrequency (RF) field was characterized using infrared thermography. Chapter 7 describes synthesis and RC heating of magnetic hydrogel nanocomposites of poly (ethylene glycol) (PEG). Nanocomposites with various iron oxide nanoparticle loadings were heated at different AMF amplitudes, and the resultant temperatures were recorded. A model was developed for the heat transfer process, and the temperature data of the PEG systems was found to be accurately

predicted by the model. Furthermore, the correlations were used to simulate the temperatures of the nanocomposite and the surrounding tissue *in vivo* for potential hyperthermia cancer treatment applications. The conclusions of this dissertation are presented in chapter 8.

1.2 References

[1] R. Langer, N.A. Peppas, Advances in biomaterials, drug delivery, and bionanotechnology. AIChE J. 49(12) (2003) 2990-3006.

[2] E.S. Gil, S.M. Hudson, Stimuli-reponsive polymers and their bioconjugates. Prog. Polym. Sci. 29(12) (2004) 1173-1222.

[3] X. Wang, H. Gu, Z. Yang, The heating effect of magnetic fluids in an alternating magnetic field. J. Magn. Magn. Mater. 293 (2005) 334-340.

[4] C.J. Gannon, P. Cherukuri, B.I. Yakobson, L. Cognet, J.S. Kanzius, C. Kittrell, R.B. Weisman, M. Pasquali, H.K. Schmidt, R.E. Smalley, S.A. Curley, Carbon nanotube-enhanced thermal destruction of cancer cells in a noninvasive radiofrequency field. Cancer 110(12) (2007) 2654-2665.

[5] R. Yoshida, K. Sakai, T. Okano, Y. Sakurai, Modulating the phase transition temperature and thermosensitivity in N-isopropylacrylamide copolymer gels. J. Biomater. Sci., Polym. Ed. 6 (1994) 585-598.

[6] A. Hawkins, N. Satarkar, J. Hilt, Nanocomposite degradable hydrogels: demonstration of remote controlled degradation and drug release. Pharm. Res. 26(3) (2009) 667-673.

[7] S. Chaterji, I.K. Kwon, K. Park, Smart polymeric gels: Redefining the limits of biomedical devices. Prog. Polym. Sci. 32(8-9) (2007) 1083-1122.

[8] H.G. Schild, Poly(N-isopropylacrylamide): experiment, theory, and application. Prog. Polym. Sci. 17 (1992) 163-249.

[9] J. Melin, S.R. Quake, Microfluidic large-scale integration: The evolution of design rules for biological automation. Annu. Rev. Biophys. Biomol. Struct. 36(1) (2007) 213-231.

[10] G.M. Whitesides, The origins and the future of microfluidics. Nature 442(7101) (2006) 368-373.

CHAPTER 2

BACKGROUND

This Chapter is based in part on

- Book chapter published as:

  N.S. Satarkar, A.M. Hawkins, J.Z. Hilt, Hydrogel nanocomposites in biology and medicine: Applications and interactions, In: R. Bizios and D. Puleo, eds. Biological interactions on materials surfaces, Springer, 2009.

- Review article published as:

  N.S. Satarkar, D. Biswal, J.Z. Hilt, Hydrogel nanocomposites: A review of applications as remote controlled biomaterials, Soft Matter, In Press.

2.1 Introduction

Hydrogels are three dimensional polymeric networks with the ability to swell several times their dry weight by absorption of water and other biological fluids. Hydrogels are currently considered for numerous biomedical and pharmaceutical applications including drug delivery devices, contact lenses, tissue engineering scaffolds, biosensors, sutures, and components of microfluidic devices.[1-4] Responsive hydrogels are a class of hydrogels with swelling properties dependent on environmental factors like pH, temperature, ionic strength, and the presence of a particular molecule.[5-7] Temperature and pH responsive hydrogels have been widely investigated for applications as drug

delivery devices, sensors, and actuators.[8-11] For example, poly (N-isopropylacrylamide) (PNIPAAm) is a negative temperature-responsive hydrogel with a lower critical solution temperature (LCST) of 34^{o}C.[12] PNIPAAm is in swollen state below LCST and is collapsed (less swollen) above LCST. The appropriate choice of the PNIPAAm hydrogel composition allows tuning the LCST close to body temperature to dictate the temperature where the collapse will occur.[13] This aspect has allowed for PNIPAAm systems to be used for temperature triggered drug release and in microfluidic devices in other temperature regimes.[14, 15]

Hydrogel nanocomposites can be obtained by incorporating different types of nanoparticles, such as metallic, clay, and carbon nanotubes, into a hydrogel matrix. Hydrogel nanocomposites have unique properties such as improved mechanical strength, stimuli-responsive behavior, biological interactions, optical properties, and ability of remote actuation.[16-18] For example, the high water content and elasticity of hydrogels typically leads to inferior mechanical performance and limits their applications. The incorporation of nanoparticulate material like hydroxyapatite has improved the mechanical properties and made the nanocomposites attractive materials for a broader range of tissue engineering applications.[19] In cases where the nanoparticle could induce an undesired biological response, the hydrogel can prevent the direct interaction of the nanoparticle with the biological system.

Additionally, hydrogels can be made responsive to external stimuli by incorporation of stimuli-specific nanoparticulates. In order to impart remote controlled (RC) capabilities, a variety of approaches have been employed including the incorporation of magnetic nanoparticles,[20] gold nanoparticles,[21] or carbon nanotubes.[22] Magnetic

nanoparticles are well known for their ability to generate heat when exposed to alternating magnetic fields (AMF) through Neel and Brownian relaxations.[23] In contrast, gold nanoparticles (e.g., nanoshells and nanorods) exhibit photothermal effects by selective absorption of near-infrared (near-IR) light.[24] In addition, research with carbon nanotubes (CNT) has shown that CNTs can be selectively heated when exposed to radiofrequency fields (RF) or near-IR light.[25, 26] Thus, nanocomposites can be remotely heated with specific stimuli through the incorporation of these nanoparticles into polymeric systems.

In the following sections, the recent developments in RC nanocomposites consisting of crosslinked hydrogels and various inorganic nanoparticles are discussed. Some of the common methods of nanocomposite synthesis are described initially. The primary focus of additional sections is on the applications of bulk hydrogel nanocomposites in drug delivery, sensors and actuators, and other therapeutic areas.

2.2 Synthesis and RC actuation of hydrogel nanocomposites

Hydrogel nanocomposites can be roughly divided into three categories based on their size: bulk nanocomposites, particle nanocomposites, and core-shell nanocomposites (**figure 2.1**). The bulk hydrogel nanocomposites are predominantly synthesized in the form of thin films. The nanocomposites in particle form can range from tens of nanometers to microns in diameter and can contain several to many nanoparticle fillers. The core-shell nanocomposites, on the other hand, consist of a single nanoparticle core or small agglomerate of nanoparticles surrounded by a hydrogel shell. The important synthesis routes of these different types of nanocomposites are highlighted below.

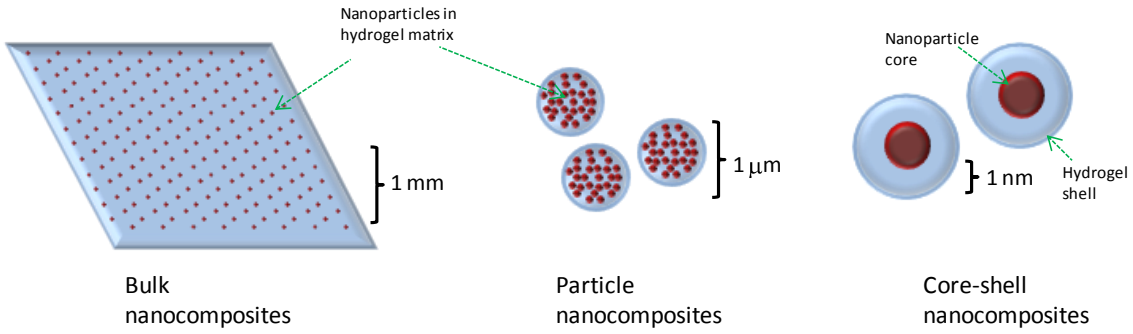

Figure 2.1. Different forms of hydrogel nanocomposites: Bulk nanocomposites, particle nanocomposites, and core-shell nanocomposites

2.2.1 Bulk nanocomposites

Two major routes for the synthesis of bulk polymer nanocomposites have been reported in literature. The first approach involves the dispersion of nanoparticles in the monomer solution followed by polymerization. The other approach consists of synthesis of hydrogel followed by precipitation of nanoparticles within the preformed network to obtain a nanocomposite. Although the presence of reactive groups on the nanoparticle surface can allow for the covalent attachment to the polymer network, the nanoparticles can also be physically entrapped within the polymer. For example, Hilt and associates dispersed the magnetic iron oxide (Fe_3O_4) nanoparticles in N-isopropylacrylamide (NIPAAm)-based monomer solution and carried out free radical polymerization to obtain magnetic hydrogel nanocomposites.[27]

Furthermore, the incorporation of Fe_3O_4 nanoparticles into a hydrogel matrix can impart the ability to remotely heat the hydrogel nanocomposites using an AMF. The extent of PNIPAAm nanocomposite heating in 300 kHz AMF has been shown to be proportional to magnetic nanoparticle loadings.[20] In addition to magnetic nanoparticles, a few

researchers have looked at the addition of gold nanoparticulates to achieve remote heating with near-IR light.[21]

2.2.2 Particle nanocomposites

Particle nanocomposites can provide solutions to problems where bulk or macro-scale systems fail. The size alone can enable their use in applications where this is a critical aspect (e.g., intravenous administration, passive tumor targeting, etc.). Due to smaller diffusion path, nanocomposite micro- and nano-particles exhibit a faster swelling response than the bulk nanocomposites. A variety of emulsion polymerization methods have been developed for particle nanocomposite synthesis.[28-31] The other major route for obtaining particle nanocomposites involves reduction or precipitation of metal nanoparticles within the preformed network of polymer particles.[32] In another example of integration of nanoparticles after hydrogel particle synthesis, gold nanorods have been mixed with swollen hydrogel particles and stabilized in the network by electrostatic forces.[33]

Similar to bulk nanocomposites, the particle nanocomposites can also be actuated by remote stimuli such as magnetic fields or light. For example, Budhlall et al. synthesized (PNIPAAm-co-AAm)-gold microgels and demonstrated remote actuation by application of light and microwave irradiations.[29] In another study, Das and associates obtained RC collapse of (NIPAAm-maleic acid)-gold nanorod particle nanocomposite by irradiation with 809 nm laser light.[33]

2.2.3 Core-shell nanocomposites

Magnetic and gold nanoparticles modified to obtain biocompatible hydrogel surface coatings hold promise in biomedical applications such as drug delivery and contrast agents.[34, 35] These polymers can be chemically bound or physically adsorbed on the nanoparticle surfaces to form thin single or multiple layers. The polymer coatings can provide stabilization, particle size control, and binding selectivity. Examples of different ways to synthesize hydrogel coated nanoparticles (e.g., magnetic and gold cores) include single inverse microemulsion polymerization,[36] emulsion polymerization,[37] photochemical methods,[38] and atom transfer radical polymerization(ATRP).[39] For example, Frimpong and co-workers have synthesized PNIPAAm-based hydrogel coating on magnetic nanoparticles via ATRP. After the ligand exchange over the magnetic particle surface by alkyl bromide or bromosilane, they carried out the ATRP polymerization with PNIPAAm as monomer and various crosslinkers.[39]

2.3 Hydrogel nanocomposite applications in drug delivery

The field of controlled drug delivery continues to be one of the key areas of current research in pharmaceutics and medicine. Due to unique and tailorable properties, hydrogels have been extensively studied as materials for drug delivery applications.[3, 11, 40] For example, the hydrophilicity and porosity of hydrogel network can be controlled by choice of the monomer(s) and the crosslinker. The manipulation of network design allows for the development of drug delivery systems with a desired release profile for a given drug.[41] The incorporation of nano- and micro-scale materials in the hydrogel matrix allows additional control on the network properties (e.g., potential for RC actuation). The various types of hydrogel nanocomposites have been developed in the

past few years, and their swelling and drug release properties have been extensively studied. Here, we review some of the key drug delivery applications of hydrogel nanocomposites.

2.3.1 Hydrogel nanocomposites for RC drug delivery

In many applications, drug delivery systems are designed to release a drug at a constant rate for long periods of time. In other situations, therapeutics such as peptides and hormones often require pulsatile release to match their natural release profile in the body. In the design of pulsatile drug delivery systems, devices have been created that are pre-programmed, self-regulating depending on the presence of a specific molecule, and externally actuated with specific stimuli.[42-45] The design of RC pulsatile drug delivery systems can be tailored by the choice of nanoparticulates, the hydrogel matrix, and the external stimulus. The inherent advantage of these systems over other approaches is that the drug release profile can be altered after implanting the device in the body.

The idea of RC polymer composites was first pursued by Langer and co-workers.[46, 47] They embedded magnetic steel beads in an ethylene-vinyl polymer matrix and release of macromolecules was regulated by application of a low frequency oscillating magnetic field. In their further studies, a magnetic polymer composite containing insulin was implanted subcutaneously in diabetic rats, and effective control of glucose levels was demonstrated with an oscillating magnetic field.[48] The remote control of drug release has attracted a lot of attention, and hydrogel nanocomposites responsive to various stimuli like alternating magnetic field (AMF),[20] direct current (DC) magnetic fields,[49] and light have been investigated.[50] Some of the studies on RC release are highlighted in the sections that follow.

2.3.1.1 Modulation of drug release with AMF

Since AMFs are minimally absorbed by tissue, the use of these fields for RC materials and devices is attractive for *in vivo* applications. In particular, these systems can allow for the simultaneous application of thermal- and chemo-therapies. Demonstration of AMF controlled drug delivery by Hilt and co-workers is described in chapters 3 and 4. A few other researchers have also looked at drug release from magnetic hydrogel nanocomposites with AMF application.[51, 52] For example, Muller-Schulte and Schmitz-Rode applied an AMF (360 kHz, 20 kA/m) to magnetic-PNIPAAm particles and demonstrated triggered release of model drugs such as rhodamine B.[31] In another study, Fe_3O_4 nanoparticles were incorporated in a gelatin hydrogel matrix, and the pulsed release of Vitamin B_{12} was observed on application of a high frequency magnetic field. The effect of magnetic particle size (10-250 nm) was also studied to obtain maximum pulse effect. It was speculated that pulsed release was obtained due to heating of magnetic the particles leading to heating, and resultant shrinking, of gelatin network. The underlying mechanism for this phenomenon in ferrogels is not completely understood.[52]

In one of the first studies of the biocompatibility of hydrogel nanocomposites, *in vitro* analysis of magnetic PNIPAAm nanocomposites with NIH3T3 fibroblasts indicated minimal cytotoxicity.[53] In additional studies, poly(ethylene glycol) magnetic nanocomposites were demonstrated as potential implant for thermal ablation and hyperthermia cancer treatment, along with capabilities of RC drug delivery.[54]

Magnetic nanocomposites in particle form can also be used to control drug release from an implant. In an interesting device design, iron oxide nanoparticles and PNIPAAm based

particles were embedded into an ethyl cellulose membrane. This membrane was fixed on a sodium fluorescein drug reservoir. Application of an AMF heated the magnetic particles and increased local temperatures, which caused the hydrogel nanoparticles to shrink. This process opened the pores and allowed the drug to diffuse at enhanced rates. When the AMF was turned off, the device cooled, and the hydrogel particles reswelled. This led to the drug release being turned off. The temperature profile of the sample chamber for multiple AMF cycles and the differential flux of sodium fluorescein out of the membrane were recorded. The cytotoxicity analysis of the membranes to a broad range of cell types (fibroblasts, macrophages, and mesothelial cells) showed over 90% viability. Furthermore, a membrane implanted subcutaneously in rats for 45 days was found to retain its inductive heating ability. This device holds promise as a long term on-demand drug delivery implant.[55]

2.3.1.2 Modulation of drug release with DC magnetic fields

In addition to AMF actuation systems, magnetic nanocomposite researchers have explored DC magnetic fields for RC drug delivery.[56] Chen and colleagues showed that application of a DC magnetic field to a PVA nanocomposite resulted in accumulation of drug around the ferrogel, this situation was designated as “close” configuration of pores. When the field was switched OFF, the pores opened and the drug was released.[49] Studies with different size particles showed that hydrogels with larger sized particles exhibited better actuation profiles due to stronger saturation magnetization and smaller coercive forces. Overall, the release profiles showed reduced drug release on application of magnetic fields. Further studies with the system tested nanocomposites with various particle loadings in an attempt to achieve the optimum magnetic-responsive behavior.

Various system parameters like permeability coefficient, partition coefficient, space restriction, and magnetization were investigated.[56] A similar effect with DC magnetic field was observed on drug release from magnetic nanocomposites of gelatin hydrogels.[57] In another study, nanocomposites were fabricated by in-situ synthesis of magnetic particles using a coprecipitation method. Vitamin B_{12} was used as a model drug for the release study, and reduced drug release was obtained by application of the magnetic field.[58]

A few other studies have looked at RC application of the nanocomposites *in vivo*. For example, Chen et al. synthesized about 1 μm diameter magnetic polyvinylpyrrolidone hydrogel particles, and loaded with chemotherapeutic drug Bleomycin A5 Hydrochloride (BLM). The microparticles were injected (intra-arterial) in rabbits with an auricular VX2 tumor. A permanent magnet (magnetic flux 0.5T) was placed directly over the tumor surface for 24 hours following the injection. The size of the tumor was measured for 2 weeks. The treatment with microparticles followed by magnet showed significant reduction in tumor size as compared to the animals with other treatment variations. The microparticles containing BLM were selectively accumulated at the tumor site due to the magnet, and slowly released BLM leading to tumor recession.[30, 59] In another study, effective targeting was also demonstrated by Sun et al. when they injected magnetic polyacrylamide particle nanocomposites into rabbits. A DC magnetic field was applied to the right back leg of the rabbit, and the accumulation of particles there was found to be two times higher after 90 minutes of injection, as compared to the left back leg.[60]

2.3.1.3 Modulation of drug release with light

Near-infrared (near-IR) light is an alternative method to achieve RC actuation of materials and devices. Of particular interest is near-IR light with wavelengths between 800-1200 nm which can be transmitted through tissue for short (e.g., couple centimeters) distances with very little attenuation.There is significant interest in the addition of gold nanoparticulates or CNTs in PNIPAAm hydrogels, where light can be used to induce remote heating and collapse. In an interesting demonstration, DNA-CNT/nanohorn conjugates were synthesized and incorporated in PNIPAAm matrix. The irradiation by 1064 nm near-IR light heated the nanocomposites and released the DNA conjugates, while hydrogels without CNT/nanohorns were not affected by the laser irradiation.[22]

West and co-workers synthesized gold nanoshells with optical absorbance properties that can be tuned by appropriate choice of the geometry and composition. They incorporated nanoshells in a PNIPAAm matrix and showed that selective absorption of near-IR light at 832 nm can cause the nanocomposite swelling transition.[61] The extent of such a collapse could be tailored by varying the nanoshell concentration and strength of the laser light. Gold-PNIPAAm nanocomposites were further used to modulate the release of proteins including insulin, bovine serum albumin (BSA), and lysozyme. The SDS-PAGE gel analysis of the released proteins indicated no significant degradation in molecular weights, suggesting that the released drugs may still be biologically active.[50]

In a notable demonstration, Niidome et al. looked at RC actuation of the nanocomposites *in vivo*. They synthesized PNIPAAm coated gold nanorods via colloidal-template polymerization and silica etching. The core-shell nanocomposites exhibited photothermal phase transition with the application of near-IR light, and the nanocomposite swelling

properties could be controlled by irradiation power. The nanocomposites were intravenously injected into mice followed by the irradiation of near-IR laser light to the right kidney. The organs were subsequently collected, and the amounts of the gold nanorods were analyzed. For the case without near-IR irradiation, most of the nanoparticles were trapped in lungs. The application of near-IR light to the right kidney caused particle collapse and aggregation resulting in significant accumulation. No accumulation was observed in the left kidney, and the amount of gold in the blood was lower than in the case without laser irradiation.[62]

2.3.2 Hydrogel-clay nanocomposites for enhanced release profile

In addition to remote actuation, nanoparticles can also be utilized to manipulate transport properties of hydrogel networks. Clay is one of the most widely studied filler materials that affect the hydrophilicity of hydrogel networks in order to modulate drug release. The incorporation of clay in hydrogel matrices can result into nanocomposites with unique properties including high mechanical strength, better optical properties, and controlled response to stimuli. Hectorite, hydrotalcite, montmorillonite, and synthetic mica are some of the examples of clay incorporated in hydrogels.[63-67] For example, Haraguchi and co-workers synthesized nanocomposite hydrogels with water-swellable inorganic clay.[68] The mechanism of formation of clay-PNIPAAm composite was studied in order to investigate the reasons for the unique nanocomposite properties. These studies revealed that polymerization proceeded on the clay particles, which act as multi-functional crosslinking agents. The clay nanoparticles acted as active components of the network structure and allowed additional control of the crosslink density.[69]

Lee and Chen prepared nanocomposites of poly(acrylic acid-*co*-poly(ethylene glycol) methyl ether acrylate) hydrogels with hydrotalcite clay.[70] The results showed that clay incorporation affected slightly the pH swelling response of the hydrogels; moreover, the gels became more hydrophilic with increased clay content. Hydrotalcite clay has a positive charge on its surface, while acrylic acid networks have a negative charge. Hence, incorporation of various amounts of clay could control the charge of the nanocomposite. Drug release studies were conducted using model chemical compounds with different charge properties to study the effects of drug-composite interaction. The release profile of crystal violet, a cationic model chemical compound, was altered significantly by clay loading.[49]

In another study, the charge properties of PNIPAAm were adjusted by using anionic clay (mica) and/or a cationic monomer (trimethyl (acrylamido propyl) ammonium iodide). The various properties of the resultant nanocomposite, including temperature-responsive swelling and drug release behavior, were studied. In that case, drug release behavior depended on the charge properties of the clay and the chemical compounds tested.[71]

2.4 Hydrogel nanocomposites applications as sensors and actuators

In addition to drug delivery, another area of hydrogel nanocomposite applications of great interest is sensors and actuators. Hydrogel nanocomposites have unique properties that make them attractive as sensing elements and actuators. For example, incorporation of gold nanoparticles or carbon nanotubes in temperature responsive hydrogels can result into dramatic change in electrical properties of the composite with changes in swelling state and temperature.[72, 73] The change in electrical properties can be harnessed for applications in sensors (e.g., temperature and humidity sensors). Furthermore, the

composite properties and response can be tuned by type and concentration of monomers, crosslinkers, and nanoparticulates.

The incorporation of nanoparticulates can also result in hydrogel nanocomposites that can change shape or swelling state in response to external signals. Hydrogel nanocomposites have been demonstrated to be responsive to electric and magnetic fields, making them attractive as valves, pumps, and artificial muscles.[74, 75] In addition, incorporation of magnetic nanoparticles or gold-nanoshells in temperature responsive hydrogels can heat them with stimuli such as magnetic fields, or light. Hence, they can be actuated at a distance.[76] In this section, we highlight some of the high interest applications of hydrogel nanocomposites as sensors and actuators.

2.4.1 Hydrogel nanocomposites as sensors

There is a lot of interest in tuning the electrical properties of temperature responsive hydrogels by adding gold nanoparticles for applications as temperature sensors. Zhao and others functionalized gold nanoparticles with vinyl groups and dispersed them in temperature-responsive PNIPAAm monomer solution. On polymerization, hydrogel nanocomposites with well dispersed gold nanoparticles attached covalently to the polymer matrix were obtained. The nanocomposite was incorporated on an electrode and showed excellent thermo-switchable electrical properties. The electrical conductivity of the gold-PNIPAAm nanocomposite was changed by two orders of magnitude around the transition temperature. The reversible change in electrical conductivity was observed for multiple temperature cycles.[77] It was hypothesized that lower electrical conductivity was observed at lower temperatures because the large inter-particle distance acted as barrier to electron hopping through the PNIPAAm. As temperature was increased,

PNIPAAm started collapsing and the distance between gold particles decreased. Above the transition temperature, gold nanoparticles became close-packed and developed a conductive path that increased conductivity of the nanocomposite construct. Further studies showed that the transition temperature could be adjusted from 0^{o}C to 40^{o}C by variation of the concentration of gold nanoparticles, the composition of the monomer, and the degree of crosslinking.[72]

In addition to gold nanoparticles, carbon nanotubes are also studied as materials to impart unique electrical properties to hydrogels. Carbon nanotubes are attractive because they can also increase the mechanical properties of the composites. For example, Yang et al. synthesized multi-walled carbon nanotubes (MWCNT) arrays and filled the inter-MWCNT spaces with PNIPAAm monomer solution. After polymerization, nanocomposites of PNIPAAm with aligned MWCNT arrays were obtained. The resistance of the nanocomposites decreased linearly with an increase in temperature. This is because the PNIPAAm films collapsed with an increase in temperature, reducing the distance between MWCNTs and increasing conductance of the film. Also, the addition of water increased resistance of the gel, and as water evaporated, the resistance decreased. Furthermore, the nanocomposite showed fast wetting/dewetting behavior as opposed to pure hydrogel as well as random MWCNT-hydrogel nanocomposites. Finally, it was observed that the resistance of the nanocomposite was also sensitive to the humidity of its environment. The hydrogel/MWCNT-array nanocomposites showed faster sensitivity to change in humidity than pure CNT samples. The unique properties of this NIPAAm-MWCNT nanocomposites are significant for use as temperature/humidity sensors and dewetting materials.[73]

2.4.2 Hydrogel nanocomposites as actuators

In addition to sensors, hydrogel nanocomposites are being pursued for actuator applications. The swelling phenomenon of hydrogels is diffusion limited and, hence, actuators at small size scales can result in faster response. This aspect leads to hydrogels being attractive components of micro- and nanodevices. Beebe and colleagues introduced pH-responsive hydrogels as both a sensor and actuator for flow control in microfluidic devices.[10] The ability to change shape on application of specific stimuli is discussed in this section with emphasis on RC actuators.

2.4.2.1 Actuation with electric fields

Shi and colleagues showed that carbon nanotube-PVA nanocomposites can exhibit bending effects in an electric field. MWCNT were converted to an acid form and then to sodium salts. The PVA nanocomposites were then synthesized using a freeze-thaw method. On application of a DC electric field, Na-MWCNT/PVA hydrogel strips quickly bended towards the cathode. This is because cations (Na+) in the gel migrated towards the negative electrode, while anions were immobilized with the nanotubes. An osmotic pressure difference was established in the gel leading to its bending. A reversible bending phenomenon was observed when the polarity of the electric field was switched for multiple cycles**.**[74]

In another study, swelling and electroresponsive properties of MWCNT-gelatin nanocomposites were studied. The swelling studies showed a decrease in equilibrium swelling with increased MWCNT loadings due to the hydrophobic property of MWCNT. The application of DC electric field induced a two-stage bending phenomenon attributed

to the osmotic pressure difference: initial bending towards the anode followed by bending towards the cathode.[78]

2.4.2.2 Actuation with magnetic fields

The use of magnetic fields (AMF or DC magnetic fields) can allow remote actuation of hydrogel nanocomposites. Zrinyi and co-workers were the first ones to demonstrate that DC magnetic fields could be used to induce remote shape change in hydrogel composites.[79] They prepared magnetic nanocomposites of PVA hydrogels containing 10-12 nm Fe_3O_4 particles. The application of a spatially non-uniform magnetic field to the magnetic nanocomposite generated forces within the matrix. The hydrogel matrix moved because the particles in the matrix were attracted to stronger fields. The elongation of magnetic nanocomposite was dependent on magnetic field gradient and concentration of nanoparticles.[80] Other studies reported in the literature characterize the magnetic field response of the PNIPAAm based nanocomposites for different particle loadings and field amplitude.[79, 81] Magnetic and elastic interactions are the key parameters that control the motion of nanocomposites.[75] In another report, cobalt nanoparticles were covalently attached to poly (2-hydroxyethyl methacrylate) network. The resultant nanocomposites exhibited enhanced properties including flexibility, shape memory, and response to DC magnetic fields.[82]

In addition to DC magnetic fields, AMF has also been pursued for actuator applications. For example, Kato et al. applied a 2 kHz AMF to magnetic PNIPAAm nanocomposites inducing RC heating and collapse. The change in volume in this case was demonstrated as a magnetically controlled chemomechanical device to lift weights.[83] Hydrogel nanocomposites can be used as valves to regulate flow in microfluidic channels.

Hydrogels are easy to fabricate in microchannels and can potentially eliminate the need for complex external components that are necessary in traditional pneumatic flow control. Much of the initial work with hydrogels as valves has been with pH or temperature responsive hydrogels.[9] Magnetic fields or light as a stimuli have more potential than pH or temperature because they can be applied remotely to a microfluidic device. The demonstration of AMF controlled microfluidic valves by Hilt and co-workers is discussed in chapter 5. Recently, Ghosh et al. have also studied AMF controlled microfluidic valves. They showed that response time can be improved by using valves of smaller dimensions.[84]

2.4.2.3 Actuation with light

In another study of RC valves, West and co-workers incorporated gold-PNIPAAm nanocomposites at a T-junction in a microfluidic device. One valve in the device contained a gold-colloid hydrogel nanocomposite while the other contained a gold-nanoshell hydrogel nanocomposite. The study demonstrated that both of the hydrogel valves can be independently addressed using light of different wavelengths.[76] RC actuators can thus be potentially useful as valves, mixers, pumps, and flow sorters for on-chip microfluidic devices. Light as a stimulus has potential limitations for actuation of valves in multi-layered devices. Magnetic fields on the other hand can potentially penetrate deeper and have a wider-range of applications.

Gold-PNIPAAm nanocomposites have also been demonstrated as tunable microlens with light as a stimulus. In an attractive demonstration, multiple micropost structures of gold-PNIPAAm hydrogels were patterned around a lens aperture. Hydrogel swelling state was controlled by IR light irradiation, which in turn changed the curvature of liquid-liquid

interface and, thus, the focal length of the lens. Light controlled microlenses have potential to replace current technology that uses mechanical or electrical signals.[85]

2.5 Hydrogel nanocomposites for other therapeutic applications

In addition to drug delivery, sensors, and actuators, hydrogel nanocomposites are also attractive for various other therapeutic applications such as thermal therapy, and antimicrobial materials. Thermal therapy for cancer treatment is based on the concept of heating magnetic nanoparticles remotely by magnetic fields. On the other hand, the antimicrobial activity of hydrogels can arise from the incorporation of silver nanoparticles. This section briefly addresses the aforementioned two applications.

2.5.1 Thermal therapy applications

In the last few years, hyperthermia, which uses heat as a therapy, has attracted much interest in the treatment of cancer cells. It is interesting to note that hyperthermia is actually one of the oldest cancer therapies known.[86] Recent advances in thermal therapy systems (e.g., those based on nanoparticle systems) allow better control of the spatial and temporal delivery of thermal energy. As a result, there has been renewed interest in investigating the effect of hyperthermia in combination with radiation, chemotherapy, immunotherapy, and drug delivery modalities.[87-89]

Magnetic hydrogel nanocomposites can be potentially used for hyperthermia applications. For example, Wang and co-workers developed a Bioglass based degradable magnetic composite and demonstrated selective treatment of lung carcinoma cells by use of an AMF.[90] In another study, Hilt and co-workers synthesized magnetic poly(ethylene glycol) nanocomposites and showed ability to kill glioblastoma cells *in*

vitro with magnetic nanocomposites exposed to AMF.[54] Heating analysis of magnetic hydrogel nanocomposites, modeling, and simulations for hyperthermia treatment is described in chapter 7.

2.5.2 Antimicrobial applications

Metallic nanoparticles can be toxic to microorganisms. For example, silver nanoparticles exhibit antimicrobial effects by binding to microbial DNA, preventing bacterial replication, and also causing inactivation of bacteria function.[91, 92] Researchers have studied silver nanocomposites of various types of hydrogel systems, including poly (acrylamide-co-acrylic acid), poly (NIPAAm-co-sodium acrylate), and poly (vinyl pyrolidone) interpenetrated with poly(acrylamide).[92-95] Silver-hydrogel nanocomposites demonstrated excellent antibacterial effects when tested using *Escherichia Coli (E. Coli)*.[93, 94] Lee and Tsao studied the effect of particle concentration on various properties including swelling kinetics, gel strength, electrical conductivity, and anti-microbial activity.[54] Additionally, the antibacterial activity of hydrogel nanocomposites was enhanced by reducing the nanoparticle size and increasing the nanoparticle loading.[92]

2.6 Concluding remarks

In this chapter, the rapidly emerging field of hydrogel nanocomposites was discussed. Hydrogel nanocomposites containing different types of nanoparticulates including iron oxide, clay, silver, gold, and carbon naotubes were highlighted. The versatile synthesis techniques have allowed for the creation of nanocomposites with tailored size and compositions that are suitable for a wide-range of applications. The enhanced and unique properties of these nanocomposite biomaterials were emphasized. The primary focus of

this chapter was on the RC hydrogel nanocomposites, and the applications of hydrogel nanocomposites in drug delivery, sensors, actuators, antimicrobial materials, and thermal therapy were discussed.

Based on this detailed background study, following observations are made.

1. There is increasing interest in RC drug delivery from hydrogel nanocomposites using a variety of approaches. However, the detailed understanding of the underlying mechanism has not been investigated, particularly with AMF actuated magnetic nanocomposites.

2. Hydrogel nanocomposites are attractive materials for microfluidic flow control. There is limited information on applications of magnetic hydrogel nanocomposites as AMF actuated RC microfluidic valves.

3. Radiofrequency actuation of carbon nanotube-hydrogel nanocomposites remains unexplored.

4. Although RC heating of a variety of hydrogel nanocomposites has been explored, there are no reports of modeling the heating response. Development of analytical model can help further understanding and can also be a useful tool for simulating hydrogel response in a different heat transfer condition (e.g., *in vivo* hyperthermia).

2.7 References

[1] A.M. Lowman, N.A. Peppas, Hydrogels. in: E. Mathiowitz (Ed.), Encyclopedia of Controlled Drug Delivery, Vol. 1, Wiley, New York, 1999, pp. 397-418.

[2] N.A. Peppas, J.Z. Hilt, A. Khademhosseini, R. Langer, Hydrogels in biology and medicine: from molecular principles to bionanotechnology. Adv. Mater. 18 (2006) 1345-1360.

[3] N.A. Peppas, P. Bures, W. Leobandung, H. Ichikawa, Hydrogels in pharmaceutical formulations. European Journal of Pharmceutics and Biopharmaceutics 50 (2000) 27-46.

[4] A.S. Hoffman, Hydrogels in biomedical applications. Adv. Drug Deliver. Rev. 43 (2002) 3-12.

[5] S. Chaterji, I.K. Kwon, K. Park, Smart polymeric gels: Redefining the limits of biomedical devices. Prog. Polym. Sci. 32(8-9) (2007) 1083-1122.

[6] R.V. Ulijn, N. Bibi, V. Jayawarna, P.D. Thornton, S.J. Todd, R.J. Mart, A.M. Smith, J.E. Gough, Bioresponsive hydrogels. Materials Today 10(4) (2007) 40-48.

[7] T. Miyata, N. Asami, T. Uragami, A reversibly antigen-responsive hydrogel. Nature 399(6738) (1999) 766-769.

[8] J.Z. Hilt, A.K. Gupta, R. Bashir, N.A. Peppas, Ultrasensitive biomems sensors based on microcantilevers patterned with environmentally responsive hydrogels. Biomedical Microdevices 5(3) (2003) 177-184.

[9] L. Dong, H. Jiang, Autonomous microfluidics with stimuli-responsive hydrogels. Soft Matter 3(10) (2007) 1223-1230.

[10] D.J. Beebe, J.S. Moore, J.M. Bauer, Q. Yu, R.H. Liu, C. Devadoss, B.-H. Jo, Functional hydrogel structures for autonomous flow control inside microfluidic channels. Nature 404(6778) (2000) 588-590.

[11] Y. Qiu, K. Park, Environment-sensitive hydrogels for drug delivery. Adv. Drug Deliver. Rev. 53(3) (2001) 321-339.

[12] H.G. Schild, Poly(N-isopropylacrylamide): experiment, theory, and application. Prog. Polym. Sci. 17 (1992) 163-249.

[13] R. Yoshida, K. Sakai, T. Okano, Y. Sakurai, Modulating the phase transition temperature and thermosensitivity in N-isopropylacrylamide copolymer gels. J. Biomater. Sci., Polym. Ed. 6 (1995) 585-598.

[14] A.S. Hoffman, Applications of thermally reversible polymers and hydrogels in therapeutics and diagnostics. J. Control. Rel. 6(1) (1987) 297-305.

[15] A.K. Agarwal, L. Dong, D.J. Beebe, H. Jiang, Autonomously-triggered microfluidic cooling using thermo-responsive hydrogels. Lab Chip 7(3) (2007) 310-315.

[16] R.A. Frimpong, J.Z. Hilt, in: N. A. Peppas, J. Z. Hilt and J. B. Thomas (Eds.), Nanotechnology in Therapeutics: Current Technology and Applications, Horizon Scientific Press, Norfolk, 2007, pp. 241-256.

[17] V. Thomas, M. Namdeo, Y.M. Mohan, S.K. Bajpai, M. Bajpai, Review on polymer, hydrogel and microgel metal nanocomposites: A facile nanotechnological approach. J. Macromol. Sci., Part A: Pure Appl. Chem. 45(1) (2008) 107-119.

[18] K.M. Gattas-Asfura, Y. Zheng, M. Micic, M.J. Snedaker, X. Ji, G. Sui, J. Orbulescu, F.M. Andreopoulos, S.M. Pham, C. Wang, R.M. Leblanc, Immobilization of quantum dots in the photo-cross-linked poly(ethylene glycol)-based hydrogel. J. Phys. Chem. B 107(38) (2003) 10464-10469.

[19] H. Xu, Y.J. Wang, Y.D. Zheng, X.F. Chen, L. Ren, G. Wu, X.S. Huang, Preparation and characterization of bioglass/polyvinyl alcohol composite hydrogel. Biomedical Materials 2(2) (2007) 62-66.

[20] N.S. Satarkar, J.Z. Hilt, Nanocomposite hydrogels as remote controlled biomaterials. Acta Biomater. 4 (2008) 11-16.

[21] A. Shiotani, T. Mori, T. Niidome, Y. Niidome, Y. Katayama, Stable incorporation of gold nanorods into N-Isopropylacrylamide hydrogels and their rapid shrinkage induced by near-infrared laser irradiation. Langmuir 23(7) (2007) 4012-4018.

[22] E. Miyako, H. Nagata, K. Hirano, T. Hirotsu, Photodynamic thermoresponsive nanocarbon-polymer gel hybrids. Small 4(10) (2008) 1711-1715.

[23] X. Wang, H. Gu, Z. Yang, The heating effect of magnetic fluids in an alternating magnetic field. J. Magn. Magn. Mater. 293 (2005) 334-340.

[24] A.O. Govorov, H.H. Richardson, Generating heat with metal nanoparticles. Nanotoday 2(1) (2007) 30-38.

[25] C.J. Gannon, P. Cherukuri, B.I. Yakobson, L. Cognet, J.S. Kanzius, C. Kittrell, R.B. Weisman, M. Pasquali, H.K. Schmidt, R.E. Smalley, S.A. Curley, Carbon nanotube-enhanced thermal destruction of cancer cells in a noninvasive radiofrequency field. Cancer 110(12) (2007) 2654-2665.

[26] N.W.S. Kam, M. O'Connell, J.A. Wisdom, H. Dai, Carbon nanotubes as multifunctional biological transporters and near-infrared agents for selective cancer cell destruction. Proc. Natl. Acad. Sci. U. S. A. 102(33) (2005) 11600-11605.

[27] R.A. Frimpong, S. Fraser, J.Z. Hilt, Synthesis and temperature response analysis of magnetic-hydrogel nanocomposites. J. Biomed. Mater. Res. A 80A(1) (2007) 1-6.

[28] Z.Z. Xu, C.C. Wang, W.L. Yang, Y.H. Deng, S.K. Fu, Encapsulation of nanosized magnetic iron oxide by polyacrylamide via inverse miniemulsion polymerization. Journal of Magnetism and Magnetic Materials 277(1-2) (2004) 136-143.

[29] B.M. Budhlall, M. Marquez, O.D. Velev, Microwave, photo- and thermally responsive PNIPAAm gold nanoparticle microgels. Langmuir 24(20) (2008) 11959-11966.

[30] J. Chen, L. Yang, Y. Liu, G. Ding, Y. Pei, J. Li, G. Hua, J. Huang, Preparation and characterization of magnetic targeted drug controlled-release hydrogel microspheres. Macromol. Symp. 225(1) (2005) 71-80.

[31] D. Müller-Schulte, T. Schmitz-Rode, Thermosensitive magnetic polymer particles as contactless controllable drug carriers. J. Magn. Magn. Mater. 302(1) (2006) 267-271.

[32] X. Jiang, D.A. Xiong, Y. An, P. Zheng, W. Zhang, L. Shi, Thermoresponsive hydrogel of poly(glycidyl methacrylate-co-N-isopropylacrylamide) as a nanoreactor of gold nanoparticles. Journal of Polymer Science Part A: Polymer Chemistry 45(13) (2007) 2812-2819.

[33] M. Das, N. Sanson, D. Fava, E. Kumacheva, Microgels loaded with gold nanorods: Photothermally triggered volume transitions under physiological conditions Langmuir 23(1) (2006) 196-201.

[34] H. Chirra, D. Biswal, J.Z. Hilt, in: D. T. Pathak (Ed.), Nanoparticulate Drug Delivery Systems (NPDDS) II: Formulation and Characterization, Informa Healthcare, New York, 2009, in press, pp. 90-114.

[35] R.A. Frimpong, J.Z. Hilt, Magnetic nanoparticles in biomedicine: Properties, synthesis, and functionalization. Nanomedicine (Under review).

[36] P.A. Dresco, V.S. Zaitsev, R.J. Gambino, B. Chu, Preparation and Properties of Magnetite and Polymer Magnetite Nanoparticles. Langmuir 15(6) (1999) 1945-1951.

[37] J.-H. Kim, T.R. Lee, Thermo- and pH-Responsive Hydrogel-Coated Gold Nanoparticles. Chemistry of Materials 16(19) (2004) 3647-3651.

[38] P. Gong, J. Yu, H. Sun, J. Hong, S. Zhao, D. Xu, S. Yao, Preparation and characterization of OH-functionalized magnetic nanogels under UV irradiation. Journal of Applied Polymer Science 101(3) (2006) 1283-1290.

[39] R.A. Frimpong, J.Z. Hilt, Poly(n-isopropylacrylamide)-based hydrogel coatings on magnetite nanoparticles via atom transfer radical polymerization. Nanotechnology 19(17) (2008) 175101-175107.

[40] T.R. Hoare, D.S. Kohane, Hydrogels in drug delivery: Progress and challenges. Polymer 49(8) (2008) 1993-2007.

[41] C.-C. Lin, A.T. Metters, Hydrogels in controlled release formulations: Network design and mathematical modeling. Adv. Drug Deliver. Rev. 58(12-13) (2006) 1379-1408.

[42] A. Kikuchi, T. Okano, Pulsatile drug release control using hydrogels. Adv. Drug Deliver. Rev. 54 (2002) 53-77.

[43] J. Kost, R. Langer, Responsive polymeric delivery systems. Adv. Drug Deliver. Rev. 46 (2001) 125-148.

[44] S.R. Sershen, J.L. West, Implantable, polymeric systems for modulated drug delivery. Adv. Drug Deliver. Rev. 54 (2002) 1225-1235.

[45] T. Bussemer, I. Otto, R. Bodmeier, Pulsatile drug-delivery systems. Crit. Rev. Ther. Drug. 18(5) (2001) 433-458.

[46] E.R. Edelman, J. Kost, H. Bobeck, R. Langer, Regulation of drug release from polymer matrices by oscillating magnetic fields. J. Biomed. Mater. Res. 19(1) (1985) 67-83.

[47] D. S. T. Hsieh, R. Langer, J. Folkman, Magnetic modulation of release of macromolecules from polymers. Proc. Natl. Acad. Sci. U. S. A. 78(3) (1981) 1863-1867.

[48] J. Kost, J. Wolfrum, R. Langer, Magnetically enhanced insulin release in diabetic rats. J. Biomed. Mater. Res. 21 (1987) 1367-1373.

[49] T.Y. Liu, S.H. Hu, D.M. Liu, S.Y. Chen, Magnetic-sensitive behavior of intelligent ferrogels for controlled release of drug. Langmuir 22(14) (2006) 5974-5978.

[50] M. Bikram, A.M. Gobin, R.E. Whitmire, J.L. West, Temperature-sensitive hydrogels with SiO2-Au nanoshells for controlled drug delivery. J. Control. Rel. 123(3) (2007) 219-227.

[51] M. Babincova, J. Novotny, J. Rosenecker, P. Babinec, Remote radio-control of siRNA release from magnetite-hydrogel composite. Optoelectronics and Advanced Materials – Rapid Communications 1(11) (2007) 644-647.

[52] S.-H. Hu, T.-Y. Liu, D.-M. Liu, S.-Y. Chen, Controlled pulsatile drug release from a ferrogel by a high-frequency magnetic field. Macromolecules 40(19) (2007) 6786-6788.

[53] S.A. Meenach, A.A. Anderson, M. Suthar, K.W. Anderson, J.Z. Hilt, Biocompatibility analysis of magnetic hydrogel nanocomposites based on poly(N-isopropylacrylamide) and iron oxide. Journal of Biomedical Materials Research Part A 91A(3) (2009) 903-909.

[54] S.A. Meenach, J.Z. Hilt, K.W. Anderson, Poly(ethylene glycol)-based magnetic hydrogel nanocomposites for hyperthermia cancer therapy. Acta Biomater. 6(3) (2010) 1039.

[55] T. Hoare, J. Santamaria, G.F. Goya, S. Irusta, D. Lin, S. Lau, R. Padera, R. Langer, D.S. Kohane, A magnetically triggered composite membrane for on-demand drug delivery. Nano Lett. 9(10) (2009) 3651-3657.

[56] T.-Y. Liu, S.-H. Hu, K.-H. Liu, D.-M. Liu, S.-Y. Chen, Study on controlled drug permeation of magnetic-sensitive ferrogels: Effect of Fe3O4 and PVA. J. Control. Rel. 126(3) (2008) 228-236.

[57] T.-Y. Liu, S.-H. Hu, K.-H. Liu, D.-M. Liu, S.-Y. Chen, Preparation and characterization of smart magnetic hydrogels and its use for drug release. J. Magn. Magn. Mater. 304 (2006) e397-e399.

[58] S.-H. Hu, T.-Y. Liu, D.-M. Liu, S.-Y. Chen, Nano-ferrosponges for controlled drug release. J. Control. Rel. 121(3) (2007) 181-189.

[59] A. Kamulegeya, J. Huang, G. Ding, J. Chen, Y. Liu, Self assembled magnetic PVP/PVA hydrogel microspheres; magnetic drug targeting of VX2 auricular tumours using pingyangmycin. J. Drug Targeting 14(4) (2006) 243-253.

[60] H. Sun, L. Zhang, X. Zhang, C. Zhang, Z. Wei, S. Yao, 188Re-labeled MPEG-modified superparamagnetic nanogels: preparation and targeting application in rabbits. Biomedical Microdevices 10(2) (2008) 281-287.

[61] S.R. Sershen, S.L. Westcott, N.J. Halas, J.L. West, Temperature-sensitive polymer-nanoshell composites for photothermally modulated drug delivery. J. Biomed. Mater. Res. 51(3) (2000) 293-298.

[62] T. Kawano, Y. Niidome, T. Mori, Y. Katayama, T. Niidome, PNIPAM Gel-Coated Gold Nanorods for Targeted Delivery Responding to a Near-Infrared Laser. Bioconjugate Chemistry 20(2) (2009) 209-212.

[63] J. Ma, Y. Xu, Q. Zhang, L. Zha, B. Liang, Preparation and characterization of pH- and temperature-responsive semi-IPN hydrogels of carboxymethyl chitosan with poly (N-isopropyl acrylamide) crosslinked by clay. Colloid & Polymer Science 285(4) (2007) 479-484.

[64] Y. Xiang, Z. Peng, D. Chen, A new polymer/clay nano-composite hydrogel with improved response rate and tensile mechanical properties. Eur. Polym. J. 42(9) (2006) 2125-2132.

[65] M. Kokabi, M. Sirousazar, Z.M. Hassan, PVA-clay nanocomposite hydrogels for wound dressing. Eur. Polym. J. 43(3) (2007) 773-781.

[66] K. Haraguchi, H.-J. Li, Control of the coil-to-globule transition and ultrahigh mechanical properties of PNIPA in nanocomposite hydrogels. Angew. Chem. 117(40) (2005) 6658-6662.

[67] K. Haraguchi, Nanocomposite hydrogels. Current Opinion in Solid State and Materials Science 11(3-4) 47-54.

[68] K. Haraguchi, T. Takehisa, Nanocomposite hydrogels: A unique organic-inorganic network structure with extraordinary mechanical, optical, and swelling/de-swelling properties. Adv. Mater. 14(16) (2002) 1120-1124.

[69] K. Haraguchi, H.J. Li, K. Matsuda, T. Takehisa, E. Elliott, Mechanism of forming organic/inorganic network structures during in-situ free-radical polymerization in PNIPA-clay nanocomposite hydrogels. Macromolecules 38(8) (2005) 3482-3490.

[70] W.-F. Lee, Y.-C. Chen, Effect of hydrotalcite on the physical properties and drug-release behavior of nanocomposite hydrogels based on poly[acrylic acid-co-poly(ethylene glycol) methyl ether acrylate] gels. J. Appl. Polym. Sci. 94(2) (2004) 692-699.

[71] W.-F. Lee, K.-T. Tsao, Effect of intercalant content of mica on the various properties for the charged nanocomposite poly(N-isopropyl acrylamide) hydrogels. J. Appl. Polym. Sci. 104(4) (2007) 2277-2287.

[72] X. Zhao, X. Ding, Z. Deng, Z. Zheng, Y. Peng, C. Tian, X. Long, A kind of smart gold nanoparticle-hydrogel composite with tunable thermo-switchable electrical properties. New J. Chem. 30(6) (2006) 915-920.

[73] Z. Yang, Z. Cao, H. Sun, Y. Li, Composite films based on aligned carbon nanotube arrays and a poly(N-isopropyl acrylamide) hydrogel. Adv. Mater. 20(11) (2008) 2201-2205.

[74] J. Shi, Z.X. Guo, B. Zhan, H. Luo, Y. Li, D. Zhu, Actuator Based on MWNT/PVA Hydrogels. J. Phys. Chem. B 109(31) (2005) 14789-14791.

[75] G. Filipcsei, I. Csetneki, A. Szilagyi, M. Zrinyi, Magnetic field-responsive smart polymer composites Adv. Polym. Sci. 206 (2007) 137-189.

[76] S.R. Sershen, G.A. Mensing, M. Ng, N.J. Halas, D.J. Beebe, J.L. West, Independent optical control of microfluidic valves formed from optomechanically responsive nanocomposite hydrogels. Adv. Mater. 17(11) (2005) 1366-1368.

[77] X. Zhao, X. Ding, Z. Deng, Z. Zheng, Y. Peng, X. Long, Thermoswitchable electronic properties of a gold nanoparticle/hydrogel composite. Macromol. Rapid Commun. 26(22) (2005) 1784-1787.

[78] S. Haider, S.-Y. Park, K. Saeed, B.L. Farmer, Swelling and electroresponsive characteristics of gelatin immobilized onto multi-walled carbon nanotubes. Sensors and Actuators B: Chemical 124(2) (2007) 517-528.

[79] M. Zrínyi, Intelligent polymer gels controlled by magnetic fields. Colloid & Polymer Science 278(2) (2000) 98-103.

[80] M. Zrinyi, L. Barsi, A. Buki, Deformation of ferrogels induced by nonuniform magnetic fields. The Journal of Chemical Physics 104(21) (1996) 8750-8756.

[81] R.V. Ramanujan, L.L. Lao, The mechanical behavior of smart magnet-hydrogel composites. Smart Materials and Structures 15(4) (2006) 952-956.

[82] R. Fuhrer, E.K. Athanassiou, N.A. Luechinger, W.J. Stark, Crosslinking metal nanoparticles into the polymer backbone of hydrogels enables preparation of soft, magnetic field-driven actuators with muscle-like flexibility. Small 5(3) (2009) 383-388.

[83] N. Kato, Y. Takizawa, F. Takahashi, Magnetically driven chemomechanical device with poly(N-isopropylacrylamide) hydrogel containing gamma-Fe2O3. Journal of Intelligent Material Systems and Structures 8 (7) (1997) 588-595.

[84] S. Ghosh, C. Yang, T. Cai, Z. Hu, A. Neogi, Oscillating magnetic field-actuated microvalves for micro- and nanofluidics. J. Phys. D: Appl. Phys. 42(13) (2009) 135501.

[85] X. Zeng, H. Jiang, Tunable liquid microlens actuated by infrared light-responsive hydrogel. Appl. Phys. Lett. 93(15) (2008) 151101.

[86] B. Hildebrandt, P. Wust, O. Ahlers, A. Dieing, G. Sreenivasa, T. Kerner, R. Felix, H. Riess, The cellular and molecular basis of hyperthermia. Critical Reviews in Oncology/Hematology 43(1) (2002) 33-56.

[87] D.S. Coffey, R.H. Getzenberg, T.L. DeWeese, Hyperthermic biology and cancer therapies: A hypothesis for the "Lance Armstrong Effect". JAMA: The Journal of the American Medical Association 296(4) (2006) 445-448.

[88] M.R. Horsman, J. Overgaard, Hyperthermia: a potent enhancer of radiotherapy. Clinical Oncology 19(6) (2007) 418-426.

[89] D.E. Meyer, B.C. Shin, G.A. Kong, M.W. Dewhirst, A. Chilkoti, Drug targeting using thermally responsive polymers and local hyperthermia. J. Control. Rel. 74(1-3) (2001) 213-224.

[90] Tzu-Wei Wang, Hsi-Chin Wu, Wei-Ren Wang, Feng-Huei Lin, Pei-Jen Lou, Ming-Jium Shieh, Tai-Horng Young, The development of magnetic degradable DP-Bioglass for hyperthermia cancer therapy. Journal of Biomedical Materials Research Part A 83A(3) (2007) 828-837.

[91] I. Sondi, B. Salopek-Sondi, Silver nanoparticles as antimicrobial agent: a case study on E. coli as a model for Gram-negative bacteria. J. Colloid Interface Sci. 275(1) (2004) 177-182.

[92] V. Thomas, M.M. Yallapu, B. Sreedhar, S.K. Bajpai, A versatile strategy to fabricate hydrogel-silver nanocomposites and investigation of their antimicrobial activity. J. Colloid Interface Sci. 315(1) (2007) 389-395.

[93] P.S.K. Murthy, Y. Murali Mohan, K. Varaprasad, B. Sreedhar, K. Mohana Raju, First successful design of semi-IPN hydrogel-silver nanocomposites: A facile approach for antibacterial application. J. Colloid Interface Sci. 318(2) (2008) 217-224.

[94] Y. Murali Mohan, K. Lee, T. Premkumar, K.E. Geckeler, Hydrogel networks as nanoreactors: A novel approach to silver nanoparticles for antibacterial applications. Polymer 48(1) (2007) 158-164.

[95] Y. Murali Mohan, T. Premkumar, K. Lee, K.E. Geckeler, Fabrication of silver nanoparticles in hydrogel networks. Macromol. Rapid Commun. 27(16) (2006) 1346-1354.

CHAPTER 3

MAGNETIC HYDROGEL NANOCOMPOSITES: SYNTHESIS AND REMOTE HEATING

This chapter is based on work published as:

N.S. Satarkar, J.Z. Hilt, Hydrogel nanocomposites as remote-controlled biomaterials, Acta Biomater 4 1(2008) 11-16.

3.1 Summary

Nanocomposite hydrogels are a new class of intelligent materials, which have recently attracted interest as biomaterials. In this chapter, magnetic nanocomposites of temperature sensitive hydrogels have been developed and demonstrated to be responsive to alternating magnetic field (AMF). Nanocomposites were synthesized by incorporation of superparamagnetic Fe_3O_4 nanoparticles in negative temperature sensitive poly (N-isopropylacrylamide) hydrogels. The systems were characterized for temperature responsive swelling, remote heating on application of AMF, and also for remote controlled (RC) drug delivery applications. The rise in temperature with application of an AMF depends on Fe_3O_4 particle loading of the system. Preliminary studies on RC drug release showed reduced release in the presence of an AMF.

3.2 Introduction

Hydrogels are crosslinked hydrophilic polymers that can absorb water or biological fluids and swell several times of their dry volume. Due to high composition of water and elastic structure, hydrogels are considered as excellent biocompatible materials.[1] There are numerous applications of hydrogels in the medical and pharmaceutical sectors such as contact lenses, membranes for biosensors, sutures, drug delivery devices, matrices for repair and regeneration of tissues and organs.[2-4]

Hydrogels can show swelling behavior depending on changes in the external environment. Some of the factors that can affect the swelling of responsive hydrogels include pH, ionic strength, and temperature.[5] Hydrogels can also be made to respond to diverse external stimuli such as light, electric current, ultrasound, magnetic field, and presence of a particular molecule. The unique property of responsiveness has resulted in their applications in sensors,[6, 7] self regulated and externally actuated intelligent drug delivery systems,[8-11] and microfluidic devices.[12, 13]

Hydrogel nanocomposites have recently attracted considerable attention due to their accelerated response and capability of action at a distance. The properties of the nanocomposites can be easily tailored by manipulating properties of hydrogel and the composite material. Hydrogel nanocomposites with magnetic nanoparticles have been demonstrated as potential candidates for pulsatile drug delivery and soft actuator applications. Zrinyi and co-workers have reported that magnetic composites of poly (vinyl alcohol) undergo quick, controllable changes in response to applied magnetic field and thus can be used in soft actuator type of applications.[14, 15] Further studies on magnetic composites of N-isopropylacrylamide (NIPAAm) showed that magnetic

nanoparticles do not affect the temperature sensitivity of the hydrogel network including the lower critical transition temperature (LCST).[16]

One of the first approaches to achieve an externally controlled drug delivery system using biomaterials was by Langer and co-workers.[17-20] They embedded macroscale magnetic beads (~1 mm diameter) in ethylene vinyl acetate along with various macromolecular drugs like insulin. Both in vivo and in vitro studies showed that application of an oscillating magnetic field lead to increased release rates. The release rates could be modulated by altering the geometry of the implant; the position, orientation, and magnetic strength of the embedded materials, as well as changing the amplitude and frequency of the magnetic field. Recently, Liu et al. demonstrated gelatin and poly (vinyl alcohol) hydrogels with Fe_3O_4 nanoparticles as "on" and "off" drug delivery devices.[21, 22] When direct current (D.C.) magnetic field was applied, there was reduced release and when the field was switched off, the drug was released rapidly. The release rate depends on magnetic field amplitude, particle size, and switching duration time.

For our current studies with magnetic nanocomposites, NIPAAm was used due to its temperature responsiveness while superparamagnetic iron oxide (Fe_3O_4) nanoparticles (20-30 nm diameter) were used as they have been widely considered for remote heating in case of hyperthermia.[23-25] The application of an alternating magnetic field (AMF) to the nanocomposite will lead to heat generation which can drive the swelling transition of the hydrogel. This is the first demonstration utilizing an AMF for the remote control of drug release from nanocomposite hydrogels, and we expect these systems to find application in implantable biomedical devices. Although this chapter only demonstrates

remote control for short release durations, the release profiles can be easily modulated by altering the nanocomposite hydrogel composition (e.g., physical size, crosslinking percentage, molecular weight between crosslinks, etc.). Currently, additional studies are under way to look into systems that can demonstrate control over extended periods of time. In addition, on/off control of the release is possible through tailoring the nanocomposite hydrogel composition, and this is currently being studied. **Figure 3.1** includes a schematic of the nanocomposite systems for remote controlled (RC) drug delivery in case of negative and positive temperature sensitive systems.

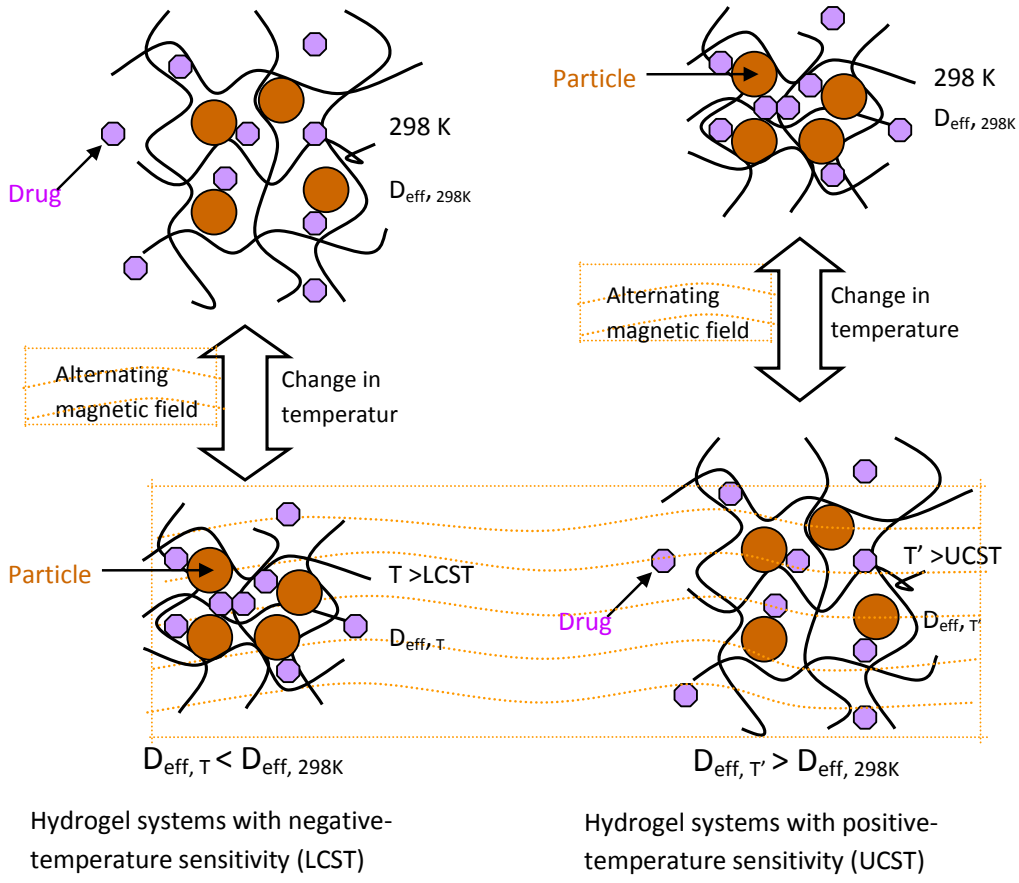

Figure 3.1. Schematic of proposed RC drug delivery system for negative and positive temperature sensitive systems.

The synthesis and swelling behavior of NIPAAm based magnetic nanocomposites has been described earlier with special emphasis on effect of type of crosslinker.[26] In this work, we report the characterization of the magnetic nanocomposites; which includes the effect of degree of crosslinking on swelling behavior, their remote heating response on application of AMF, and preliminary results of RC drug delivery.

3.3 Materials and methods

3.3.1 Hydrogel synthesis

Hydrogel nanocomposites were synthesized by UV photopolymerization with various crosslinking densities and magnetic nanoparticle loadings. The hydrogel systems were based on N-isopropylacrylamide (Sigma-Aldrich) as monomer with poly (ethylene glycol) 400 dimethacrylate (Polysciences, Inc) as crosslinker. 2,2-dimethoxy-2-phenylacetophenone (Sigma-Aldrich) was used as the photosensitive initiator for UV photopolymerization. Iron oxide nanoparticles (Fe_3O_4 Nanostructured and Amorphous Materials Inc.) used for magnetic nanocomposite synthesis were spherical with mean size of 20 to 30 nm.

N-isopropylacrylamide (NIPAAm) and poly (ethylene glycol) 400 dimethacrylate (PEG400DMA) mixtures were prepared in molar compositions of 90:10, 80:20, and 70:30 and dissolved in equal weight of ethanol as the solvent. The nanocomposites were synthesized for 90:10 molar ratio with the Fe_3O_4 nanoparticles added to the monomer mixtures prior to polymerization. The nanoparticle loadings were varied as 0, 1, 2.5, and 5 % of combined weight of monomer and crosslinker. The uniform dispersion of nanoparticles was ensured in monomer mixtures by probe sonication (Fisher Scientific

Sonic Dismembrator Model 500) for 10 minutes followed by ultrasonic bath for 10 minutes. Initiator was added 1% by weight of monomer and crosslinker together and manual shaking was continued until complete dissolution. The mixtures were then pipetted into two 15 x 15 cm^2 clamped glass plates separated by a 500 μm Teflon spacer. The glass plate assembly was then transferred to UV source (LESCO) preset at 365 nm wavelength and adjusted to give the intensity of 17.5 mW/cm^2. Photopolymerization was carried out for 5 minutes and the gel was carefully removed and placed in deionized water. For hydrogel nanocomposites, uniform UV light exposure of both sides of gel was ensured during polymerization. The hydrogel films were washed daily by changing deionized water. UV analysis of the wash water samples was performed with deionized water as baseline. Washing was continued until no significant peaks were observed (Cary 50 UV Spectrophotometer). The gels were then taken out of water, cut into discs of diameter 15 mm and dried in air. The discs were stored in vacuum oven for at least 24 hours to ensure complete drying.

3.3.2 Characterization of swelling behavior

The swelling studies were carried out for pure hydrogel discs and 5 wt% particle loaded 90:10 molar discs at 15 to 45°C, and volume swelling ratio Q was calculated by methods described in appendix D.1.[26]

3.3.3 Remote heating on application of AMF

The heating response of the nanocomposites to electromagnetic field was characterized using a Taylor Winfield induction power supply model MMF-3-135/400-2 (solenoid of 15 mm diameter and 5 turns). Dry hydrogel discs with NIPAAm: PEG400DMA of molar

compositions of 90:10 and various particle loadings were placed in a petri dish on top of the solenoid and subjected to AMF of amplitude 33.5 kA/m (calculations described in appendix D.2) and frequency 297 kHz. An IR camera (AGEMA Thermovision 470) was used to acquire thermal images and record the resulting increase in surface temperature. The heating was continued for 5 minutes and the results were averaged over three samples.

3.3.4 Demonstration of RC drug delivery

Pyrocatechol violet dye was used as a model drug for the release studies. The hydrogel discs with 0 and 5 wt% nanoparticles and molar composition of NIPAAm: PEG400DMA as 90:10 were loaded with the dye by imbibition in a 1 mg/ml dye solution at room temperature (22°C) for 48 h. To observe the effect of an AMF on dye release, release study was carried out with one set of discs placed in AMF at center of solenoid (59.5 kA/m, 297 kHz), while another set outside the field. The set inside the field was subjected to 10 min ON and 5 min OFF cycle. Infinite dilution method was used for release studies for first 1 hour by changing supernatant solution every 15 minutes. Final supernatant was collected at 24 hours and cumulative release was quantified as M_{inf}. The supernatant was quantified by UV spectrophotometer for peak at 443 nm.

3.4 Results and discussion

3.4.1 Characterization of swelling behavior

The swelling behavior of the gels was analyzed at different temperatures to characterize the effect of crosslinking density and particle loading on the swelling transition temperature. The swelling studies on NIPAAm based system with varying crosslinker

density of PEG400DMA at temperatures of 15 to 45°C show that, for a given system, equilibrium volume swelling ratio (Q) decreases with increase in temperature (**figure 3.2**). This trend is expected since NIPAAm is negative temperature-sensitive hydrogel with LCST of about 34°C for pure NIPAAm.[27] As temperature increases, the hydrogen bonds of the network break, resulting in decrease in hydrophilicity. This forces water out of the hydrogel network and results in decreased swelling. Thus, at 15°C, the gel is in swollen state and hence equilibrium volume swelling ratio observed is greater than that at 45°C, where it is in the collapsed state.

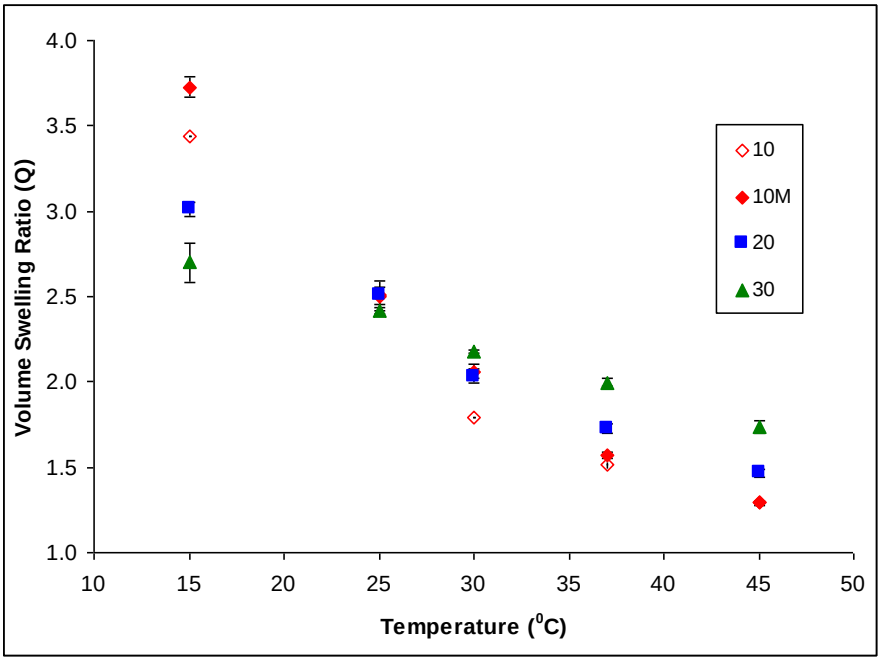

Figure 3.2. Effect of temperature on equilibrium swelling of hydrogels. 10, 20, and 30 represents molar % PEG400DMA in NIPAAm-PEG400DMA system. M represents magnetic nanocomposite. (N=3, ±SD)

As seen in prior research, we observe here that the swelling transition is broadened due to effect of PEG400DMA crosslinking.[26] At temperatures below the critical transition

range, higher degree of crosslinking (less NIPAAm content) leads to smaller Q values (less equilibrium swelling) due to smaller mesh size. There is a larger reduction in equilibrium swelling with increase in temperature for systems with a lower degree of crosslinking (higher NIPAAm content). As a result, Q values above the critical transition temperature range are higher for systems with a higher degree of crosslinking. The comparison between swelling ratios of gels with and without nanoparticles shows that 5 wt% magnetic nanoparticles do not have significant effect on swelling behavior. Similar observations were reported in prior research incorporating lower amounts of particle loadings in NIPAAm systems.[26]

3.4.2 Remote heating on application of AMF

Dry NIPAAm: PEG400DMA hydrogel nanocomposite discs with 5 wt% Fe_3O_4 nanoparticles were subjected to AMF of amplitude 33.5 kA/m and frequency 297 kHz. IR camera images (**figure 3.3(a, b)**) show that the surface temperature at the centre of disc rises from an initial temperature of 22°C to about 55°C within the first minute. When AMF is applied, superparamagnetic Fe_3O_4 particles heat due to Neel and Brownian relaxations (discussed in appendix D.3) and high temperatures are generated at the nanoscale.[28] This leads to increase in temperature of the hydrogel matrix. The field intensity of the solenoid varies with maximum amplitude at the centre leading to a temperature distribution in the heated disc.

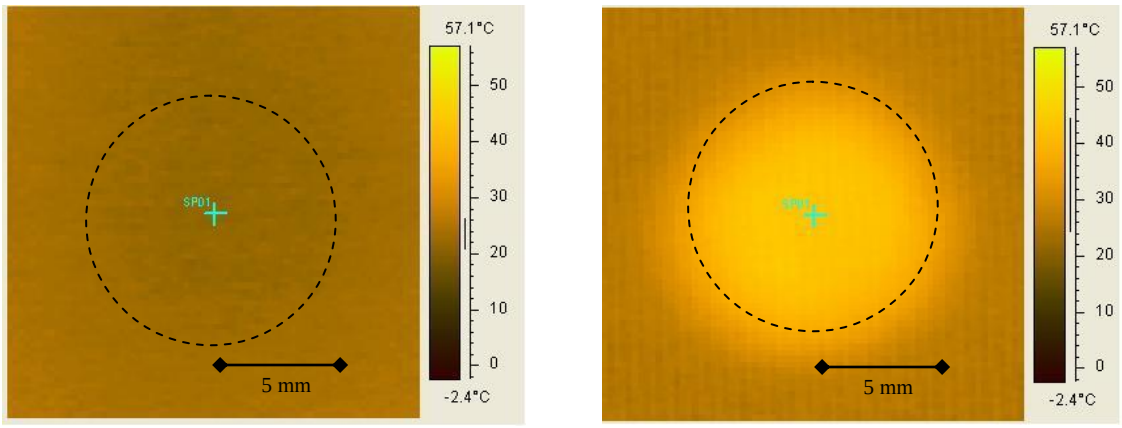

(a) (b)

Figure 3.3. Heating effect of nanocomposites in electromagnetic field. (a) IR image of 5 wt% particle disc at 0 sec (b) IR image of 5 wt% particle disc at 60 sec (Dotted circle shows the disc area).

Figure 3.4 shows the results of detailed magnetic field effect on dry hydrogel nanocomposite discs of NIPAAm: PEG400DMA systems with varying particle loadings. Hydrogel nanocomposites with no nanoparticles showed minimal resistive heating, while increase in particle loading increased the maximum temperature achieved in field. Higher temperatures are expected with increase in particle loading since heat generation is proportional to amount of nanoparticles present. It should be noted that the disc was open to air, and hence temperature rise also depends on heat transfer to the air by convection. Initial temperature rise is fast, which is followed by a slow continuous increase in temperature.

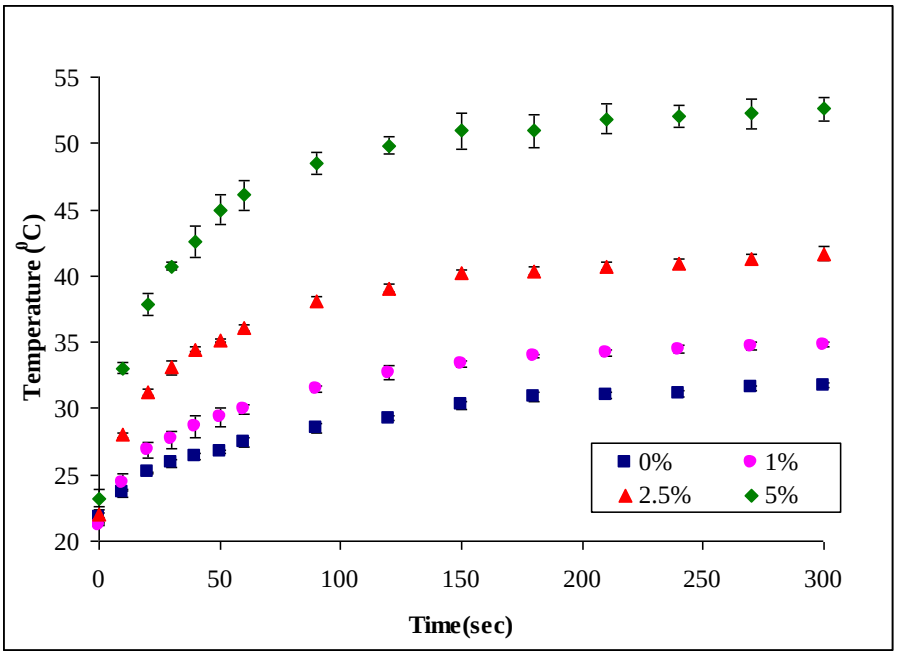

Figure 3.4. Temperature increase of nanocomposites with varying particle loadings subjected to electromagnetic field. % represents particle loading by weight in NIPAAm-PEG400DMA nanocomposite. (N=3, ±SD)

3.4.3 Demonstration of RC drug delivery

Release studies were conducted for the system with molar composition of NIPAAm: PEG400DMA as 90:10 (0 wt% and 5 wt% magnetic nanoparticles) using Pyrocatechol Violet dye as model drug. One set of discs was placed in AMF of amplitude 59.5 kA/m and frequency 297 kHz, while another set outside the field. The cumulative drug release was plotted versus time showing that most of the drug was released in 1 hour (**figure 3.5**). Faster release rate is expected when swollen (the mesh size of the systems is large) resulting in faster diffusion. Results of the set placed outside the field show that magnetic nanoparticles only slightly reduce drug release rate.

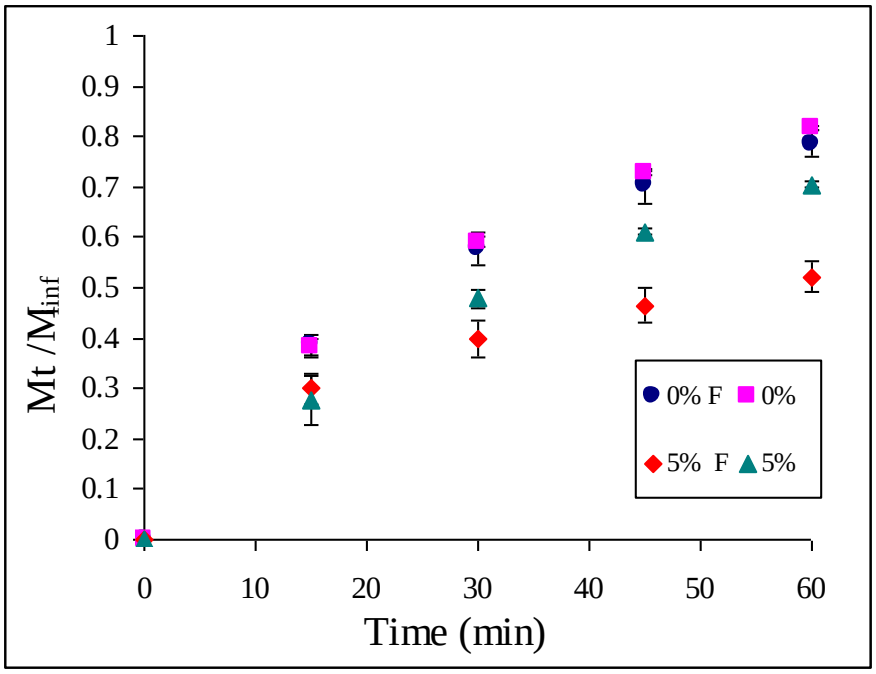

Figure 3.5. Controlled drug release from nanocomposites in electromagnetic field. % represents particle loading by weight in NIPAAm-PEG400DMA nanocomposite. F represents application of magnetic field. (N=3, ±SD)

On application of AMF, the hydrogel nanocomposite gives about 25% reduction in dye release in 1 hour. On the other hand, the hydrogel with no nanoparticles is unaffected by field. We speculate that this suppression in release is a result of the collapse of the hydrogel network with heating. As observed in dry heating (**figure 3.4**), application of AMF leads to high temperatures. If the temperatures generated are above LCST, they can cause negative temperature sensitive network of NIPAAm to collapse, shrinking the mesh size. Even when field is not applied, there is a slight decrease in release from the nanocomposite hydrogel systems as compared to that of hydrogel systems with no nanoparticles. This effect potentially can be attributed to affinity between nanoparticles and drug, and it is currently being further studied.

The analysis of diffusion aspects of dye release was done by early time release data using methods described in appendix D.4.[29] The calculated power law exponent and effective diffusivity values are presented in **table 3.1**. The effective diffusivity in case of the 5 wt% nanocomposite with field ON is less by a factor of 5 than the other cases. This supports that the hydrogel network is collapsed as temperature increases above LCST. Thus, drug release can be remotely controlled by application of AMF. Extensive analysis as per heating time and ON-OFF durations is in progress to gain further insight into the effects of an AMF and the effects of the resultant heating on drug release rate. Some of the factors that can be used to modulate the release rate are hydrogel composition, nanoparticles loading, field exposure time, and field amplitude.

Table 3.1. Pyrocatechol violet diffusion coefficients and power law exponents with varying particle loadings and electromagnetic field.

Sample	Particles	Field	Pyrocatechol Violet diffusion coefficient (x10^8 cm^2/s)	Power law exponent, n
0%	0%	OFF	3.064	0.59
0%F	0%	ON	2.616	0.55
5%	5%	OFF	2.870	0.73
5%F	5%	ON	0.672	0.40

3.5 Conclusions

In conclusion, magnetic nanocomposites of NIPAAm show negative temperature sensitivity. The temperature sensitivity and swelling transition temperature can be controlled by composition of NIPAAm in the hydrogel system. When exposed to external AMF, heating of superparamagnetic Fe_3O_4 nanoparticles lead to rise in temperature of the nanocomposite system. The rise in temperature can be controlled by particle loadings of the system. RC drug release was demonstrated from magnetic nanocomposites using an AMF. The suppression in release is speculated to be a result of the collapse of the hydrogel network with heating. This class of biomaterials holds promise in RC drug delivery systems for pulsatile release of drug molecules on demand. In the following chapter, analysis to further understand the factors that control drug delivery rate is presented.

3.6 References

[1] N.A. Peppas, P. Bures, W. Leobandung, H. Ichikawa, Hydrogels in pharmaceutical formulations. European Journal of Pharmceutics and Biopharmaceutics 50 (2000) 27-46.

[2] A.S. Hoffman, Hydrogels in biomedical applications. Adv. Drug Deliver. Rev. 43 (2002) 3-12.

[3] A.M. Lowman, N.A. Peppas, Hydrogels. in: E. Mathiowitz (Ed.), Encyclopedia of Controlled Drug Delivery, Vol. 1, Wiley, New York, 1999, pp. 397-418.

[4] N.A. Peppas, J.Z. Hilt, A. Khademhosseini, R. Langer, Hydrogels in biology and medicine: from molecular principles to bionanotechnology. Adv. Mater. 18 (2006) 1345-1360.

[5] N.A. Peppas, in: B. D. Ratner, A. S. Hoffman, F. J. Schoen and J. E. Lemons (Eds.), Biomaterials science, Second Ed.: An introduction to materials in medicine, Academic Press, New York 2004, pp. 100-107.

[6] R. Bashir, J.Z. Hilt, O. Elibol, A. Gupta, N.A. Peppas, Micromechanical cantilever as an ultrasensitive pH microsensor. Appl. Phys. Lett. 81(16) (2002) 3091-3093.

[7] J.Z. Hilt, A.K. Gupta, R. Bashir, N.A. Peppas, Ultrasensitive biomems sensors based on microcantilevers patterned with environmentally responsive hydrogels. Biomedical Microdevices 5(3) (2003) 177-184.

[8] S.R. Sershen, J.L. West, Implantable, polymeric systems for modulated drug delivery. Adv. Drug Deliver. Rev. 54 (2002) 1225-1235.

[9] R. Yoshida, K. Sakai, T. Okano, Y. Sakurai, Pulsatile drug delivery systems using hydrogels. Adv. Drug Deliver. Rev. 11(1-2) (1993) 85-108.

[10] S.R. Sershen, S.L. Westcott, N.J. Halas, J.L. West, Temperature-sensitive polymer-nanoshell composites for photothermally modulated drug delivery. J. Biomed. Mater. Res. 51(3) (2000) 293-298.

[11] T. Miyata, N. Asami, T. Uragami, A reversibly antigen-responsive hydrogel. Nature 399(6738) (1999) 766-769.

[12] S.R. Sershen, G.A. Mensing, M. Ng, N.J. Halas, D.J. Beebe, J.L. West, Independent optical control of microfluidic valves formed from optomechanically responsive nanocomposite hydrogels. Adv. Mater. 17(11) (2005) 1366-1368.

[13] D.J. Beebe, J.S. Moore, J.M. Bauer, Q. Yu, R.H. Liu, C. Devadoss, B.-H. Jo, Functional hydrogel structures for autonomous flow control inside microfluidic channels. Nature 404(6778) (2000) 588-590.

[14] M. Zrinyi, D. Szabo, H.-G. Kilian, Kinetics of the shape change of magnetic field sensitive polymer gels. Polymer Gels and Networks 6 (1998) 441-454.

[15] M. Zrínyi, Intelligent polymer gels controlled by magnetic fields. Colloid & Polymer Science 278(2) (2000) 98-103.

[16] P.M. Xulu, G. Filipcsei, M. Zrinyi, Preparation and response properties of magnetically soft poly(N-isopropylacrylamide) gels. Macromolecules 33 (2000) 1716-1719.

[17] D.S. Hsieh, L. R, F. J, Magnetic modulation of release of macromolecules from polymers. Proc. Natl. Acad. Sci. U. S. A. 78(3) (1981) 1863-1867.

[18] E.R. Edelman, J. Kost, H. Bobeck, R. Langer, Regulation of drug release from polymer matrices by oscillating magnetic fields. J. Biomed. Mater. Res. 19(1) (1985) 67-83.

[19] J. Kost, R. Noecker, E. Kunica, R. Langer, Magnetically controlled release systems: effect of polymer composition. J. Biomed. Mater. Res. 19 (1985) 935-940.

[20] J. Kost, J. Wolfrum, R. Langer, Magnetically enhanced insulin release in diabetic rats. J. Biomed. Mater. Res. 21 (1987) 1367-1373.

[21] T.Y. Liu, S.H. Hu, D.M. Liu, S.Y. Chen, Magnetic-sensitive behavior of intelligent ferrogels for controlled release of drug. Langmuir 22(14) (2006) 5974-5978.

[22] T.-Y. Liu, S.-H. Hu, K.-H. Liu, D.-M. Liu, S.-Y. Chen, Preparation and characterization of smart magnetic hydrogels and its use for drug release. J. Magn. Magn. Mater. 304 (2006) e397-e399.

[23] L.L. Lao, R.V. Ramanujan, Magnetic and hydrogel composite materials for hyperthermia applications. J. Mater. Sci.: Mater. Med. 15 (2004) 1061-1064.

[24] M. Babincová, D. Leszczynska, P. Sourivong, P. Cicmanec, P. Babinec, Superparamagnetic gel as a novel material for electromagnetically induced hyperthermia. J. Magn. Magn. Mater. 225(1-2) (2001) 109-112.

[25] R. Hergt, W. Andra, C.G. d'Ambly, I. Hilger, W.A. Kaiser, U. Richter, H.G. Schmidt, Physical limits of hyperthermia using magnetite fine particles. Magnetics, IEEE Transactions on 34(5) (1998) 3745-3754.

[26] R.A. Frimpong, S. Fraser, J.Z. Hilt, Synthesis and temperature response analysis of magnetic-hydrogel nanocomposites. J. Biomed. Mater. Res. A 80A(1) (2007) 1-6.

[27] S. Hirotsu, Y. Hirokawa, T. Tanaka, Volume-phase transitions of ionized N-isopropylacrylamide gels. The Journal of Chemical Physics 87(2) (1987) 1392-1395.

[28] X. Wang, H. Gu, Z. Yang, The heating effect of magnetic fluids in an alternating magnetic field. J. Magn. Magn. Mater. 293 (2005) 334-340.

[29] J.Z. Hilt, M.E. Byrne, N.A. Peppas, Microfabrication of intelligent biomimetic networks for recognition of d-glucose. Chem. Mater. 18(25) (2006) 5869-5875.

CHAPTER 4

MAGNETIC HYDROGEL NANOCOMPOSITES FOR REMOTE CONTROLLED PULSATILE DRUG RELEASE

This chapter is based on work published as:

N.S. Satarkar, J.Z. Hilt, Magnetic hydrogel nanocomposites for remote controlled pulsatile drug release, J Control Rel 130 3(2008) 246-251.

4.1 Summary

Hydrogel nanocomposites are novel macromolecular biomaterials that promise to impact various applications in medical and pharmaceutical fields. In this chapter, magnetic nanocomposites of temperature responsive hydrogels were used to illustrate remote controlled (RC) drug delivery. Alternating magnetic field (AMF) was used to trigger the on demand pulsatile drug release from the nanocomposites. Nanocomposites were synthesized by incorporation of superparamagnetic Fe_3O_4 particles in negative temperature sensitive poly (N-isopropylacrylamide) hydrogels. Pulses of AMF were applied to the nanocomposites and the kinetics of collapse and recovery were characterized. The application of an AMF resulted in uniform heating within the nanocomposites leading to accelerated collapse and squeezing out large amounts of imbibed drug (release at a faster rate). Remote controlled pulsatile drug release was characterized for different drugs as well as for different ON-OFF durations of the AMF.

4.2 Introduction

For many controlled drug delivery applications, zero order release of therapeutics over prolonged period of time is the goal. On the other hand, pulsatile release systems are attractive for release of therapeutics that need varying plasma concentrations with time. Pulsatile release can match the body's release of specific peptides or hormones leading to optimum drug delivery.[1, 2] Pulsatile drug delivery systems can be pre-programmed,[3, 4] self-regulated depending on presence of specific molecule, or can be externally actuated by applying various stimuli from outside the body.[5-7] In this chapter, externally actuated drug release was achieved from magnetic hydrogel nanocomposites by application of alternating magnetic field (AMF).

Hydrogels can be defined as crosslinked polymer networks which may absorb large amounts of water or biological fluids. Hydrogels are currently being considered for various biological applications such as components of drug delivery devices, microfluidic devices, biosensors, tissue implants, and contact lenses.[8-10] Responsive hydrogels are a class of hydrogels that can respond to specific changes in their external environment. For many years, researchers have developed and characterized responsive hydrogels showing swelling behavior dependent on pH, ionic strength, temperature, or presence of a specific molecule.[11-13] Unique properties can be achieved by incorporation of various nano- and micro-scale materials such as metal particles or biological molecules into the hydrogel matrix.[14-16] In particular, nanocomposites of responsive hydrogels can exhibit unique dual-responsive properties with capability of actuation at a distance. Recent studies have shown that the nanocomposites of temperature responsive hydrogels

can be actuated by external stimuli like light or magnetic field and thus can be used as externally actuated drug delivery systems,[6, 17, 18] and in microfluidic devices.[19]

In particular, the concept of using external magnetic fields to achieve pulsatile release from polymer composites was first pursued by Langer and others. They demonstrated an externally controlled on-demand insulin release from magnetic composite of ethylene vinyl acetate by application of low frequency oscillating magnetic field.[20] Recently, Paoli et al. demonstrated enhancement in dextran release by application of low frequency oscillating magnetic field to magnetic nanocomposites of collagen.[21] The low frequency oscillating magnetic field application relies on interactions between magnetic particles and resultant mechanical deformation of the gel to squeeze out the drug.[22] Use of AMF to actuate magnetic particles is also rapidly emerging as an important research area in externally controlled drug delivery systems.[23, 24] However, there has been very limited research on using AMF to control release from temperature responsive polymer nanocomposites. It was only very recently that pulsatile release from magnetic nanocomposites of gelatin hydrogels was obtained by application of alternating magnetic field (50-100 kHz),[17] but the detailed analysis of effect on AMF on composites of temperature responsive hydrogels and applications to externally actuated drug delivery still remain unexplored.

In this work with hydrogel nanocomposites, superparamagnetic (20-30 nm diameter) iron oxide (Fe_3O_4) nanoparticles were incorporated into N-isopropylacrylamide (NIPAAm)-based matrix. Fe_3O_4 nanoparticles are currently being considered in various medical applications such as magnetic resonance imaging contrast agents, targeted drug delivery, and hyperthermia treatment of cancer.[25] Application of alternating magnetic field

(AMF) to Fe_3O_4 nanoparticles generates heat due to Neel and Brownian relaxations.[26] The main advantage of using AMF of around 300 kHz is it can penetrate deep in the body with minimal energy absorption by tissue.[27] N-isopropylacrylamide (NIPAAm) is a negative temperature responsive hydrogel with lower critical transition temperature (LCST) between 30 and 35^{o}C.[28] Initial work of using NIPAAm based hydrogels for temperature triggered drug release was done by Hoffman and others.[29, 30] When AMF is applied to magnetic nanocomposites of NIPAAm, heat generation by the nanoparticles will lead to rise in temperature of the polymer matrix. If resulting temperatures are above LCST, the gel will collapse leading to expulsion of water. Thus, AMF can be used to drive the swelling transition of the gel at a distance. **Figure 4.1** shows the schematic of actuation at a distance and resultant squeezing effect for the negative temperature responsive NIPAAm system. This unique phenomenon can be used to externally actuate biomedical implants like drug delivery systems as well as microfluidic devices.

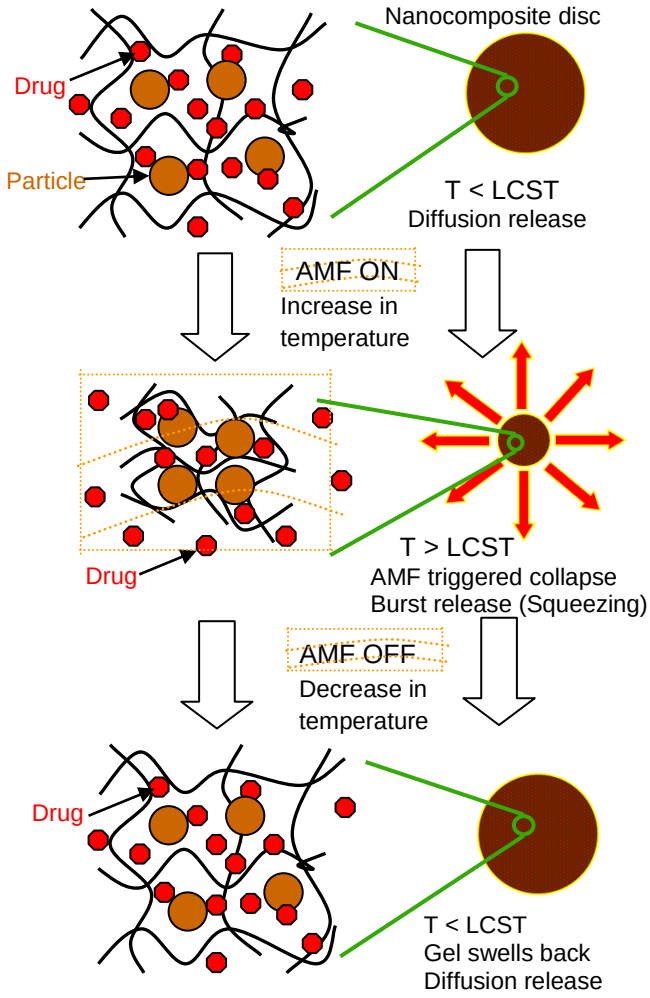

Figure 4.1. Schematic showing the effect of ON-OFF cycles of AMF to the magnetic nanocomposites of NIPAAm. It shows the AMF triggered collapse and resultant burst release due to squeezing effect.

In previous publications, it was demonstrated that composition of NIPAAm gels can be tailored to get temperature response,[31] while the loadings of Fe_3O_4 nanoparticles in the gel can be manipulated to get the desired remote heating on application of AMF.[32] In addition, chapter 3 presented a system that showed reduced release with application of AMF.[32] Here, pulsatile release from nanocomposites, the investigation of mechanism behind release, and evaluation of various factors that can control release profile is

presented. Specifically, nanocomposites were characterized for the kinetics of AMF triggered collapse along with reproducibility of gel collapse and recovery. The effects of collapse of the nanocomposite on application of AMF to the collapse achieved by raising the temperature of surrounding solution above LCST were compared. Vitamin B_{12} and methylene blue were used as model drugs for analysis of remote controlled drug release. AMF was applied in form of short pulses and control on drug release over extended periods of time was analyzed. In addition, the effect of variation of pulse durations on drug release profile was characterized.

4.3 Materials and methods

N-Isopropylacrylamide (NIPAAm), ammonium persulfate (APS), N,N,N`,N`-tetramethylethylenediamine (TEMED), methylene blue, and vitamin B_{12} were purchased from Sigma-Aldrich. Tetra (ethylene glycol) dimethacrylate (TEGDMA) was purchased from Polysciences, Inc. Dispersible iron oxide nanoparticles (Fe_3O_4 with ~0.2% PVP coated) were obtained from Nanostructured and Amorphous Materials Inc. The spherical particles have mean size of 25 nm. Scanning electron microscope (SEM) Hitachi S 4300 was used to collect the SEM pictures. Taylor Winfield induction power supply model MMF-3-135/400-2 (solenoid of 15 mm diameter and 5 turns) was used to generate AMF of frequency 297 kHz. AGEMA Thermovision 470 IR camera was used for thermal imaging. All reagents were used as received.

4.3.1 Hydrogel synthesis

Hydrogel nanocomposites were synthesized with NIPAAm as monomer and TEGDMA as crosslinker by redox polymerization. NIPAAm and TEGDMA mixtures were prepared

in molar ratio of 95:5 and dissolved in equal weight of ethanol. For nanocomposite systems, Fe_3O_4 nanoparticles were added at 5% of combined weight of NIPAAm and TEGDMA, and the nanoparticles were dispersed uniformly by bath sonication for 10 minutes. Oxygen present in monomer solution was removed by passing nitrogen for 5 minutes. Redox initiator APS (1.5% of combined weight of NIPAAm and TEGDMA) was dissolved in 200 μl deionized water and added to the monomer solution. Accelerator TEMED (2.25% of combined weight of NIPAAm and TEGDMA) was then added and mixed to initiate the redox reaction. The solution was then poured into a mold of two 15 x 15 cm^2 clamped glass plates separated by a 1500 μm Teflon spacer. The reaction was continued for 24 h at 25^oC, and then the hydrogel film was removed from the mold and placed in deionized water. The control set was made with no particles using identical polymerization procedures. Hydrogel films were washed daily by changing water until no significant UV absorbance peaks were observed (Cary 50 UV Spectrophotometer). The gels were then cut into discs of diameter 15 mm and dried in air followed by vacuum oven for 24 hours.

4.3.2 Response to AMF

Dry hydrogel discs with 0 and 5% particle loadings were placed in a petri dish on top of the solenoid and subjected to an alternating magnetic field of amplitude 33.5 kA/m and frequency 297 kHz. The rise in surface temperature of nanocomposites was recorded by IR camera. The field heating was continued for 5 minutes and the results were averaged over three samples

4.3.3 AMF triggered deswelling

Hydrogel nanocomposite and control hydrogels were cut into discs of diameter 15 mm and allowed to come to equilibrium in phosphate buffered solution (PBS) at 25 ^{o}C. The discs were placed in centrifuge tube with 10 ml PBS solution and subjected to AMF (amplitude 59.5 kA/m and frequency 297 kHz). The field was kept continuously ON for 50 minutes. The weight of the disc was measured at regular time intervals and PBS solution was replaced by fresh solution at 25^{o}C. In order to compare kinetics of surface collapse with that of collapse due to uniform internal heating, a set of hydrogels swollen at 25^{o}C was immersed in a water bath at 45^{o}C. The discs were removed periodically, and their weight was measured at regular time intervals.

4.3.4 Reproducibility analysis of AMF triggered collapse

Nanocomposite discs were swollen in PBS solution at 25^{o}C. AMF was applied as a pulse (amplitude 59.5 kA/m and frequency 297 kHz) for 5 minutes every 2 hours. The solution temperature was maintained at 25^{o}C except when AMF was applied. The disc weight was measured before and after AMF was applied.

4.3.5 Drug release studies

Vitamin B_{12} (MW 1355) and methylene blue (MW 320) were used as model drugs for controlled drug release demonstration. These two compounds were chosen as model drugs due to high aqueous solubilities and different molecular weights. Aqueous solutions of vitamin B_{12} (12.5 mg/ml solution prepared in PBS) and methylene blue (5 mg/ml solution prepared in PBS) were used to imbibe the dry hydrogel discs for 48 hours at 25°C. The discs were removed from loading solution and then rinsed in PBS for 5

minutes. Subsequently, the release behavior of loaded discs was studied in centrifuge tubes containing PBS solution. The AMF used for these studies had amplitude 59.5 kA/m and frequency 297 kHz. The final supernatant was collected at 48 hours and cumulative release was quantified as mass released at time t, M_t, over the total mass released, M_{inf}. Vitamin B_{12} and methylene blue release was quantified by UV-Vis spectrophotometer at 360.9 nm and 291.5 nm, respectively. All studies were done in triplicates. The details of methods for accelerated and pulsatile release are described below.

4.3.5.1 Demonstration of accelerated drug release

One set of discs was immersed in a water bath at 25°C with no exposure to the AMF. The supernatant was changed quickly at every time point. The centrifuge tubes containing the second set of discs were placed in the center of solenoid and subjected continuously to AMF. Identical analysis was done for control as well as nanocomposite hydrogels for 45 minutes.

4.3.5.2 Demonstration of pulsatile drug release

Vitamin B_{12} loaded discs were allowed to release in PBS solution at 25°C for 14 hours. A pulse of AMF was applied to one set for a few minutes every few hours and solution was collected before and after application of AMF. Another set of loaded discs had no application of AMF. This analysis was done for control hydrogels as well as nanocomposites. Additionally, the effect of surface collapse of hydrogel disc as opposed to AMF collapse was studied by a release study at 45°C.

Methylene blue release studies were carried out only for the nanocomposites. The loaded discs were allowed to release in PBS solution at 25°C for 7 hours. The goal here was to

observe effect of variation of AMF cycles on release profile. One set had no application of AMF, AMF was applied to the second set for a few minutes every few hours, while the third set was subjected to AMF for 10 min ON and 20 min OFF cycles.

4.4 Results and discussion

4.4.1 Characterization of hydrogel nanocomposite

Figure 4.2 is an SEM image of the cross-section of the nanocomposite. As shown, the magnetic nanoparticles were embedded in hydrogel matrix and showed relatively uniform dispersion. This good dispersion leads to a uniform heating response of the nanocomposite on application of AMF and will be further discussed in the following sections.

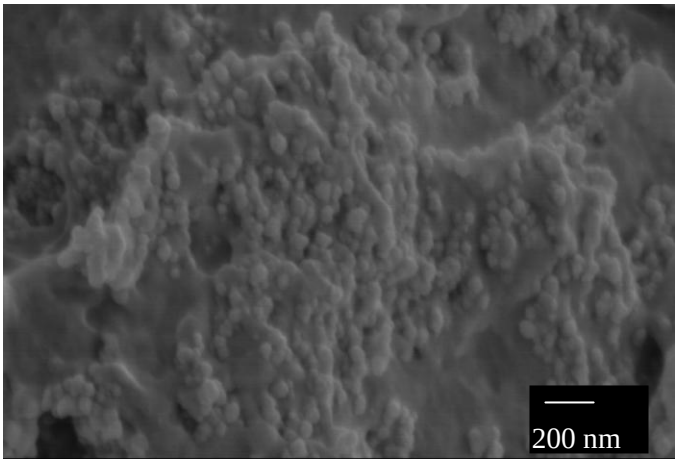

Figure 4.2. Cross-sectional SEM showing magnetic nanoparticles dispersed in NIPAAm-TEGDMA matrix.

4.4.2 Response to AMF

Surface temperatures of dry NIPAAm: TEGDMA hydrogel discs are plotted in **figure 4.3**. In the case of nanocomposites, application of AMF selectively heated magnetic

particles, led to a rise in temperature of the hydrogel discs. The control hydrogels showed minimal resistive heating. Increasing particle loading led to increased heating of the discs and a higher surface temperature, as discussed in earlier studies.[32] The temperature of 1500 μm thick discs used here increased to 69°C in 5 minutes, as opposed to 55°C in case of 500 μm thick discs used in earlier work. The transport of heat from the nanocomposite surface to its surroundings was primarily due to convection between the surface and the surrounding air. Increasing the thickness of the samples led to a decrease in the surface area to volume ratio. Thus, the thicker disc increased the total heat source and heat generation, while the rate of heat dissipation from surface to surrounding air changed only slightly. Thus, higher equilibrium temperatures were achieved by increasing the thickness of nanocomposite.

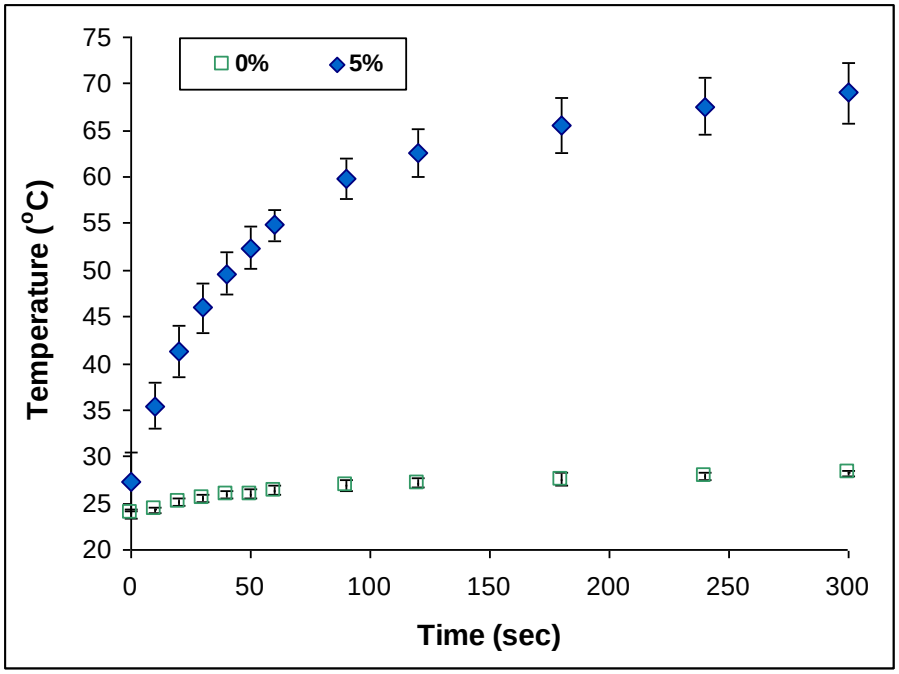

Figure 4.3. Temperature increase of nanocomposites subjected to continuously ON AMF. % represents particle loading by weight in NIPAAm-TEGDMA nanocomposite. (N=3, ±SD)

4.4.3 AMF triggered deswelling

Weight swelling ratio (q) was calculated as

$$q = \frac{\text{Weight}_{t=t}}{\text{Dry Weight}} \tag{4.1}$$

The swelling ratios are plotted in **figure 4.4**. The plot shows that nanocomposites collapsed on application of AMF, while the field had negligible effect on the control set. Heat generated in nanocomposites was sufficient to increase the internal temperature of swollen NIPAAm: TEGDMA matrix above its LCST. This led to expulsion of water and decrease in the weight of nanocomposites as soon as AMF was switched ON. The rate of

collapse was fast for initial 10 minutes which suggests that a large amount of water was expelled from the hydrogel matrix. This phenomenon can be used to achieve pulse release of drug molecules by application of AMF.

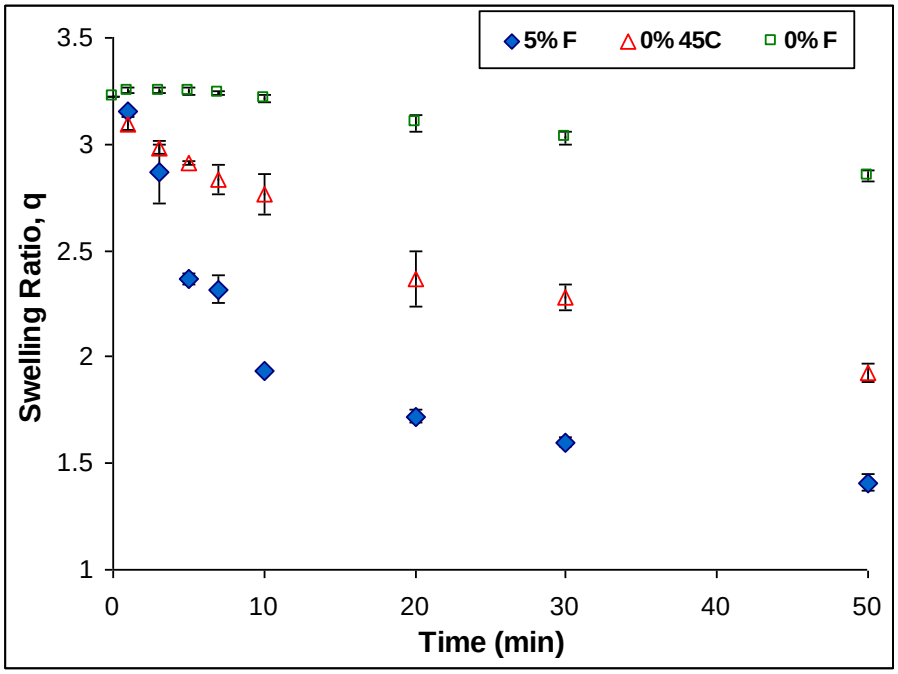

Figure 4.4. AMF triggered de-swelling of nanocomposites. % represents particle loading by weight in NIPAAm-TEGDMA nanocomposite. F represents application of AMF. (N=3, ±SD)

The rise in temperatures in swollen state is limited due to presence of water. Although dry discs showed surface temperatures of 69°C, actual temperatures in presence of water are expected to be much lower. More studies are underway to investigate the heat and mass transfer implications of field triggered heating and collapse. The nanocomposite disc exposed to field collapsed faster as compared to disc placed at 45^{o}C. Placing the discs in 45^{o}C water causes a skin layer to form (surface collapses first), leading to slower diffusion of water out of gel, and hence slower collapse.[33] Furthermore, the uniform

heating in nanocomposites is significantly faster process since it internally heats hydrogel as opposed to raising temperature of the surrounding solution. Since the AMF did not heat control hydrogels, it is implied that the AMF will induce minimal heating in tissues when used for implant type of applications.

4.4.4 Reproducibility analysis of AMF triggered collapse

The calculated swelling ratios (q) are plotted in **figure 4.5**. The plot shows that fast collapse was observed when AMF is applied, but the recovery of the discs to original swelling state required significant time. Thus, rapid heating and resulting high temperatures de-swell the discs rapidly, but the slower dissipation of the heat and diffusion of water into gel resulted in a relatively slow swelling and recovery process. It is to be noted that the geometry and thickness of the samples will dictate the kinetics of the recovery process. Discs of smaller thickness are expected to recover faster due to faster water diffusion. The discs were subjected to AMF for several cycles, and no irreversible changes in swelling properties were observed. It is also observed that the disc eventually came back to its original swelling state. Although these studies were conducted for 14 hours, similar hydrogel response is expected for longer durations. Hence, these nanocomposites are feasible for applications in remotely actuated ON-OFF type devices.

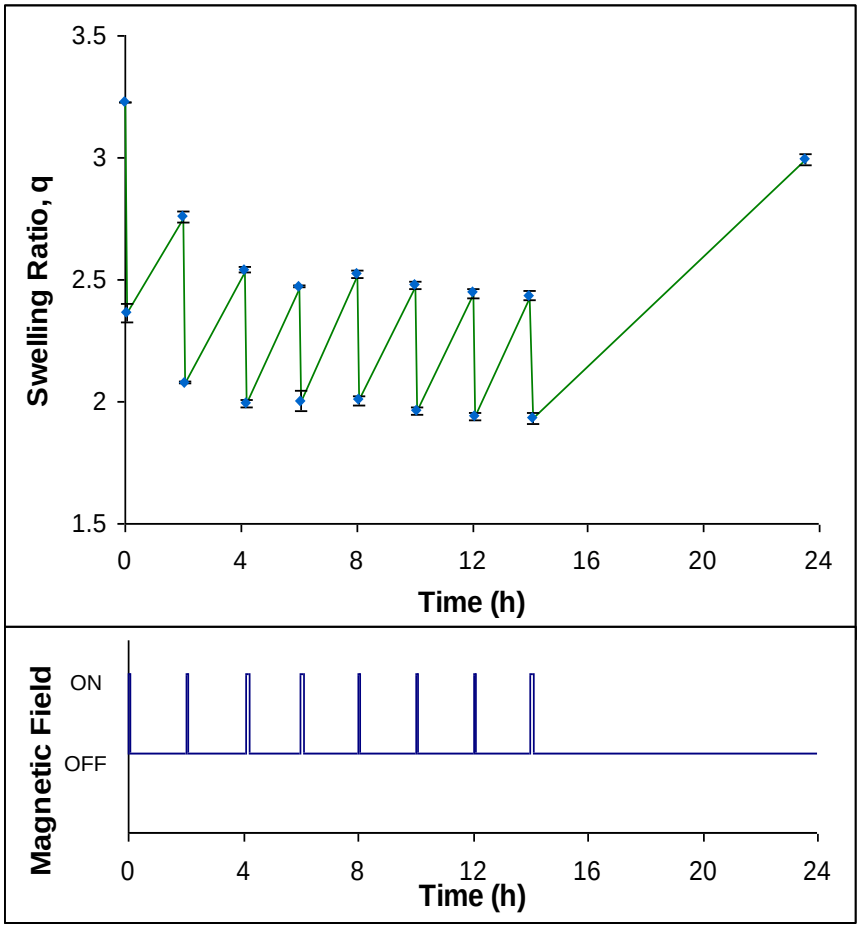

Figure 4.5. NIPAAm-TEGDMA nanocomposite discs subjected to ON-OFF cycles of AMF. (N=3, ±SD)

4.4.5 Drug release studies

4.4.5.1 Accelerated release with field ON

The release of vitamin B_{12} from hydrogel nanocomposite is plotted as cumulative release with time in **figure 4.6**. Continuous application of AMF led to fast release from nanocomposite. Applied AMF heated and hence collapsed hydrogel disc causing expulsion of large amounts of the imbibed water, led to an enhancement in the release rate of the loaded drug. It is speculated that there will be slight enhancement in release

rates due to increased drug diffusivity at higher temperatures. Hence, the release can be accelerated by application of AMF. The AMF did not significantly heat the control hydrogels and hence had minimal effect on release. The control hydrogels thus continued to release in a Fickian profile. The rise in temperature inside hydrogel needs to be controlled precisely to ensure stability of drug molecules. It is expected that the rise in temperature and resulting burst release can be tailored by variation of field exposure duration, field amplitude, and particle loadings.

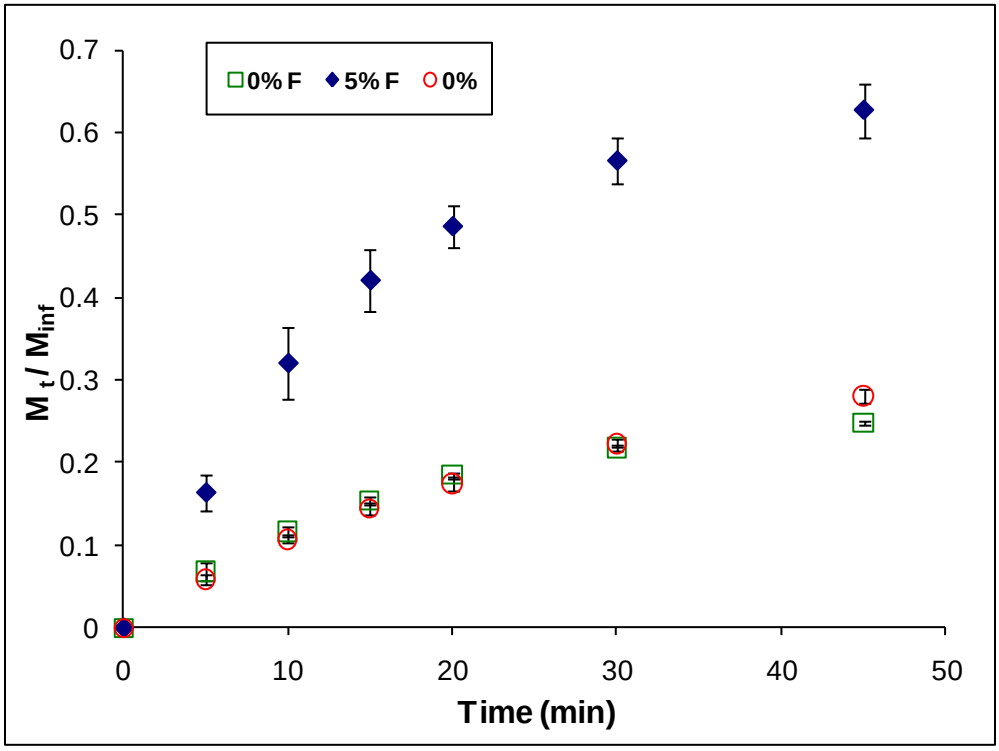

Figure 4.6. Accelerated vitamin B_{12} release from nanocomposites in continuous ON AMF. % represents particle loading by weight in NIPAAm-TEGDMA nanocomposite. F represents application of AMF. M_t represents cumulative mass released at the time. M_{inf} represents cumulative mass released at the time. M_{inf} represents cumulative mass released over 48 hours. (N=3, ±SD)

4.4.5.2 Demonstration of pulsatile release

The release rates and cumulative release of vitamin B_{12} from nanocomposite and control hydrogels is plotted in **figure 4.7**. The plot of release rate with time shows that Fickian release was observed from nanocomposites as well as control hydrogels. When a pulse of the AMF was applied to the nanocomposite, the system collapsed and a corresponding burst in the vitamin B_{12} release was observed. The enhancement in release rate on application of AMF was approximately 6 times more than Fickian release rate. Since AMF was applied only for short durations, the gel recovered slowly back to the swollen state in the OFF cycle. However, the drug had a reduced diffusivity in the collapsed network, resulting into slower release rates during the OFF cycle. Hence, a significant fraction of drug was released during small timeframe when the AMF pulse was applied. Also, when the network mesh size becomes comparable or less than size of the drug, release can be "turned OFF". The drug content of the disc decreased with time and hence limited actuation was achieved in the later stages. Application *in vivo* as implantable drug delivery device typically needs release for weeks to months. It is expected that modifications in hydrogel network properties, shape of the gel, and procedures for drug loading can lead to longer release durations.

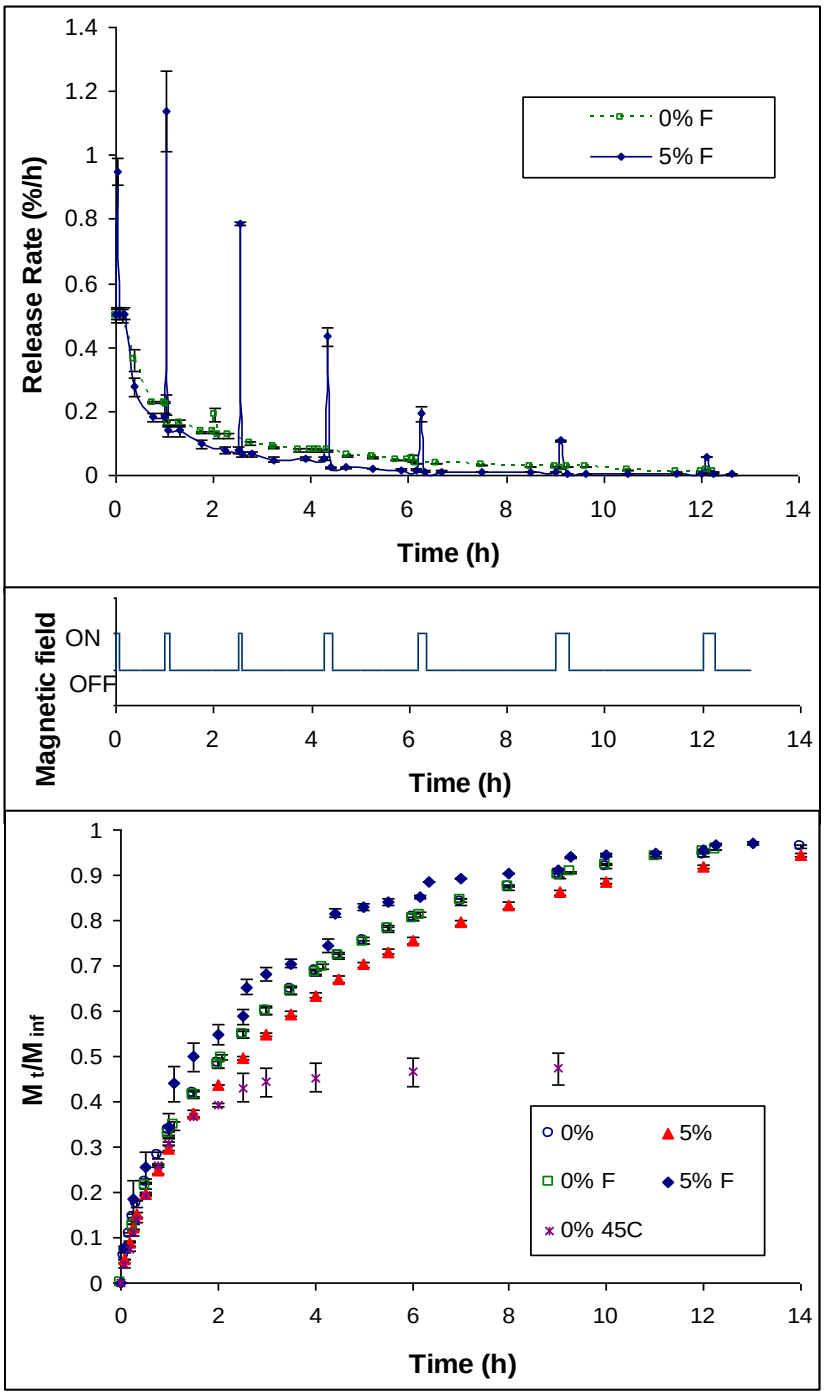

Figure 4.7. Vitamin B12 release from nanocomposites on pulsed application of AMF. % represents particle loading by weight in NIPAAm-TEGDMA nanocomposite. F represents application of AMF. Mt represents cumulative mass released at the time. Minf represents cumulative mass released over 48 hours. (N=3, ±SD)

The cumulative release with time shows that application of AMF pulses had negligible effect on release profile from control hydrogel discs. Similar to earlier studies, presence of particles caused a slight reduction in release rate when AMF was not applied.[32] This is hypothesized to result from hindered diffusion of drug due to the physical presence of the nanoparticles in the network and also potentially from affinity interactions between the drug and the nanoparticles. On the other hand, AMF application to nanocomposites resulted in a stepwise, on-demand release pattern. These remote controlled biomaterials can hence be used to obtain a continuous Fickian release with time and an additional pulsed release when desired by application of external AMF pulse.

When discs were placed in 45°C PBS, the release profile followed 25°C release for first 2 hours and it stopped after about 3 hours. Placing in hot bath (>LCST) led to gradual shrinking of disc as shown in **figure 4.3**. This effect is significantly different than the squeezing effect of the uniform heating due to the applied AMF. Here, the surface starts collapsing first and hence it completely hinders transport of drug from core of the disc to the outside.[33]

Release rates and cumulative release of methylene blue from nanocomposites is plotted in **figure 4.8**. For methylene blue the effect of variation of AMF exposure cycles on release profile was also observed.

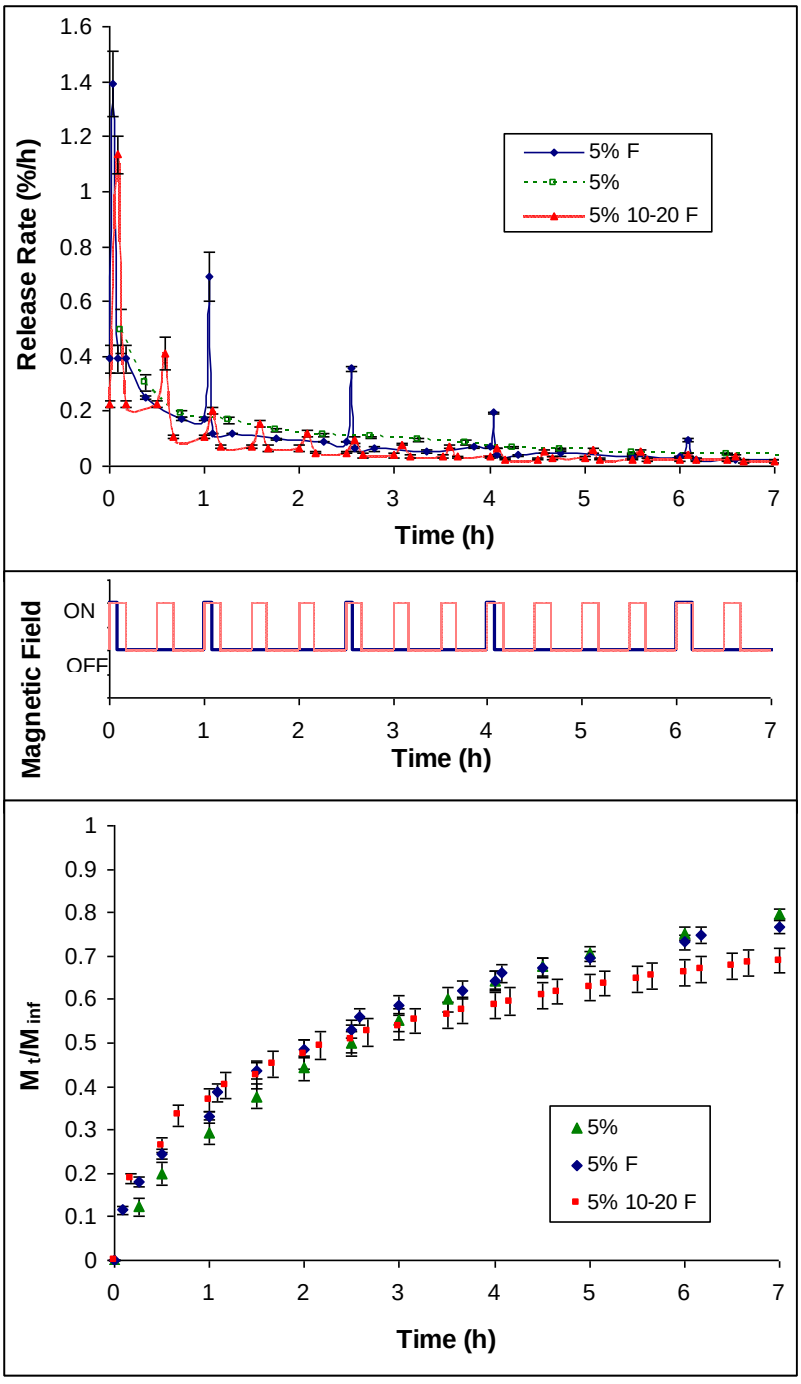

Figure 4.8. Methylene blue release from nanocomposites on pulsed application of AMF. % represents particle loading by weight in NIPAAm-TEGDMA nanocomposite. F represents application of AMF. M_t represents cumulative mass released at the time. M_{inf}

represents cumulative mass released over 48 hours. 10-20 indicates AMF cycle of 10 minutes ON and 20 minutes OFF. (N=3, ±SD)

Release rate profile of methylene blue on pulse application of AMF is similar to that of vitamin B_{12} and emphasizes that effective modulation in release can be obtained by pulse application. A significant fraction of methylene blue was released when AMF pulse was applied. However, methylene blue has an increased diffusivity making the content of the drug in disc deplete faster. So, the magnitude of burst effect decreased faster with time as compared to Vitamin B_{12}.

Release rates from 10 min ON- 20 min OFF cycles indicate that modulation of release was limited. Due to smaller OFF durations, the collapsed network did not recover back to swollen state. Hence the gel stayed mostly in collapsed state, the diffusion became slow, and the Fickian release rate shifted to lower values. Longer AMF ON durations thus limit the diffusion of water into hydrogel matrix and can be used to get reduced drug transport out of gel, as observed in earlier studies.[32]

The comparison of the timeframe of cumulative release of the two drugs shows that methylene blue (MW 320) released faster than vitamin B_{12} (MW 1355). It is expected that for compounds with comparable hydrophilicity, the smaller molecules will have greater effective diffusivity and hence will release faster. However, the design of hydrogel can be modified for smaller drugs by an increased crosslinker density leading to a smaller mesh size. This will allow prolonged release and effective actuation of the release of smaller drugs. Since methylene blue has a greater effective diffusivity, it continued diffusing out in the OFF cycle although the disc was in collapsed state. Hence,

the methylene blue release profiles of the control and short pulse field applications did not differ significantly, as opposed to nice stepwise release of vitamin B_{12}. The graph of cumulative release also shows that 10 ON 20 OFF field exposure profile had a stronger initial burst and reduced overall release. This is because the field squeezed drug faster initially but later on disc remained mostly in collapsed state, reducing the release rate.

Thus, the data from methylene blue and vitamin B_{12} release suggests that this nanocomposite system has potential as an implantable drug delivery device. AMF has potential to penetrate deep regions in body with negligible absorption by tissue. Hence, this system can potentially be implanted in any part of the body. An essential modification to the system includes shifting the LCST to above physiological temperatures (~37^{o}C), which can be achieved by incorporation of hydrophilic comonomer like acrylamide.[34] Furthermore, tailoring the comonomer and crosslinker compositions can yield the mesh size desirable for specific therapeutics. This would control the duration of release and magnitude of actuation. Similarly, manipulating the magnitude and duration of AMF pulse can tailor the burst release to desired magnitude and can even result into reduced release with prolonged AMF durations. In addition to matrix type of drug delivery devices, these nanocomposites can also be used as a valve in implantable reservoir types of devices. More studies are underway to demonstrate the applications of nanocomposites as remotely actuated valves in a drug delivery device.

4.5 Conclusions

Nanocomposite hydrogels have been successfully demonstrated as remote controlled biomaterials. The application of an AMF selectively heated magnetic particles and led to a rise in temperature of nanocomposite hydrogel systems. The nanocomposite

temperature increased above the LCST resulting into accelerated collapse of the gel. The discs were subjected to AMF for several cycles, and reversibility of the swelling response was observed. Hence, the nanocomposites are feasible for applications in remotely actuated ON-OFF type devices, where drug release can be turned ON by application of AMF. The collapse of the hydrogel discs expelled large amounts of imbibed water, resulting in drug release at an increased rate. Release profiles of methylene blue and vitamin B_{12} showed effective modulation in release by pulse application of AMF. Magnetic nanocomposites can thus give pulsed release when needed in addition to continuous Fickian release profile. These novel intelligent biomaterials promise numerous potential applications in externally actuated drug delivery systems for release of drug molecules.

4.6 References

[1] T. Bussemer, I. Otto, R. Bodmeier, Pulsatile drug-delivery systems. Crit. Rev. Ther. Drug. 18(5) (2001) 433-458.

[2] B.-B.C. Youan, Chronopharmaceutics: gimmick or clinically relevent approach to drug delivery? J. Control. Rel. 98 (2004) 337-353.

[3] B.G. Stubbe, S.C.D. Smedt, J. Demeester, "Programmed Polymeric Devices" for pulsed drug delivery. Pharm. Res. 21(10) (2004) 1732-1740.

[4] A.C.R. Grayson, I.S. Choi, B.M. Tyler, P.P. Wang, H. Brem, M.J. Cima, R. Langer, Multi-pulse drug delivery from a resorbable polymeric microchip device. Nat. Mater. 2 (2003) 767 - 772.

[5] J. Kost, R. Langer, Responsive polymeric delivery systems. Adv. Drug Deliver. Rev. 46 (2001) 125-148.

[6] S.R. Sershen, J.L. West, Implantable, polymeric systems for modulated drug delivery. Adv. Drug Deliver. Rev. 54 (2002) 1225-1235.

[7] A. Kikuchi, T. Okano, Pulsatile drug release control using hydrogels. Adv. Drug Deliver. Rev. 54 (2002) 53-77.

[8] N.A. Peppas, J.Z. Hilt, A. Khademhosseini, R. Langer, Hydrogels in biology and medicine: from molecular principles to bionanotechnology. Adv. Mater. 18 (2006) 1345-1360.

[9] A.M. Lowman, N.A. Peppas, Hydrogels. in: E. Mathiowitz (Ed.), Encyclopedia of Controlled Drug Delivery, Vol. 1, Wiley, New York, 1999, pp. 397-418.

[10] S. Nayak, L.A. Lyon, Soft nanotechnology with soft nanoparticles. Angew. Chem. Int. Ed. 44(47) (2005) 7686-7708.

[11] Z.M.O. Rzaev, S. Dincer, E. Piskin, Functional copolymers of N-isopropylacrylamide for bioengineering applications. Prog. Polym. Sci. 32(5) (2007) 534-595.

[12] S. Chaterji, I.K. Kwon, K. Park, Smart polymeric gels: Redefining the limits of biomedical devices. Prog. Polym. Sci. 32(8-9) (2007) 1083-1122.

[13] C. He, S.W. Kim, D.S. Lee, In situ gelling stimuli-sensitive block copolymer hydrogels for drug delivery. J. Control. Rel. 127(3) (2008) 189-207.

[14] E.S. Gil, S.M. Hudson, Stimuli-reponsive polymers and their bioconjugates. Prog. Polym. Sci. 29(12) (2004) 1173-1222.

[15] R.A. Frimpong, J.Z. Hilt, in: N. A. Peppas, J. Z. Hilt and J. B. Thomas (Eds.), Nanotechnology in Therapeutics: Current Technology and Applications, Horizon Scientific Press, Norfolk, 2007, pp. 241-256.

[16] G. Filipcsei, I. Csetneki, A. Szilagyi, M. Zrinyi, Magnetic field-responsive smart polymer composites Adv. Polym. Sci. 206 (2007) 137-189.

[17] S.-H. Hu, T.-Y. Liu, D.-M. Liu, S.-Y. Chen, Controlled pulsatile drug release from a ferrogel by a high-frequency magnetic field. Macromolecules 40(19) (2007) 6786-6788.

[18] A. Suzuki, T. Tanaka, Phase transition in polymer gels induced by visible light. Nature 346(6282) (1990) 345-347.

[19] S.R. Sershen, G.A. Mensing, M. Ng, N.J. Halas, D.J. Beebe, J.L. West, Independent optical control of microfluidic valves formed from optomechanically responsive nanocomposite hydrogels. Adv. Mater. 17(11) (2005) 1366-1368.

[20] J. Kost, J. Wolfrum, R. Langer, Magnetically enhanced insulin release in diabetic rats. J. Biomed. Mater. Res. 21 (1987) 1367-1373.

[21] V.M.D. Paoli, S.H.D.P. Lacerda, L. Spinu, B. Ingber, Z. Rosenzweig, N. Rosenzweig, Effect of an oscillating magnetic field on the release properties of magnetic collagen gels. Langmuir 22 (2006) 5894-5899.

[22] T.-Y. Liu, S.-H. Hu, K.-H. Liu, D.-M. Liu, S.-Y. Chen, Study on controlled drug permeation of magnetic-sensitive ferrogels: Effect of Fe3O4 and PVA. J. Control. Rel. 126(3) (2008) 228-236.

[23] Z. Lu, M.D. Prouty, Z. Guo, V.O. Golub, C.S.S.R. Kumar, Y.M. Lvov, Magnetic switch of permeability for polyelectrolyte microcapsules embedded with Co@Au nanoparticles. Langmuir 21 (2005) 2042-2050.

[24] A.M. Derfus, G.v. Maltzahn, T.J. Harris, T. Duza, K.S. Vecchio, E. Ruoslahti, S.N. Bhatia, Remotely triggered release from magnetic nanoparticles. Adv. Mater. 19 (2007) 3932-3936.

[25] Q.A. Pankhurst, J. Connolly, S.K. Jones, J. Dobson, Applications of magnetic nanoparticles in biomedicine. J. Phys. D: Appl. Phys. 36 (2003) R167-R181.

[26] P.P. Vaishnava, R. Tackett, A. Dixit, C. Sudakar, R. Naik, G. Lawes, Magnetic relaxation and dissipative heating in ferrofluids. J. Appl. Phys. 102 (2007) 063914.

[27] W. Andra, in: W. Andra and H. Nowak (Eds.), Magnetism in medicine, Wiley-VCH, Berlin, 1998, pp. 455-470.

[28] H.G. Schild, Poly(N-isopropylacrylamide): experiment, theory, and application. Prog. Polym. Sci. 17 (1992) 163-249.

[29] A.S.H. Tae Gwan Park, Deswelling characteristics of poly(N-isopropylacrylamide) hydrogel. J. Appl. Polym. Sci. 52(1) (1994) 85-89.

[30] A.S. Hoffman, Applications of thermally reversible polymers and hydrogels in therapeutics and diagnostics. J. Control. Rel. 6(1) (1987) 297-305.

[31] R.A. Frimpong, S. Fraser, J.Z. Hilt, Synthesis and temperature response analysis of magnetic-hydrogel nanocomposites. J. Biomed. Mater. Res. A 80A(1) (2007) 1-6.

[32] N.S. Satarkar, J.Z. Hilt, Nanocomposite hydrogels as remote controlled biomaterials. Acta Biomater. 4 (2008) 11-16.

[33] Y. Kaneko, R. Yoshida, K. Sakai, Y. Sakurai, T. Okano, Temperature-responsive shrinking kinetics of poly (N-isopropylacrylamide) copolymer gels with hydrophilic and hydrophobic comonomers. J. Membr. Sci. 101(1-2) (1995) 13-22.

[34] R. Yoshida, K. Sakai, T. Okano, Y. Sakurai, Modulating the phase transition temperature and thermosensitivity in N-isopropylacrylamide copolymer gels. J. Biomater. Sci., Polym. Ed. 6 (1995) 585-598.

CHAPTER 5

MAGNETIC HYDROGEL NANOCOMPOSITES AS REMOTE CONTROLLED MICROFLUIDIC VALVES

This chapter is based on work published as:

N.S. Satarkar, W. Zhang, R. Eitel, J.Z. Hilt, Magnetic hydrogel nanocomposites as remote controlled microfluidic valves, Lab Chip 9 (2009) 1773-1779.

5.1 Summary

In recent years, hydrogels have attracted attention as active components in microfluidic devices. Here, we present a demonstration of remote controlled flow regulation in a microfluidic device using a hydrogel nanocomposite valve. To create the nanocomposite hydrogel, magnetic nanoparticles were dispersed in temperature responsive N-isopropylacrylamide (NIPAAm) hydrogels. The swelling and collapse of the resultant nanocomposite can be remotely controlled by application of alternating magnetic field (AMF). A ceramic microfluidic device with Y-junction channels was fabricated using low temperature co-fired ceramic (LTCC) technology. The nanocomposite was incorporated as a valve in one of the channels of the device. An AMF of frequency 293 kHz was then applied to the device and ON-OFF control on flow was achieved. A pressure transducer was placed at the inlet of the channel and pressure measurements were done for multiple AMF ON-OFF cycles to evaluate the reproducibility of the valve.

Furthermore, the effect of the hydrogel geometry on the response time was characterized by hydrogels with different dimensions. Magnetic hydrogel nanocomposite films of different thicknesses (0.5, 1, 1.5 mm) were subjected to AMF and the kinetics of collapse and recovery were studied.

5.2 Introduction

Microfluidic technology is attractive because of numerous benefits including reduced reagent consumption, short analysis time, portability, low cost, and high sensitivity.[1] The current microfluidic technology typically utilizes pneumatically actuated valves with significant off-chip controls. A promising alternative to this approach is the incorporation of hydrogels as active materials for a wide range of microfluidic functions. Hydrogels have been developed as valves, pumps, mixers, and flow sorters for various on-chip applications as well as for drug delivery devices.[2, 3] However, there has been limited work on externally actuated hydrogel valves. Here, we present the incorporation of NIPAAm based hydrogel nanocomposites as valves in the low temperature co-fired ceramic (LTCC) microdevice and the demonstration of ON-OFF flow control with the application of radio frequency alternating magnetic field (AMF). LTCC is a versatile technique that can be used to conveniently fabricate complex microfluidic geometries. A brief introduction to LTCC and the commercial fabrication process is discussed in appendix A.

Hydrogels are hydrophilic polymeric networks with physical or chemical crosslinks.[4, 5] Stimuli-responsive hydrogels or smart hydrogels are a class of hydrogels that can respond to changes in external environment and show significant changes in swelling properties. Stimuli-responsive hydrogels can respond to changes in pH, temperature, light, magnetic

field, electric field, presence of specific molecules, or a combination of environmental triggers.[6, 7] The combination of stimuli-responsive hydrogels with nanoparticulates can lead to a nanocomposite matrix with unique properties including the capability to heat them remotely.[8] In particular, nanocomposites consisting of temperature responsive hydrogels and metallic nanoparticles can respond to external stimuli such as light or magnetic field. This leads to potential applications as remote controlled drug delivery devices, microfluidic valves, and soft actuators.[9-12]

Stimuli-responsive hydrogels are attractive as components of microfluidic devices because the swelling response of hydrogel systems is typically diffusion limited, and thus, hydrogels at the small scales are more efficient (i.e., shorter response times). In addition, hydrogels are easy to fabricate in microchannels and eliminate the need for integrated electronics, controls, and power source that are required for active components. One of the first demonstrations of stimuli responsive hydrogels as microfluidic valves was by Beebe and colleagues. They showed that pH responsive hydrogels can act as both a sensor and actuator for flow control.[13, 14] Several additional studies have demonstrated pH-responsive hydrogels as valves.[15] [16] [17, 18] Similarly, there has been increasing interest in using temperature responsive hydrogels as microfluidic actuators.[19-24] An important advantage of thermally versus pH actuated valves is that they do not need contact with a controlling solution (high and low pH) and hence can be controlled from outside the device. They can also be used over wide range of pH.

The concept of using external stimuli to actuate temperature-responsive hydrogel valves has received only limited attention from researchers. Remote controlled valves are

attractive for applications like pulsatile drug release from an implantable device, where the dose can be varied easily by variation of external stimuli. Sershen and others demonstrated that light can be used as stimuli to achieve independent control on operation of gold-NIPAAm nanocomposite valves.[10] Chen et al. showed that heating from the absorption of light directed to NIPAAm plug can open and close it on-demand with fast kinetics and good repeatability.[25] In another study, a chromophore was functionalized in NIPAAm valves, and independent control on multiple valves was demonstrated by local light irradiation.[26] However, light as a stimulus has potential limitations for actuation of valves in multi-layered devices or in implanted devices. To the best of our knowledge, this is the very first demonstration on use of magnetic fields to control microfluidic valves.

Previous chapters presented characterization of the hydrogel nanocomposite system for optimal heating and collapse on AMF application. Remote controlled (RC) pulsatile drug delivery with hydrogel nanocomposites has also been demonstrated.[11, 27] The focus of this chapter is primarily on the demonstration of NIPAAm based magnetic nanocomposites as valves in an LTCC microdevice. **Figure 5.1** shows the schematic of the concept for the AMF controlled microfluidic valve. The application of AMF heats the Fe_3O_4 nanoparticles by Neel and Brownian relaxations and in turn heats the hydrogel matrix. As the temperature of matrix goes above the lower critical solution temperature (LCST), the hydrogel will collapse opening the channel. The valve was demonstrated for ON-OFF flow control with application of AMF. The characterization of the time needed for the valve to open/close was also conducted using a pressure sensor. Additionally,

hydrogel film thickness was varied, and the effect on kinetics of RC collapse and recovery was studied.

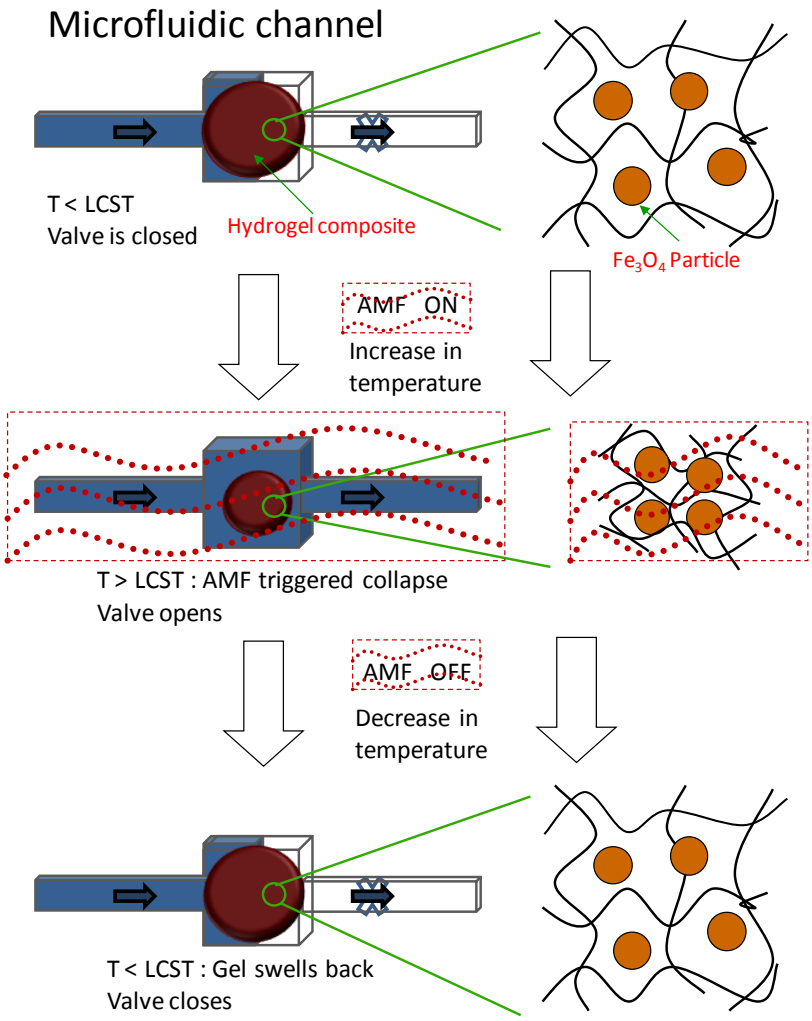

Figure 5.1. Schematic of the concept of remote controlled hydrogel nanocomposite valves with alternating magnetic field (AMF). Application of AMF results into collapse of hydrogel, leading to opening of the valve.

5.3 Materials and methods

HeraLock® HL2000 tapes which provide a sintering shrinkage in x, y direction of less than 0.2% were obtained from W.C. Heraeus Thick Film Materials Division. N-

Isopropylacrylamide (NIPAAm), ammonium persulfate (APS), and N,N,N`,N`-tetramethylethylenediamine (TEMED) were obtained from Sigma-Aldrich and used as received. Tetra (ethylene glycol) dimethacrylate (TEGDMA) was obtained from Polysciences, Inc. Dispersible iron oxide nanoparticles (Fe_3O_4, ~0.2% PVP coated, 25 nm) were obtained from Nanostructured and Amorphous Materials Inc.

5.3.1 Fabrication of ceramic microdevice

The flow system had two straight channels (width 600 μm, depth 650 μm) with a Y-shape junction, and a square cavity in the middle of one channel to anchor the hydrogel valve. The LTCC device assembly consisted of a ceramic microchannel laminate, a ceramic cover, and a transparent high density polyethylene (HDPE) gasket. The details of fabrication and assembly process are described in appendix A.

5.3.2 Synthesis of hydrogel nanocomposite

A hydrogel nanocomposite was incorporated as a valve into one channel of the microdevice. NIPAAm was used as the monomer while TEGDMA was used as the crosslinker. The NIPAAm-TEGDMA ratio was selected to obtain strong swelling response with change in temperature. The NIPAAm hydrogel system has LCST of about 32^{o}C. Further details of the effect of the hydrogel composition on temperature response can be found elsewhere.[27] NIPAAm and TEGDMA were mixed in molar ratio of 99:1 and dissolved in ethanol, which was 50 wt% of monomer and crosslinker. Magnetic particles were added as 10 wt% of NIPAAm and TEGDMA and dispersed with bath sonication for 15 minutes. Oxygen present in the pre-polymer solution was removed by bubbling nitrogen for 10 minutes. The initiator APS was weighed as 0.75 wt% of

NIPAAm and TEGDMA, dissolved in 50 μl of deionized water, and added along with equal weight of accelerator TEMED in a nitrogen environment. The pre-polymer solution was then injected into clamped glass plates separated by 500 μm spacer. Polymerization was continued at 25^{o}C for 24 hours. The hydrogel obtained was then inserted in water to wash out unreacted monomers. The hydrogel was then cut into a disc, with diameter of 4.3 mm, and placed into the valve cavity of the LTCC chip.

5.3.3 AMF heating and flow control using hydrogel valve

The device was assembled and inlets were connected to water of different colors (blue and yellow) through a syringe pump. The flow rate at both inlets was maintained at 100 μl/min. In order to evaluate the capability of actuating the hydrogel valve remotely, the microdevice was placed on top of the solenoid of a 3 kW induction heater (Taylor Winfield Corporation, MMF-3-135/400-2). The applied AMF was 293 kHz with calculated amplitude of 33.5 kA/m. IR images were collected for heating up to 2 min (Thermacam S65 HS, FLIR Systems). Images for flow control were recorded using a digital camera.

5.3.4 Analysis of flow control for multiple ON-OFF cycles

To quantify ON-OFF function, the inlet of the microchannel containing the hydrogel valve (blue channel) was connected to the syringe pump through a miniature pressure transducer (Deltran DPT-100, Utah Medical Products, Midvale, UT, USA). The pressure signals were amplified by an AC source (Model 33220A Agilent Technologies, Palo Alto, CA, USA) and recorded on a computer using a data recorder (Agilent 34970A Data Acquisition/Switch Unit, Agilent Technologies, Palo Alto, CA, USA) and a software

programmed by LabView (National Instruments, Austin, TX, USA). AMF was turned ON for 2.5 minutes followed by OFF for about 10 minutes. In order to allow accurate data collection in ON cycles, AMF was turned OFF for 2 seconds every 30 seconds. The pressure data was collected for 3-4 ON-OFF cycles.

5.3.5 Effect of hydrogel film thickness on kinetics of RC collapse and recovery

NIPAAm:TEGDMA films in a molar ratio of 95:5 with 5 wt% Fe_3O_4 nanoparticles and equal weight of ethanol as a solvent were synthesized. Different Teflon spacers were used to get films of 0.5, 1, and 1.5 mm thicknesses. Synthesis was done using polymerization methods similar to those described in section 5.3.2. The resultant hydrogel nanocomposites were washed and cut into discs of 15 mm diameter. These were then allowed to come to equilibrium in phosphate buffered solution (PBS) at 25^{o}C. The discs were placed in centrifuge tube with 10 ml PBS solution and subjected to AMF (amplitude 59.5 kA/m and frequency 297 kHz). The field was applied for 30 minutes and weight of the disc measured at regular time intervals. Then, the disc was transferred to a 25^{o}C bath. The recovery process was characterized by measuring the weight at regular time intervals until the equilibrium swelling was observed. After analysis was complete, the discs were dried in air, and the dry weight was obtained. The weight swelling ratio at different time points was calculated as swollen weight divided by dry weight.

5.4 Results and discussion

5.4.1 Fabrication of ceramic microdevice and incorporation of hydrogel valve

The pictures of assembled microfluidic device are presented in appendix A.

5.4.2 AMF heating and flow control using hydrogel valve

The hydrogel valve in the swollen state was subjected to the AMF by placing the device above the solenoid. **Figure 5.2** shows an IR picture of the microdevice after 2 minutes of heating. Starting from 21^{o}C, the valve temperature reached 27^{o}C. The picture clearly shows that the hydrogel nancomposite valve heats selectively on exposure to AMF with no effect on ceramic device. It is also noted that the HDPE gasket is only semi-IR transparent which may lead to slightly lower temperature readings. If necessary, it is known that valve heating could be increased by either increasing particle loadings and/or AMF amplitude. The effect of particle loadings on the resultant heating in AMF has been discussed elsewhere.[27]

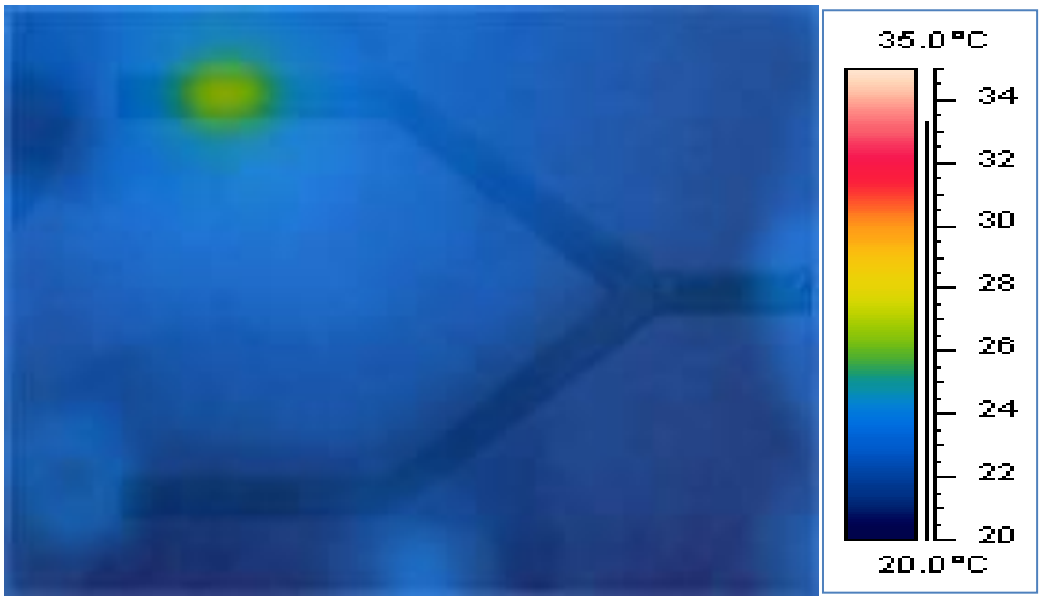

Figure 5.2. An IR image of the device after exposure to AMF for 2 minutes indicates localized remote heating of the hydrogel valve (the IR image has been superimposed on a visible image).

NIPAAm hydrogels are negative temperature responsive systems, and the effect of temperature on swelling has been studied previously.[27] **Figure 5.3** shows a series of images for visual demonstration of ON-OFF control of flow using the hydrogel valve. After flow was started, swelling of hydrogel blocked upper channel (5.3a) stopping the flow of the blue stream. Turning ON the AMF selectively heated the magnetic nanoparticles and in turn the hydrogel nanocomposite. As temperature increased above LCST, the nanocomposite hydrogel collapsed and opened the upper channel (5.3b) producing a green color in the outlet channel. When the AMF was turned OFF, the hydrogel cooled down slowly leading to swelling and a blocked upper channel. Thus, the nanocomposite hydrogel functioned effectively as a remotely controlled ON-OFF microfluidic valve.

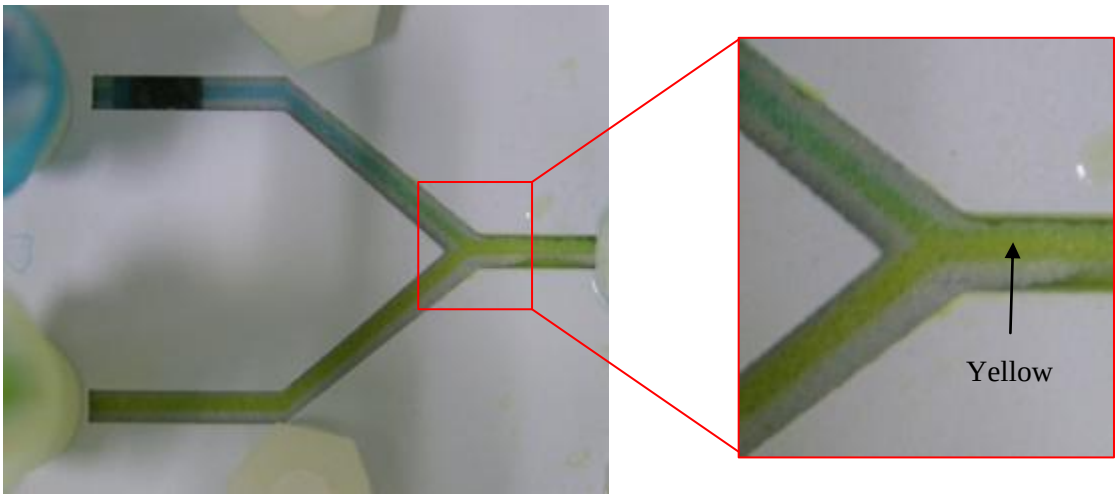

(a)

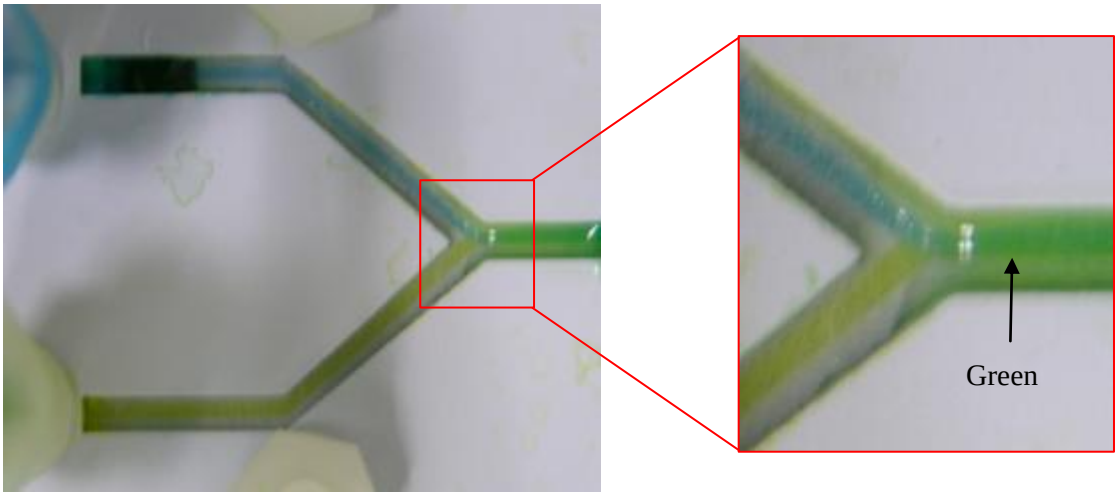

(b)

Figure 5.3. Images showing ON-OFF control of flow with the hydrogel valve. In (a) the valve OFF: swelling of hydrogel blocks upper channel preventing fluid flow. We see only yellow flowing. In (b) Valve ON: application of AMF opens upper channel allowing the blue stream to flow, leading to green color as clearly visible in the inset at right.

5.4.3 Analysis of flow control for multiple ON-OFF cycles

The pressure data was recorded at the inlet of the upper (blue) channel, and **figure 5.4** shows the pressure and temperature plot with time for 3-4 ON-OFF cycles. When flow was turned ON, the valve blocked the upper channel, and the pressure began to increase. After 10 minutes, the pressure had reached about 0.055 psi. When the AMF was turned ON, the increase in the temperature caused the collapse of the hydrogel, and the release of pressure was observed. The continued application of AMF for the next 2.5 minutes decreased the pressure to about 0.02 psi. When the AMF was turned OFF, the nanocomposite hydrogel valve swelled slowly, and the pressure in the channel increased back to over 0.06 psi in about 10 min. This was repeated for a few more cycles with a good reproducibility. Previous studies have shown that the hydrogel can undergo collapse and recovery for multiple cycles with similar response every time.[11] Hence, we can expect that these valves can work as flow regulators for long term applications.

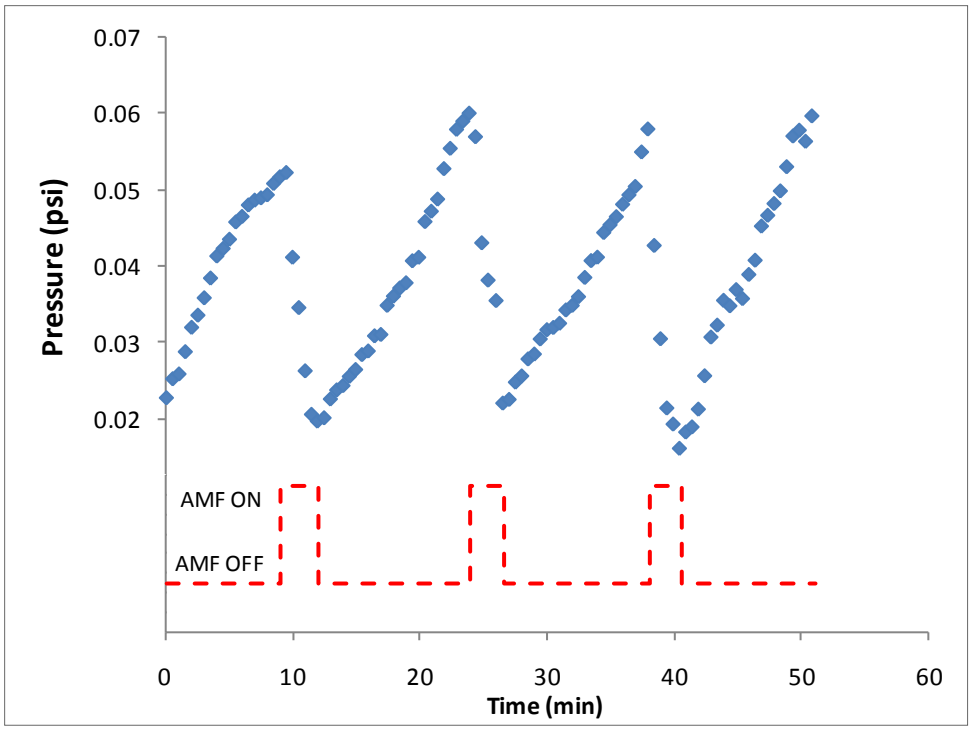

Figure 5.4. The pressure was recorded at the inlet of the upper (blue) channel and against time for 3 ON-OFF cycles, the corresponding AMF field state is indicated below.

These valves give fast collapse but need significant time for the recovery process. For many flow control applications, it is important to obtain a system that can exhibit instantaneous collapse and fast recovery. The RC collapse and recovery processes are governed by the transport of heat and water in and out of the system. The kinetics will hence be strongly influenced by the composition and geometry of the hydrogel system as well as the capability for heat generation. By increasing the heating capability, there will be a faster rise in temperatures and hence faster collapse of the valve. A couple of the possibilities for increasing the heat generation are increasing the nanoparticle loadings and incorporating nanoparticle systems with a higher heat generation capabilities. The collapse process consists of squeezing out the water and hence will depend on the dimensions of the gel. Smaller dimensions would lead to a faster collapse. The recovery

process comprises of the cooling of the hydrogel matrix and the diffusion of water into the gel. The kinetics of the recovery process are strongly governed by the hydrogel geometry. A smaller size would result in a smaller diffusion path and hence faster recovery.

5.4.4 Effect of hydrogel dimensions on kinetics of RC collapse and recovery

In order to evaluate effect of the hydrogel geometry (i.e. diffusion path) on kinetics of collapse and recovery, nanocomposite discs of 0.5, 1, and 1.5 mm thickness were studied, and **figure 5.5** shows the swelling ratio with time for these systems. The application of AMF for 30 minutes led to the collapse of the gels, and the 0.5 mm hydrogels collapsed slower than the 1 or 1.5 mm hydrogels. However, no substantial difference was observed in the collapse kinetics of 1 and 1.5 mm thickness hydrogels. The increased thickness resulted in a longer diffusion path for water and hence a reduced rate of heat transfer from the inside the film to outside water. It is thus expected that increased thickness would result in higher temperatures at the center of the gel, as observed in the case of dry heating of these nanocomposites.[11] On the contrary, smaller geometries require stronger heat generation to get fast collapse.

When the magnetic field was turned OFF, hydrogels slowly recovered back to their equilibrium swelling state and the kinetics of recovery varied dramatically with hydrogel thickness. Hydrogels with smaller thickness recovered faster. The process of recovery depends primarily on the transport of heat and water. Gels with smaller thickness lost heat faster resulting in faster recovery. Also, the smaller diffusion path in case of 500 μm film resulted into faster water transport and hence faster recovery. Preliminary analysis of the recovery kinetics implies that these systems follow length square dependence and

more studies are underway to look at heat and mass transfer processes in detail. The collapse and recovery kinetics can also be influenced by several other factors including particle loadings, hydrogel composition, and amount of crosslinking.

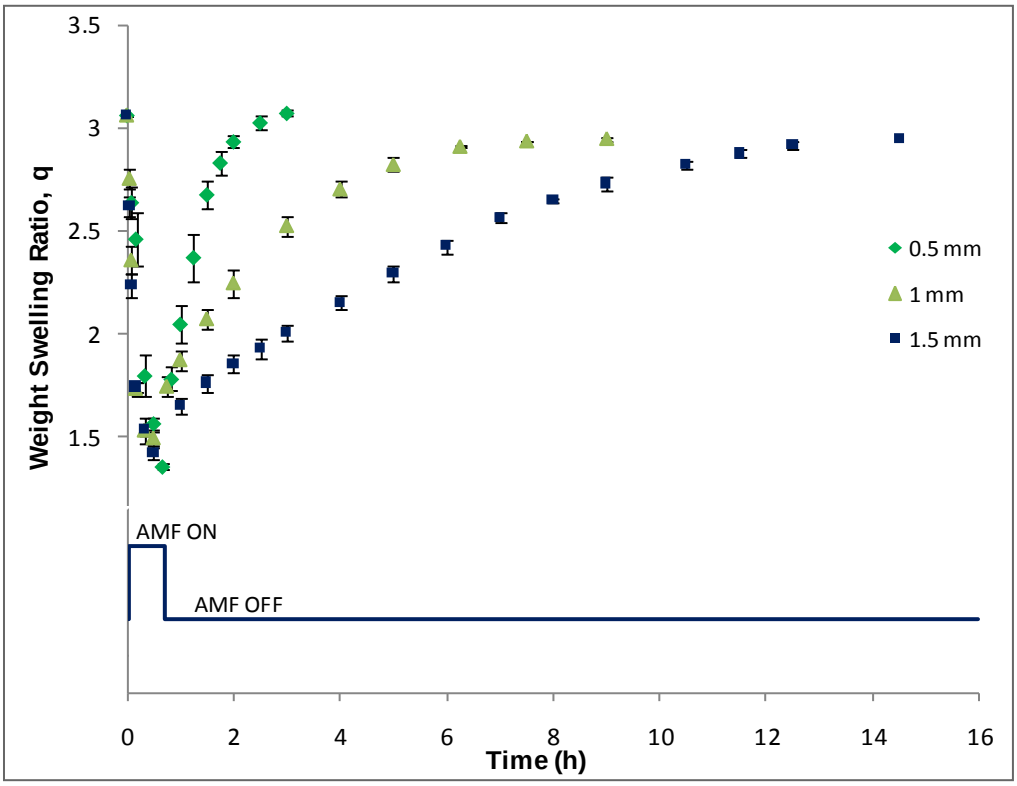

Figure 5.5. Effect of hydrogel dimensions on the kinetics of collapse and subsequent recovery. Nanocomposites of different thicknesses were collapsed by application of AMF for first 30 minutes and then allowed to swell back.

In summary, presented is a proof of concept demonstration of an RC microfluidic valve based on a magnetic hydrogel nanocomposite. The present valve geometry was chosen for the ease of assembly, observation, and characterization. Application specific optimization will be required to enhance performance of a given device. As demonstrated in the analysis of nanocomposites of different dimensions (figure 5.5), the dimensions of the valve can be decreased to significantly enhance the rate of the collapse and recovery

processes. Further studies are under way to obtain RC valves with rapid response times, which will be required for many applications.

For many LOC applications, it will be desirable to address and actuate multiple valves independently. There are several options to modify the present RC microvalve design to obtain multiple individually addressable RC valves. One of the potential approaches is using multiple off-chip solenoids of small diameters that are positioned below the individual nanocomposite valves. The solenoids will generate independent AMF in small areas, and these could be selectively turned ON to actuate the valves independently. Another approach is incorporating miniaturized solenoids on-chip at the location of the nanocomposite valve to generate localized AMF. In recent years, there has been significant interest in generating magnetic fields on-chip for a variety of applications.[28-30] In particular, there has been significant progress in fabricating inductors on-chip including examples in the LTCC platform.[31, 32]

5.5 Conclusions

In this chapter, a magnetic hydrogel nanocomposite valve was used in a microfluidic device for remote control of the flow using alternating magnetic fields. The flow circuit consisting of two inlets and one outlet was fabricated in a ceramic microfluidic device using LTCC technology. Magnetic hydrogel nanocomposites based on NIPAAm were synthesized and incorporated as a valve in one of the channels. The application of AMF led to selective heating of the hydrogel nanocomposite. As the temperature increased above LCST, the nanocomposite collapsed, leading to opening of the valve. As AMF was turned OFF, the cooling of hydrogel nanocomposite resulted in recovery leading to closing of the valve. The application of multiple ON-OFF AMF cycles to the valve along

with analysis of pressure at the inlet demonstrated that the valve can work for multiple cycles with good reproducibility. Although the response of this valve is sluggish, it can be improved by going to smaller valve dimensions. The RC collapse and recovery studies with hydrogels of different dimensions showed that hydrogels with smaller thickness exhibit slower collapse but faster recovery. The ON-OFF response of the valve can thus be precisely controlled by nanocomposite composition and geometry. Hence, magnetic hydrogel nanocomposites are potentially attractive materials as valves for remote control of flow in microfluidic devices.

5.6 References

[1] G.M. Whitesides, The origins and the future of microfluidics. Nature 442(7101) (2006) 368-373.

[2] D.T. Eddington, D.J. Beebe, Flow control with hydrogels. Adv. Drug Deliver. Rev. 56(2) (2004) 199-210.

[3] L. Dong, H. Jiang, Autonomous microfluidics with stimuli-responsive hydrogels. Soft Matter 3(10) (2007) 1223-1230.

[4] N.A. Peppas, J.Z. Hilt, A. Khademhosseini, R. Langer, Hydrogels in biology and medicine: from molecular principles to bionanotechnology. Adv. Mater. 18 (2006) 1345-1360.

[5] T.R. Hoare, D.S. Kohane, Hydrogels in drug delivery: Progress and challenges. Polymer 49(8) (2008) 1993-2007.

[6] E.S. Gil, S.M. Hudson, Stimuli-reponsive polymers and their bioconjugates. Prog. Polym. Sci. 29(12) (2004) 1173-1222.

[7] S. Chaterji, I.K. Kwon, K. Park, Smart polymeric gels: Redefining the limits of biomedical devices. Prog. Polym. Sci. 32(8-9) (2007) 1083-1122.

[8] R.A. Frimpong, J.Z. Hilt, in: N. A. Peppas, J. Z. Hilt and J. B. Thomas (Eds.), Nanotechnology in Therapeutics: Current Technology and Applications, Horizon Scientific Press, Norfolk, 2007, pp. 241-256.

[9] G. Filipcsei, I. Csetneki, A. Szilagyi, M. Zrinyi, Magnetic field-responsive smart polymer composites Adv. Polym. Sci. 206 (2007) 137-189.

[10] S.R. Sershen, G.A. Mensing, M. Ng, N.J. Halas, D.J. Beebe, J.L. West, Independent optical control of microfluidic valves formed from optomechanically responsive nanocomposite hydrogels. Adv. Mater. 17(11) (2005) 1366-1368.

[11] N.S. Satarkar, J.Z. Hilt, Magnetic hydrogel nanocomposites for remote controlled pulsatile drug release. J. Control. Rel. 130 (2008) 246-251.

[12] S.R. Sershen, S.L. Westcott, N.J. Halas, J.L. West, Temperature-sensitive polymer-nanoshell composites for photothermally modulated drug delivery. J. Biomed. Mater. Res. 51(3) (2000) 293-298.

[13] D.J. Beebe, J.S. Moore, J.M. Bauer, Q. Yu, R.H. Liu, C. Devadoss, B.-H. Jo, Functional hydrogel structures for autonomous flow control inside microfluidic channels. Nature 404(6778) (2000) 588-590.

[14] Q. Yu, J.M. Bauer, J.S. Moore, D.J. Beebe, Responsive biomimetic hydrogel valve for microfluidics. Appl. Phys. Lett. 78(17) (2001) 2589-2591.

[15] D.T. Eddington, D.J. Beebe, A valved responsive hydrogel microdispensing device with integrated pressure source. Journal of Microelectromechanical Systems 13(4) (2004) 586-593.

[16] C. Liu, P. Joong Yull, Y. Xu, S. Lee, Arrayed pH-responsive microvalves controlled by multiphase laminar flow. Journal of Micromechanics and Microengineering 17 (2007) 1985-1991.

[17] A. Baldi, G. Yuandong, P.E. Loftness, R.A. Siegel, B. Ziaie, A hydrogel-actuated environmentally sensitive microvalve for active flow control. Journal of Microelectromechanical Systems 12(5) (2003) 613-621.

[18] D.T. Eddington, R.H. Liu, J.S. Moore, D.J. Beebe, An organic self-regulating microfluidic system. Lab Chip 1(2) (2001) 96-99.

[19] M.E. Harmon, M. Tang, C.W. Frank, A microfluidic actuator based on thermoresponsive hydrogels. Polymer 44(16) (2003) 4547-4556.

[20] J. Wang, Z. Chen, M. Mauk, K.-S. Hong, M. Li, S. Yang, H.H. Bau, Self-Actuated, Thermo-Responsive Hydrogel Valves for Lab on a Chip. Biomedical Microdevices 7(4) (2005) 313-322.

[21] A. Richter, D. Kuckling, S. Howitz, G. Thomas, K.F. Arndt, Electronically controllable microvalves based on smart hydrogels: magnitudes and potential applications. Journal of Microelectromechanical Systems 12(5) (2003) 748-753.

[22] C. Yu, S. Mutlu, P. Selvaganapathy, C.H. Mastrangelo, F. Svec, J.M.J. Frechet, Flow control valves for analytical microfluidic chips without mechanical parts based on thermally responsive monolithic polymers. Anal. Chem. 75(8) (2003) 1958-1961.

[23] A.K. Agarwal, L. Dong, D.J. Beebe, H. Jiang, Autonomously-triggered microfluidic cooling using thermo-responsive hydrogels. Lab Chip 7(3) (2007) 310-315.

[24] Q. Luo, S. Mutlu, Y.B. Gianchandani, F. Svec, J.M.J. Fréchet, Monolithic valves for microfluidic chips based on thermoresponsive polymer gels. Electrophoresis 24(21) (2003) 3694-3702.

[25] G. Chen, F. Svec, D.R. Knapp, Light-actuated high pressure-resisting microvalve for on-chip flow control based on thermo-responsive nanostructured polymer. Lab Chip 8(7) (2008) 1198-1204.

[26] S. Sugiura, K. Sumaru, K. Ohi, K. Hiroki, T. Takagi, T. Kanamori, Photoresponsive polymer gel microvalves controlled by local light irradiation. Sensors and Actuators A: Physical 140(2) (2007) 176-184.

[27] N.S. Satarkar, J.Z. Hilt, Nanocomposite hydrogels as remote controlled biomaterials. Acta Biomater. 4 (2008) 11-16.

[28] N. Pamme, Magnetism and microfluidics. Lab Chip 6(1) (2006) 24-38.

[29] Y.-J. Liu, S.-S. Guo, Z.-L. Zhang, W.-H. Huang, D. Baigl, Y. Chen, D.-W. Pang, Integration of minisolenoids in microfluidic device for magnetic bead--based immunoassays. J. Appl. Phys. 102(8) (2007) 084911-084916.

[30] A.C. Siegel, S.S. Shevkoplyas, D.B. Weibel, D.A. Bruzewicz, A.W. Martinez, G.M. Whitesides, Cofabrication of electromagnets and microfluidic systems in poly(dimethylsiloxane). Angew. Chem. 118(41) (2006) 7031-7036.

[31] R. Hahn, S. Krumbholz, H. Reichl, Low profile power inductors based on ferromagnetic LTCC technology. Electronic Components and Technology Conference, 2006. Proceedings. 56th, 2006, p. 6 pp.

[32] H. Kim, Y. Kim, J. Kim, An integrated LTCC inductor embedding NiZn ferrite. Magnetics Conference, 2006. INTERMAG 2006. IEEE International, 2006, pp. 353-353.

CHAPTER 6

HYDROGEL-MWCNT NANOCOMPOSITES: SYNTHESIS, CHARACTERIZATION, AND HEATING WITH RADIOFREQUENCY FIELDS

This chapter is based on work published as:

N.S. Satarkar, D. Johnson, B. Marrs, R. Andrews et al., Synthesis and characterization of temperature responsive hydrogel-MWCNT nanocomposites, J Appl Polymer Sci, In Press.

6.1 Summary

Hydrogel nanocomposites are attractive biomaterials for numerous applications including tissue engineering, drug delivery, cancer treatment, sensors, and actuators. Here, we present a nanocomposite of multi-walled carbon nanotubes (MWCNTs) and temperature responsive N-isopropylacrylamide hydrogels. The lower critical solution temperature (LCST) of the nanocomposites was tailored for physiological applications by the addition of varying amounts of acrylamide (AAm). The addition of nanotubes contributed to interesting properties, including tailorability of temperature responsive swelling, and mechanical strength of the resultant nanocomposites. The mechanical properties of the nanocomposites were studied over a range of temperatures (25-55°C) to characterize the effect of nanotube addition. A radiofrequency (RF) field of 13.56 MHz was applied to the nanocomposite discs, and the resultant heating was characterized using infrared

thermography. This is the first report on the use of radiofrequency to remotely heat MWCNT-hydrogel nanocomposites.

6.2 Introduction

Hydrogels are hydrophilic polymeric networks that can imbibe a large amount of biological fluids including water and can swell several times their dry volume. Hydrogels have good biocompatibility and applications in medical and pharmaceutical fields including controlled drug delivery, tissue engineering, diagnostic devices, contact lenses, and biosensors.[1] Responsive hydrogels are a class of hydrogels with swelling properties dependent on the surrounding environment such as pH, temperature, the presence of a particular molecule, or ionic strength. Responsive hydrogels have been demonstrated in various applications such as sensors, pulsatile drug release devices, and valves for active flow control in microfluidic devices.[2, 3]

Hydrogel nanocomposites are synthesized by incorporating nanoparticles into a hydrogel matrix. Nanoparticulates can impart unique properties to the matrix, such as enhanced mechanical strength, drug release profile, remote actuation capabilities, and biological interactions. Several researchers have developed hydrogel nanocomposites with different particulates including clay, gold, silver, iron oxide, carbon nanotubes, hydroxyapetite, and tricalcium phosphate.[4] Hydrogel nanocomposites have been demonstrated in numerous biomedical applications such as tissue engineering scaffolds,[5] remote controlled drug delivery systems,[6] sensors,[7] and actuators.[8, 9] In recent years, interest in incorporating carbon nanotubes into hydrogel matrices has grown.

Carbon nanotubes (CNTs) are cylindrical graphite hollow tubes with one or more concentric layers. They have high aspect ratios and unique mechanical, thermal, and

electrical properties. Superior thermal and electrical properties of CNTs are useful for a wide range of applications including electrochemical and electronic devices, sensors, and probes.[10] The high mechanical strength makes them attractive materials for polymer reinforcement.[11] CNTs have attracted a lot of interest in biological applications including tissue engineering, biosensors, drug delivery, imaging, and cancer treatment.[12] Their ease of surface functionalizations allows for the attachment of desired molecules to enhance solubility, biocompatibility, and applications.[13]

The incorporation of small amounts of CNTs can significantly enhance the properties of the hydrogel matrix. It was reported that the addition of CNTs to collagen increased the electrical conductivity, and the resultant nanocomposite promoted good cell viability.[14] Bhattacharyya *et al* reported four-fold increase in the storage and loss moduli of hyaluronic acid hydrogels by incorporating 0.06 wt% of single-walled carbon nanotubes (SWCNT).[15] Similarly, a few studies have investigated the addition of CNTs into chitosan hydrogels for the purpose of mechanical enhancement,[16] and pH and electrical actuation.[17]

Hydrogel-CNT nanocomposites were also demonstrated for potential applications such as sensors and actuators. Shi et al. demonstrated actuators based on multi-walled carbon nanotubes (MWCNTs) and polyvinyl alcohol hydrogels with DC electric field as the stimulus.[18] Due to the fast electron transfer kinetics of CNTs, hydrogel-CNT nanocomposites are being pursued in sensor applications for the detection of a variety of biomolecules including ethanol, glutamate, and glucose.[19, 20] In another study, the composite films of poly-N-isopropylacrylamide (NIPAAm) and aligned MWCNT arrays showed fast wetting and dewetting behaviors. The electrical conductance of these films

was found to be dependent on temperature and water content and, hence, may have applications as temperature and humidity sensors.[7]

In addition, CNTs can be heated by microwaves,[21] radiofrequency fields,[22] and near-IR light (700-1100 nm).[23] This property can be used for a variety of applications such as cancer treatment,[22, 24] antimicrobial agents,[25] and the heating of polymer nanocomposites to drive the polymer transitions.[26-28] Near-IR light was used to remotely trigger shape memory transitions of elastomer-CNT composites.[26, 27] Fujigaya et al. embedded SWCNTs into temperature responsive NIPAAm hydrogels and showed that application of a near-IR laser could heat the nanocomposites leading to their collapse.[28] In another study, Miyako et al. showed the near-IR driven thermal transition of nanocomposites obtained by incorporating SWCNTs in NIPAAm and agarose hydrogels.[29] However, to the best of our knowledge, very little work has been reported so far on the RF heating of CNTs, with no reports on RF heating of CNT-nanocomposites.

In this chapter, we report synthesis and characterization of the MWCNT nanocomposites of NIPAAm-acrylamide (AAm). NIPAAm is a negative temperature responsive hydrogel, and the addition of AAm to NIPAAm can be used to increase the lower critical solution temperature (LCST), placing it close to the human body temperature (37^{o}C).[30] MWCNT were chosen as the nanoparticulate material because of the potential of enhancements in thermal, electrical, and mechanical properties of the resultant nanocomposites, as well as the capability to remotely heat them with RF. If the heat generated by the nanotubes is sufficient to cause a temperature increase above LCST, the NIPAAm hydrogel matrix will collapse. It is hence possible to remotely heat and actuate

the hydrogel-MWCNT nanocomposite. Although there are studies showing toxicity of MWCNTs,[31] encapsulation of MWCNTs in a non-degradable hydrogel matrix can minimize direct exposure when implanted *in vivo* and reduce their potential toxicity.

The morphology, swelling behavior, and mechanical properties of the nanocomposites were characterized to evaluate the effect of adding different amounts of MWCNTs on the hydrogel properties. Finally, a RF field of 13.56 MHz was applied to the hydrogel nanocomposite and the heating effect was characterized for different MWCNT loadings. It is possible to drive the swelling transition of CNT nanocomposites with RF application. To the best of our knowledge, this is the first report on RF heating of MWCNT hydrogel nanocomposites. These nanocomposites can be useful for a range of applications including remote controlled drug delivery, microfluidic valves/pumps, and thermal therapy.

6.3 Experimental

6.3.1 Hydrogel synthesis

N-isopropylacrylamide (NIPAAm), acrylamide (AAm), and 2,2-Azobisisobutyronitrile (AIBN) were purchased from Sigma-Aldrich. Tetra (ethylene glycol) dimethacrylate (TEGDMA) was obtained from Polysciences, Inc. MWCNTs were a generous donation from the Center for Applied Energy Research, at the University of Kentucky. MWCNT had a diameter of 20-30 nm and a length of over 80 μm. TEGO Dispers 710 was obtained from Degussa. All reagents were used as received. Fisher Scientific Sonic Dismembrator Model 500 was used for the mixing of the prepared monomer solutions. Scanning electron microscope Hitachi S4300 was used to investigate the morphology of the nanocomposites.

For the first set of hydrogels, AAm content was gradually increased to obtain gels with molar ratios of NIPAAm:AAm as 100:0, 90:10, 80:20, and 70:30. TEGDMA was added as a crosslinker to obtain 1 mol% (NIPAAm and AAm combined). Ethanol was used as the solvent for polymerization and was twice the weight of the combined monomers and crosslinker. Thermal initiator AIBN was then added as 1 wt % of the combined weight of monomers and crosslinker. The mixture was sonicated to ensure complete dissolution and uniformity. The solution was then added to an assembly of clamped glass plates separated by a 0.75 mm Teflon spacer. The assembly was then placed inside an oven at 60°C for 24 hours.

For the second set of hydrogels, NIPAAm:AAm in molar ratio of 80:20 were mixed and increasing amounts of MWCNTs were added to obtain gels with loadings of 0, 1, 2.5, and 5 wt% of the total of monomer and crosslinker. Ethanol and TEGDMA were added as mentioned above. Surfactant TEGO Dispers 710 was added at 4 times the weight of MWCNT to enhance their dispersion. Solutions were then sonicated for 5 minutes to disperse nanotubes uniformly throughout the solution. The initiator was added, and the solutions were polymerized as described above.

After polymerization, the films were removed and washed in deionized water for a week, by changing the water every day to remove unreacted components.

6.3.2 Swelling study analysis

After washing, the gels were cut into 15 mm diameter discs and placed in a vacuum oven until completely dry. The swelling studies were carried out for hydrogels with different NIPAAm:AAm ratios and with different MWCNT loadings by methods described in

appendix D.1.[32] Swelling studies were done in the temperature range of 25-55^{o}C, and the volume swelling ratio (Q) was calculated.

6.3.3 Dynamic mechanical analysis (DMA)

All mechanical analyses were completed using dynamic mechanical analysis (DMA) (TA Instruments Q800) in the *DMA multi-frequency-Strain* mode on a compression plate setup. The compression plate setup was modified to ensure that gels stay in aqueous environment throughout the analysis. DMA analysis of the nanocomposites with 0, 1, and 5 wt% MWCNTs was performed in the temperature range of 25-55°C. The nanocomposites were equilibrated at the set temperature for at least 24 hours, cut in circular discs of diameter 3 cm, and promptly placed on the compression plates. The sample chamber of the DMA was heated to the target temperature and held isothermally throughout the experiment. An amplitude of 25 µm was applied to the specimen at a test frequency of 1 Hz. Values of storage modulus, loss modulus, and tan delta were collected and averaged over 15 minutes.

6.3.4 Heating in RF fields

After washing, hydrogel films were placed in a 70^{o}C water bath for at least 24 hours to allow them to equilibrate. Hydrogel films were then cut into 15 mm diameter discs and dried in a vacuum oven. Dry hydrogel discs with 0-5 wt% of MWCNTs were subjected to RF field of 13.56 MHz and power output of 400 W for 4 minutes. RF 5S (RF Power Products) power source, with a maximum power output of 550 W, connected to a Variomatch (Dressler) matching network was used to generate the radiofrequency field. The solenoid had a diameter of 11 cm, and a total of 8 turns. Infrared (IR) camera (SC 4000, FLIR Systems) was used to collect images and record temperatures.

The surface temperatures of the disc were recorded with the IR camera, and results were averaged over three samples. The temperature readings were not affected by the changes in emissivity of samples, because the samples were black in colour (with approximate emissivity ~1.0). To avoid electrical interference, the IR camera was separately mounted far enough from the solenoid. The IR imaging technique has been used previously and proven to be effective in material characterization.[33]

6.4 Results and discussion

6.4.1 Hydrogel characterization

The dispersion of nanocomposites appeared uniform to the naked eye. 0 and 5 wt% MWCNT loaded hydrogel nanocomposites were freeze fractured and several cross-sectional SEM pictures were collected. **Figure 6.1** shows the representative images. The 5 wt% loaded nanocomposites show a homogeneous MWCNT dispersion. Uniform dispersion of nanotubes can ensure enhanced mechanical, thermal, and electrical properties. The optimal dispersion will also ensure homogeneous heating of these nanocomposites when exposed to RF fields or near-IR light.

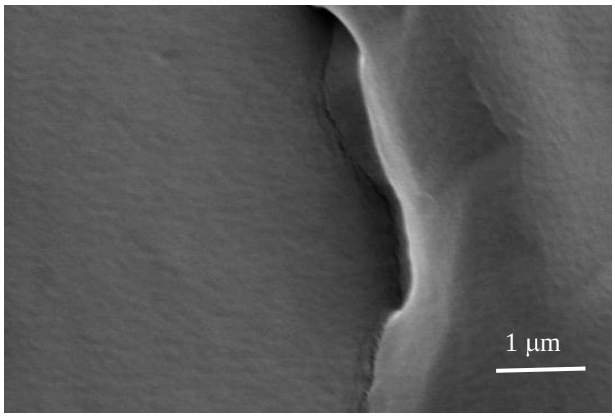

(a)

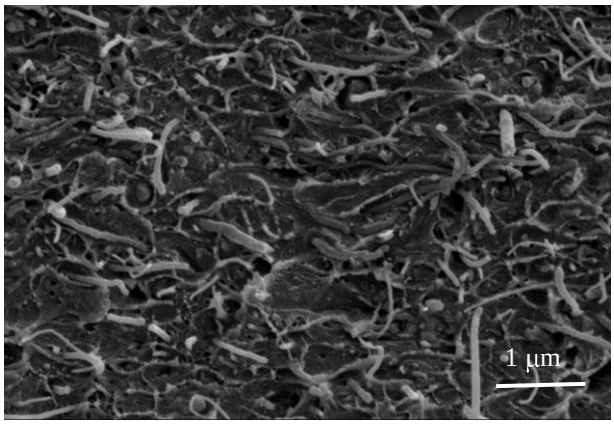

(b)

Figure 6.1. Cross-sectional SEM pictures of NIPAAm-AAm hydrogel matrix with (a) 0 and (b) 5 wt% of MWCNTs.

6.4.2 Swelling study analysis

6.4.2.1 Effect of increasing acrylamide

Swelling studies were performed at varying temperatures to look at the effect of increasing amounts of AAm on swelling transition of the hydrogel system. The purpose of varying the NIPAAm:AAm ratios was to evaluate the effect of AAm on LCST and to obtain a system with desirable actuation around human physiological conditions (37°C).

As shown in **figure 6.2**, increasing the amount of AAm shifted the LCST transition to higher temperatures. The hydrogel system without AAm collapsed completely at 32^{o}C, while the system with 30 mol% of AAm collapsed at 55^{o}C. AAm is more hydrophilic than NIPAAm, and it is expected that the addition of AAm would increase the extent of swelling. All systems follow this behavior except NIPAAm:AAm 70:30 system in temperature range of 25-32^{o}C. More analysis is needed to further understand the reasons behind this phenomenon. For efficient actuation, it is desirable to have a system that exhibits large volume changes with small changes in temperature. This is controlled to some extent by the amount of crosslinker in the hydrogels. The NIPAAm:AAm 80:20 hydrogel with 1 mol% of TEGDMA crosslinker gave significant actuation (ΔQ) around physiological temperature (37^{o}C) and hence was chosen for the addition of varying amounts of MWCNTs.

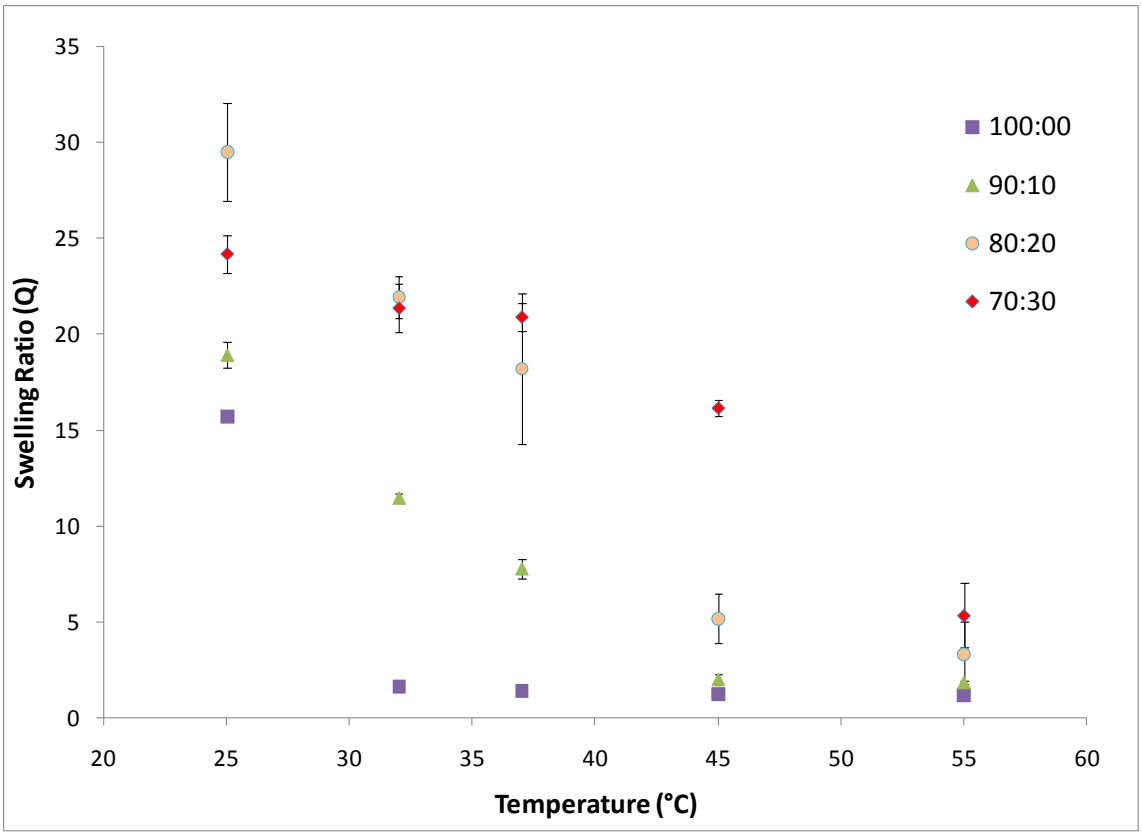

Figure 6.2. Effect of temperature on equilibrium swelling of hydrogels. The numbers indicate molar ratios of NIPAAm:AAm in hydrogels cross-linked with 1 mol% of TEGDMA. N=3±SD

6.4.2.2 Effect of MWCNT addition

Figure 6.3 shows the effect of MWCNT addition on the swelling properties of hydrogel with NIPAAm:AAm in 80:20 molar ratio and 1 mol% of TEGDMA cross-linking. It is evident that the addition of MWCNTs significantly decreased the swelling ratios, with the highest effect on addition of 5 wt% of MWCNTs. This could be attributed to the hydrophobic nature of MWCNT and is consistent with other reports in the literature that have looked at the changes in swelling properties due to the addition of MWCNTs.[15] On the other hand, the addition of MWCNTs did not affect the LCST transition

temperature range. The hydrogels were collapsed above 45°C and, hence, there was minimal effect of temperatures or MWCNT loadings above that point. In particular, the hydrogels with 5 wt% of MWCNTs gave a ΔQ of about 7 between 37 and 45°C, which is significant from the application point of view.

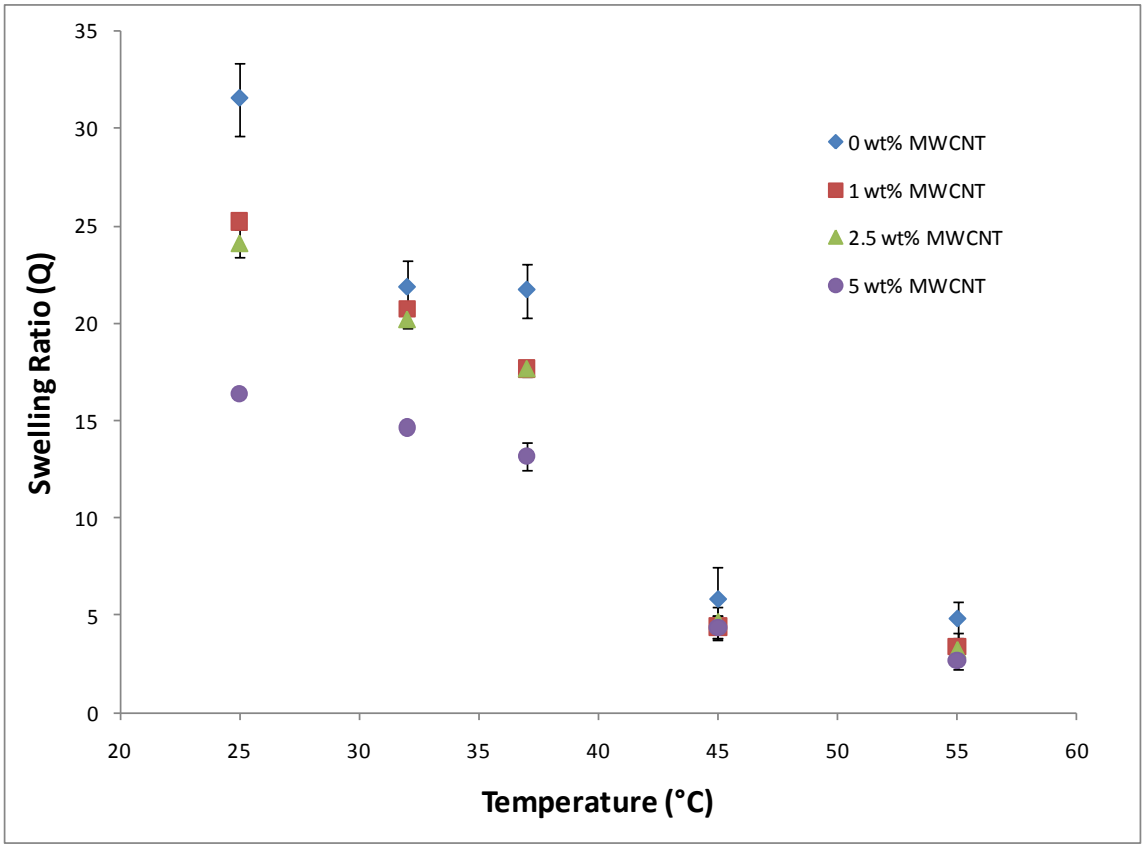

Figure 6.3. Effect of temperature on the equilibrium swelling of hydrogels with varying amounts of MWCNTs. All systems had NIPAAm:AAm in the ratio of 80:20 with 1mol% of TEGDMA as cross-linker. N=3±SD

6.4.3 Dynamic mechanical analysis

Dynamic mechanical analysis (DMA) was performed on hydrated gel discs with 3 different amounts of MWCNT loadings to compare the effects of increased nanotubes on mechanical properties. It is evident from **figure 6.4** that for every system, storage

modulus increased with increasing temperature up to 45°C. The hydrogels collapsed with increasing temperature, reducing the amount of water inside them, and thus they exhibited higher mechanical strength. The storage modulus of 0 and 1 wt% of MWCNT loaded gels peaked at 45°C. This effect was not observed for the 5 wt% of MWCNTs, and more studies are needed to understand this phenomenon.

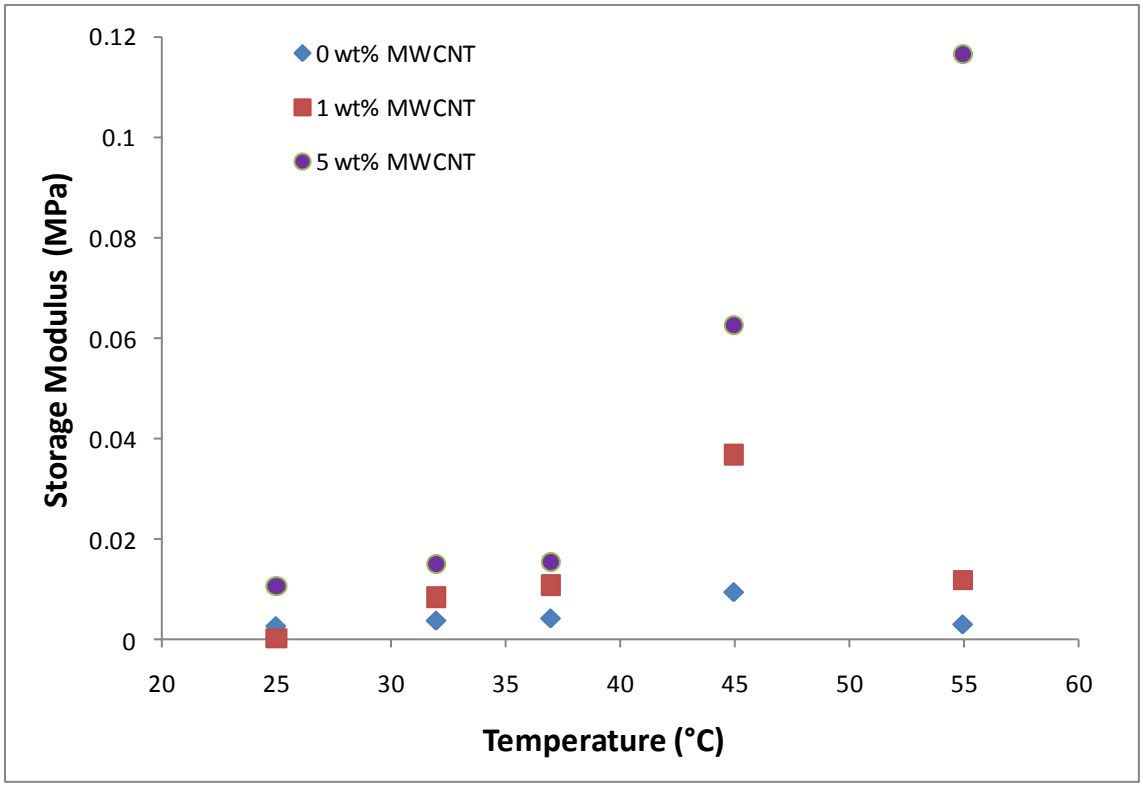

Figure 6.4. Storage modulus vs. temperature for hydrogels with varying MWCNT loadings. All systems had NIPAAm:AAm in ratio of 80:20 with 1 mol% of TEGDMA as crosslinker.

There was also an obvious enhancement in storage modulus with increasing amounts of MWCNTs. Due to addition of 20 mol% of AAm and low crosslinker content (1 mol%), these hydrogels were highly hydrated at lower temperatures and had low mechanical strength. The manipulation of mechanical properties is crucial for implant applications.

MWCNTs possess high mechanical strength and hence their addition leads to better mechanical properties. We see about a 5-fold increase in storage moduli with an addition of 5 wt% of MWCNTs in temperature range of 25-45^{o}C. In this work, non-functionalized MWCNT were physically entrapped in the hydrogel matrix. However, it is expected that the enhancements will be much more if MWCNTs were functionalized to enhance the MWCNT-polymer interactions. Favorable nanotube-polymer interfacial interactions can lead to effective load transfer from polymer to nanotubes.[34] Future studies will be done to further understand the effect of MWCNT reinforcement.

6.4.4 Heating in RF fields

There are some recent reports on the heating of MWCNT-hydrogel nanocomposites with near-IR light.[28, 29] Radiofrequency at 13.56 MHz can be used as an alternative for near-IR, and has been investigated for cancer therapy applications using CNTs.[22] The main advantage of RF over near-IR light is it can penetrate deeper in microfluidic devices or in case of *in vivo* applications. When the MWCNT nanocomposites were subjected to a RF field of 13.56 MHz, there was a significant increase in temperatures. Metallic thermocouples can heat in RF fields, hence infrared (IR) thermography was used to monitor the nanocomposite temperatures. **Figure 6.5** shows the IR images of RF heating of the dry hydrogel nanocomposites containing 2.5 wt% of MWCNTs. Starting at 25^{o}C, the surface temperature of the nanocomposite disc increased to about 46^{o}C in 4-minute RF exposure.

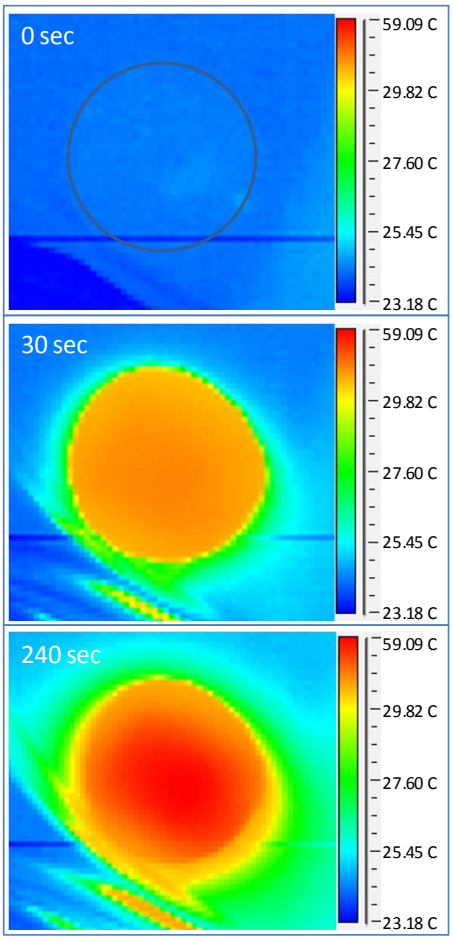

Figure 6.5. IR images of heating of dry nanocomposites with 2.5 wt% of MWCNT on RF application, at different time points.

Increase in temperatures (ΔT) was plotted for dry nanocomposites with 0-5 wt% of MWCNT loadings and is shown in **figure 6.6**. The temperature of the hydrogel with 0 wt% of MWCNTs increased by about 5^{o}C, probably due to resistive heating of polymer. The heating ability increased by increasing the amount of MWCNTs, with ΔT of about 35^{o}C in 4 minutes for the samples with 5 wt% of MWCNTs.

This study indicates a proof of concept that RF can be potentially used for remote heating of the CNT-hydrogel nanocomposites. The remotely actuated nanocomposites can be useful for a variety of biological and other applications. For example, previous studies

have demonstrated that remotely actuated magnetic hydrogel nanocomposites are attractive materials for drug delivery and for microfluidic flow control.[6, 8] The study of hydrogel nanocomposite heating in swollen state and the effect of dispersion on heating performance is underway and will be reported in future publications.

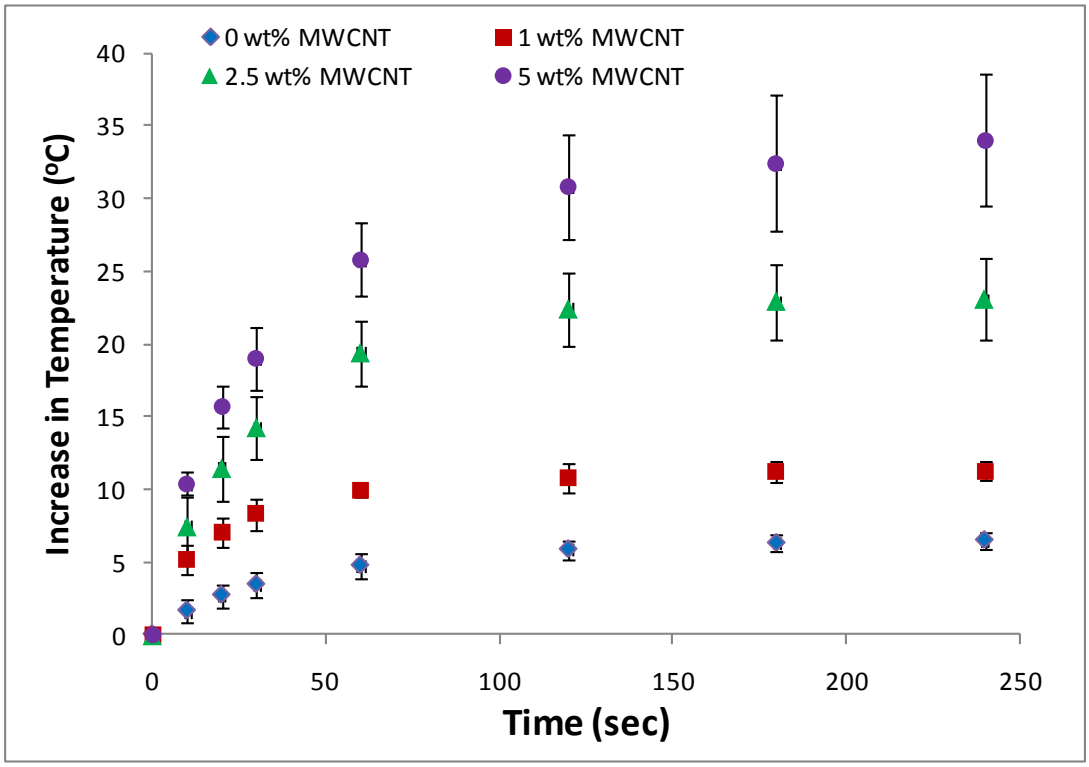

Figure 6.6. Increase in surface temperatures (ΔT) of dry hydrogel nanocomposites with different loadings of MWCNTs during a 4-minute RF exposure. N=3±SD

6.5 Conclusions

NIPAAm-MWCNT nanocomposites were successfully synthesized. The effect of varying the amount of AAm and MWCNTs on temperature responsive swelling properties of NIPAAm hydrogels was characterized. The addition of AAm to the hydrogels shifted the swelling transition (LCST) to higher temperatures, which is critical for physiological applications. The incorporation of MWCNTs to the hydrogels decreased the extent of

swelling due to hydrophobic effects. MWCNTs enhanced mechanical properties of hydrogels and the enhancement can be tailored by the concentration of MWCNTs. Applying a RF field of 13.56 MHz significantly heated the nanocomposites, and the intensity of resultant heating was dependent on MWCNT loadings. The nanocomposites showed unique properties and, therefore, they demonstrate great promise for use in different biomedical applications including tissue engineering, remote controlled drug delivery devices, and cancer treatment.

6.6 References

[1] N.A. Peppas, J.Z. Hilt, A. Khademhosseini, R. Langer, Hydrogels in biology and medicine: from molecular principles to bionanotechnology. Adv. Mater. 18 (2006) 1345-1360.

[2] E.S. Gil, S.M. Hudson, Stimuli-reponsive polymers and their bioconjugates. Prog. Polym. Sci. 29(12) (2004) 1173-1222.

[3] L. Dong, H. Jiang, Autonomous microfluidics with stimuli-responsive hydrogels. Soft Matter 3(10) (2007) 1223-1230.

[4] R.A. Frimpong, J.Z. Hilt, in: N. A. Peppas, J. Z. Hilt and J. B. Thomas (Eds.), Nanotechnology in Therapeutics: Current Technology and Applications, Horizon Scientific Press, Norfolk, 2007, pp. 241-256.

[5] M.B. Wang, Y.B. Li, J.Q. Wu, F.L. Xu, Y. Zuo, J.A. Jansen, In vitro and in vivo study to the biocompatibility and biodegradation of hydroxyapatite/poly(vinyl alcohol)/gelatin composite. Journal of Biomedical Materials Research Part A 85A(2) (2008) 418-426.

[6] N.S. Satarkar, J.Z. Hilt, Magnetic hydrogel nanocomposites for remote controlled pulsatile drug release. J. Control. Rel. 130(3) (2008) 246-251.

[7] Z. Yang, Z. Cao, H. Sun, Y. Li, Composite films based on aligned carbon nanotube arrays and a poly(N-isopropyl acrylamide) hydrogel. Adv. Mater. 20(11) (2008) 2201-2205.

[8] S.R. Sershen, G.A. Mensing, M. Ng, N.J. Halas, D.J. Beebe, J.L. West, Independent optical control of microfluidic valves formed from optomechanically responsive nanocomposite hydrogels. Adv. Mater. 17(11) (2005) 1366-1368.

[9] N.S. Satarkar, W. Zhang, R.E. Eitel, J.Z. Hilt, Magnetic hydrogel nanocomposites as remote controlled microfluidic valves. Lab Chip 9(12) (2009) 1773.

[10] R.H. Baughman, A.A. Zakhidov, W.A. de Heer, Carbon nanotubes--The route toward applications. Science 297(5582) (2002) 787-792.

[11] J.N. Coleman, U. Khan, Y.K. Gun-ko, Mechanical reinforcement of polymers using carbon nanotubes. Adv. Mater. 18 (2006) 689-706.

[12] F. Lu, L. Gu, M.J. Meziani, X. Wang, P.G. Luo, L.M. Veca, L. Cao, Y.-P. Sun, Advances in bioapplications of carbon nanotubes. Adv. Mater. 21(2) (2009) 139-152.

[13] A. Bianco, K. Kostarelos, C.D. Partidos, M. Prato, Biomedical applications of functionalised carbon nanotubes. Chemical Communications 5 (2005) 571-577.

[14] R.A. MacDonald, C.M. Voge, M. Kariolis, J.P. Stegemann, Carbon nanotubes increase the electrical conductivity of fibroblast-seeded collagen hydrogels. Acta Biomater. 4(6) (2008) 1583-1592.

[15] S. Bhattacharyya, S. Guillot, H. Dabboue, J.-F. Tranchant, J.-P. Salvetat, Carbon nanotubes as structural nanofibers for hyaluronic acid hydrogel scaffolds. Biomacromolecules 9(2) (2008) 505-509.

[16] S.-F. Wang, L. Shen, W.-D. Zhang, Y.-J. Tong, Preparation and mechanical properties of chitosan/carbon nanotubes composites. Biomacromolecules 6(6) (2005) 3067-3072.

[17] S. Ozarkar, M. Jassal, A.K. Agrawal, pH and electrical actuation of single walled carbon nanotube/chitosan composite fibers. Smart Materials and Structures 17(5) (2008) 055016.

[18] J. Shi, Z.X. Guo, B. Zhan, H. Luo, Y. Li, D. Zhu, Actuator based on MWNT/PVA hydrogels. J. Phys. Chem. B 109(31) (2005) 14789-14791.

[19] Y.-C. Tsai, J.-D. Huang, C.-C. Chiu, Amperometric ethanol biosensor based on poly(vinyl alcohol)-multiwalled carbon nanotube-alcohol dehydrogenase biocomposite. Biosensors and Bioelectronics 22(12) (2007) 3051-3056.

[20] S. Chakraborty, C.R. Raj, Mediated electrocatalytic oxidation of bioanalytes and biosensing of glutamate using functionalized multiwall carbon nanotubes-biopolymer nanocomposite. J. Electroanal. Chem. 609(2) (2007) 155-162.

[21] K.R. Paton, A.H. Windle, Efficient microwave energy absorption by carbon nanotubes. Carbon 46(14) (2008) 1935-1941.

[22] C.J. Gannon, P. Cherukuri, B.I. Yakobson, L. Cognet, J.S. Kanzius, C. Kittrell, R.B. Weisman, M. Pasquali, H.K. Schmidt, R.E. Smalley, S.A. Curley, Carbon nanotube-enhanced thermal destruction of cancer cells in a noninvasive radiofrequency field. Cancer 110(12) (2007) 2654-2665.

[23] D. Boldor, N.M. Gerbo, W.T. Monroe, J.H. Palmer, Z. Li, A.S. Biris, Temperature measurement of carbon nanotubes using infrared thermography. Chem. Mater. 20(12) (2008) 4011-4016.

[24] P. Chakravarty, R. Marches, N.S. Zimmerman, A.D.-E. Swafford, P. Bajaj, I.H. Musselman, P. Pantano, R.K. Draper, E.S. Vitetta, Thermal ablation of tumor cells with antibody-functionalized single-walled carbon nanotubes. Proceedings of the National Academy of Sciences 105(25) (2008) 8697-8702.

[25] J.-W. Kim, E.V. Shashkov, E.I. Galanzha, N. Kotagiri, V.P. Zharov, Photothermal antimicrobial nanotherapy and nanodiagnostics with self-assembling carbon nanotube clusters. Lasers in Surgery and Medicine 39(7) (2007) 622-634.

[26] H. Koerner, G. Price, N.A. Pearce, M. Alexander, R.A. Vaia, Remotely actuated polymer nanocomposites[mdash]stress-recovery of carbon-nanotube-filled thermoplastic elastomers. Nat. Mater. 3(2) (2004) 115-120.

[27] L. Yang, K. Setyowati, A. Li, S. Gong, J. Chen, Reversible infrared actuation of carbon nanotube-liquid crystalline elastomer nanocomposites. Adv. Mater. 20(12) (2008) 2271-2275.

[28] T. Fujigaya, T. Morimoto, Y. Niidome, N. Nakashima, NIR laser-driven reversible volume phase transition of single-walled carbon nanotube/poly(N-isopropylacrylamide) composite gels. Adv. Mater. 20(19) (2008) 3610-3614.

[29] E. Miyako, H. Nagata, K. Hirano, T. Hirotsu, Photodynamic thermoresponsive nanocarbon-polymer gel hybrids. Small 4(10) (2008) 1711-1715.

[30] R. Yoshida, K. Sakai, T. Okano, Y. Sakurai, Modulating the phase transition temperature and thermosensitivity in N-isopropylacrylamide copolymer gels. J. Biomater. Sci., Polym. Ed. 6 (1994) 585-598.

[31] C.A. Poland, R. Duffin, I. Kinloch, A. Maynard, W.A.H. Wallace, A. Seaton, V. Stone, S. Brown, W. MacNee, K. Donaldson, Carbon nanotubes introduced into the abdominal cavity of mice show asbestos-like pathogenicity in a pilot study. Nat Nano 3(7) (2008) 423-428.

[32] R.A. Frimpong, S. Fraser, J.Z. Hilt, Synthesis and temperature response analysis of magnetic-hydrogel nanocomposites. J. Biomed. Mater. Res. A 80A(1) (2007) 1-6.

[33] M.A. Omar, B. Gharaibeh, A.J. Salazar, K. Saito, Infrared thermography (IRT) and ultraviolet fluorescence (UVF) for the nondestructive evaluation of ballast tanks' coated surfaces. NDT & E International 40(1) (2007) 62-70.

[34] Y. Hou, J. Tang, H. Zhang, C. Qian, Y. Feng, J. Liu, Functionalized few-walled carbon nanotubes for mechanical reinforcement of polymeric composites. ACS Nano 3(5) (2009) 1057-1062.

CHAPTER 7

REMOTE ACTUATION OF HYDROGEL NANOCOMPOSITES: HEATING ANALYSIS, MODELING, AND SIMULATIONS

This chapter is based on work published as:

N.S. Satarkar, S.A. Meenach, K. Anderson, J.Z. Hilt, Remote actuation of hydrogel nanocomposites: Heating analysis, modeling, and simulations, AIChE J, Accepted.

7.1 Summary

Recently, there has been increasing interest in remote heating of polymer nanocomposites for applications as actuators, microfluidic valves, drug delivery devices, and in hyperthermia treatment of cancer. In this study, magnetic hydrogel nanocomposites of poly (ethylene glycol) (PEG) with varying amounts of iron oxide nanoparticle loadings were synthesized. The nanocomposites were remotely heated using an alternating magnetic field (AMF) at three different AMF amplitudes, and the resultant temperatures were recorded. The rate of the temperature rise and the steady state temperatures were analyzed with a heat transfer model, and a correlation of heat generation per unit mass with the nanoparticle loadings was established for different AMF amplitudes. The temperature rise data of a PEG system with different swelling properties was found to be accurately predicted by the model. Furthermore, the correlations were used to simulate the temperatures of the nanocomposite and the surrounding tissue for potential hyperthermia cancer treatment applications.

7.2 Introduction

Nanoparticulates such as iron oxide nanoparticles, gold nanorods and nanoshells, and carbon nanotubes can be remotely heated with the application of specific external stimuli such as radiofrequency fields or near-infrared light.[1] The incorporation of these nanoparticulates into a polymer matrix can result in several interesting properties including improved mechanical, thermal, or electrical behavior,[2] as well as the capability of remote actuation.[3, 4] In the last few years, there have been several studies on the remote heating of polymer nanocomposites for a variety of applications such as actuators,[5-8] microfluidic valves,[9, 10] drug delivery devices,[11-15] and for hyperthermia cancer treatment.[16-19]

For example, an alternating magnetic field (AMF) has been shown to selectively induce heating and shape transition in magnetic shape memory polymer nanocomposites.[5, 8] In another study, Hawkins et al. demonstrated that addition of iron oxide nanoparticles to a degradable hydrogel matrix can allow heating upon AMF exposure, which was in turn used to manipulate the rates of degradation and drug release.[14] AMF heating has also been explored to trigger the collapse of magnetic nanocomposites of N-isopropylacrylamide (NIPAAm), a temperature responsive hydrogel. Previous chapters demonstrate the application of this phenomenon in controlled drug release and microfluidic valve applications.[10, 11, 15] In a recent study, Meenach et al. observed favorable cell viability of magnetic NIPAAm nanocomposites with NIH 3T3 murine fibroblasts and also showed heating on the application of AMF.[18] In all these studies, heating of the nanocomposites was a key factor, and precise control of the heating would further enhance the system design.

Remote heating of nanoparticles and nanocomposites can also potentially be used for hyperthermia treatment.[16, 17] For example, Wang and co-workers developed a Bioglass based degradable magnetic composite and demonstrated selective treatment of lung carcinoma cells by use of an AMF.[19] In another study, Meenach et al. synthesized magnetic PEG nanocomposites and showed ability to kill glioblastoma cells *in vitro* with magnetic nanocomposites exposed to AMF.[20] Hyperthermia is the treatment of cancer through the application of heat (41 to 44^{o}C) and has been under investigation for several decades.[21] Recently, technical advancements in selective heating of superficial and deep-seated tumors has demonstrated significant improvements in the applicability of hyperthermia.[22] A few researchers have looked at modeling magnetic fluid hyperthermia to predict most effective treatment options.[23, 24] Additionally, combination of hyperthermia with other treatments like radiation therapy and/or chemotherapy can further enhance the treatment success.[25] In addition to those based on magnetic nanoparticles, there has been significant work with polymer nanocomposites containing gold nanoparticles,[6, 9, 12] and carbon nanotubes (CNT).[4, 7, 13]

Although there have been several interesting demonstrations of remote heating of polymer nanocomposites, modeling of the remote heating still remains unexplored to the best of the author's knowledge. In this chapter, the analysis of AMF-triggered remote heating of magnetic hydrogel nanocomposites, development of a predictive heat transfer model, and *in vivo* temperature simulations are reported. Poly(ethylene glycol) (PEG) hydrogels were selected due to their biocompatibility and their applications as biomaterials, such as in cell encapsulation and controlled therapeutic delivery.[26, 27] The analysis of PEG nanocomposite heating at different iron oxide particle loadings and

AMF amplitudes was conducted, and a heat transfer model was developed to predict the nanocomposite temperatures. Furthermore, this hydrogel system was aimed at hyperthermia cancer treatment and, hence, COMSOL was used to simulate heating of a nanocomposite disc implanted in tissue.

7.3 Development of heat transfer problem

7.3.1 A model for AMF induced heating of hydrogel disc

Figure 7.1 shows a small circular disc of a magnetic hydrogel nanocomposite subjected to AMF and exposed to air. The hydrogel disc in this study was covered in Saran wrap and suspended on top of the solenoid. At any time, the temperature of the nanocomposite disc depends on the rate of heat generation due to magnetic particles and the rate of heat loss to surroundings by convection. The small dimensions of the hydrogel disc coupled with low temperature differentials result in negligible temperature gradients in the disc. Hence, the temperature of the entire disc can be assumed equal to that of the surface.

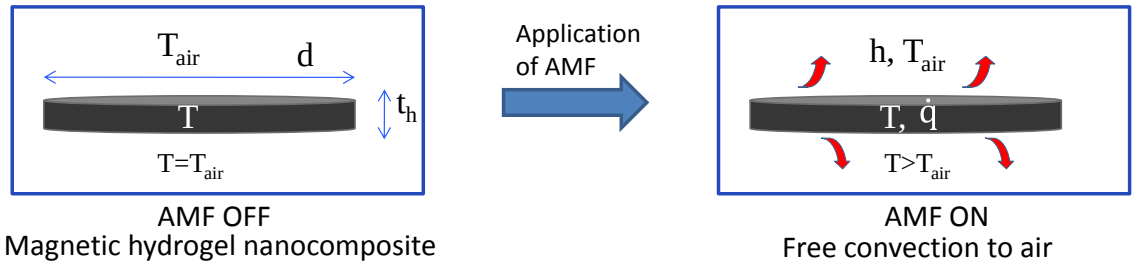

Figure 7.1. Schematic of a magnetic hydrogel nanocomposite disc subjected to AMF. Heat generation is by magnetic particles and loss is by convection to surrounding air.

The energy balance on the hydrogel disc is:

$$-hA(T - T_{air}) + \dot{q}m = \frac{d}{dt}(mC_{p,h}T) \tag{7.1}$$

where $\dot{q}$ is the rate of heat generation per unit mass of hydrogel and the surface area of the disc is defined by:

$$A = 2\Pi r^2 + 2\Pi r t_h \tag{7.2}$$

The experimental setup can be designed to minimize the change in the mass of hydrogels during heating. The heat capacity values for the hydrogel systems under consideration do not change significantly with temperature (see appendix **table B.1**). Hence, the analytical solution to equation (7.1) using separation of variables and subsequent integration is:

$$T = T_{air} + \frac{\dot{q}m}{hA}\left\{1 - \exp\left[-\frac{hA}{mC_{p,h}}t\right]\right\} \tag{7.3}$$

The value of $\dot{q}$ depends on the nanoparticle characteristics and loadings, as well as the AMF properties such as frequency and amplitude. At steady state ($t \to \infty$), equation (7.3) reduces to

$$T_{ss} = T_{air} + \frac{\dot{q}m}{hA} \qquad \text{or} \qquad \dot{q} = \frac{hA(T_{ss} - T_{air})}{m} \tag{7.4}$$

7.3.2 Formulation of the *in vivo* heat transfer problem

The $\dot{q}$ values derived from the analysis of the heat transfer to air can be used for nanocomposite heating in a different environment, if identical AMF amplitudes are achieved. The temperatures of the nanocomposite and its surroundings depend on the heat transfer process and dictate hydrogel performance as an actuator in a microfluidic device, an implant for drug delivery, or hyperthermia cancer treatment. As an example, analysis of the nanocomposite disc placed *in vivo* is discussed here with specific focus on hyperthermia applications.

In order to simulate heat transfer between the nanocomposite and surrounding tissue, finite element modeling software COMSOL3.4 was used with the bioheat equation application mode. Here, a hydrogel disc implanted at the center of a cylindrical tissue was considered as the model system (**figure 7.2**). Application of an AMF will result in selective heating of the nanocomposite disc, causing the surrounding tissue to heat.

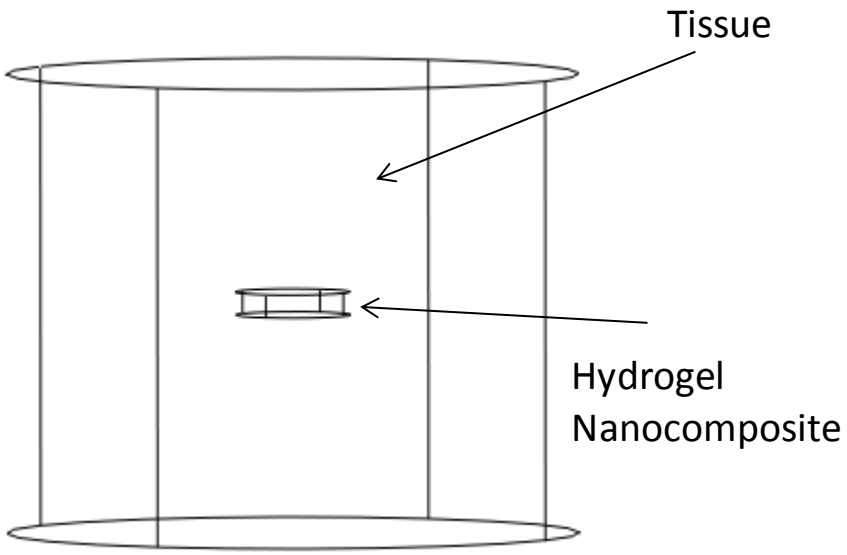

Figure 7.2. Schematic of hydrogel nanocomposite disc placed at the center of tissue.

Heat transport in the tissue is primarily by conduction with blood perfusion as the other contributing mechanism. Researchers have proposed several models for heat transfer in tissue, and Pennes bioheat equation is the most widely applied and is given below.[28, 29]

$$\rho_t C_{p,t} \frac{\partial T}{\partial t} = \nabla(k_t \nabla T) + \rho_b C_{p,b} w_b (T_b - T) + Q_{met} + Q_{ext} \qquad (7.5)$$

Heat generation from an external source (Q_{ext}) is absent in the tissue region of the model system. Temperature (T) was considered as a continuous variable in the nanocomposite

and the tissue regions of the model. The energy balance for the hydrogel nanocomposite region is:

$$\rho_h C_{p,h} \frac{\partial T}{\partial t} = \nabla(k_h \nabla T) + Q_{ext} \quad (7.6)$$

The heat generation term (Q_{ext}) is determined by particle loadings and AMF amplitude.

7.4 Experimental analysis

7.4.1 Synthesis of nanocomposites

Poly(ethylene glycol) (N=200) monomethyl ether monomethacrylate (PEG200MMA), tetra(ethylene glycol) dimethacrylate (TEGDMA) and poly(ethylene glycol) (N=400) dimethacrylate (PEG400DMA) were obtained from Polysciences, Inc. (Warrington, PA). Fe_3O_4 magnetic nanoparticles (20-30 nm diameter, 0.2% PVP-coated) were obtained from Nanostructured and Amorphous Materials, Inc. (Los Alamos, NM). Initiator ammonium persulfate (APS), accelerator N,N,N',N'-tetramethylethane-1,2-diamine (TEMED), and phosphate buffered saline (PBS) were obtained from Sigma Aldrich (St. Louis, MO). All materials were used as received.

Hydrogels were fabricated via redox polymerization using monomer, crosslinkers, and magnetic particles in varying amounts as indicated in **table 7.1**. PEG200MMA and TEGDMA were used in equimolar ratios for the hydrogel D system. Four different magnetic nanoparticle loadings were added to the hydrogel D system, to look at the effect of particle loadings on the heating in AMF. Hydrogel C2.5, on the other hand, had lower amounts of crosslinker, to test the predictive ability of the model. Ethanol was added as the solvent in 1:1 ratio in terms of total weight of the monomer and crosslinker. Various

loadings of iron oxide nanoparticles were added in case of hydrogel nanocomposites, and the prepolymer solution was bath sonicated for 20 minutes to obtain even dispersion. APS was added at 2% weight ratio and TEMED was added at 4% weight ratio of total monomer and crosslinker. After combining these materials, the solution was bath sonicated for an additional 2 minutes, and added to a glass template consisting of 2 glass plates of size 15x15 cm separated with a 0.5 mm Teflon spacer. The gels were kept in the template overnight to ensure complete polymerization and then transferred into deionized water. The water was changed every day for at least one week in order to wash out any unreacted chemicals.

Table 7.1. The compositions of 5 different types of hydrogels systems.

Abbrev.	**Monomer**	**Mol%**	**Crosslinker**	**Mol%**	**Fe_3O_4 (wt%)**
D0	PEG200MMA	50	TEGDMA	50	0
D1	PEG200MMA	50	TEGDMA	50	1
D2.5	PEG200MMA	50	TEGDMA	50	2.5
D5	PEG200MMA	50	TEGDMA	50	5
C2.5	PEG200MMA	95	PEG400DMA	5	2.5

7.4.2 Estimation of nanocomposite properties

After fabrication, the gels were removed from water, cut into circular discs of about 1.4 cm in diameter, and placed in phosphate buffered saline (PBS) solution. Swelling studies were conducted at 22 and 37^{o}C to obtain the volume swelling ratio (Q) by previously described methods (appendix D.1).[18] The volume swelling ratios were also used to estimate hydrogel density.

Heat capacity measurements were performed using differential scanning calorimeter (DSC) (TA Instruments Q200) in the quasi-isothermal modulated DSC mode with data collection for 45 minutes. Heat capacity values were measured for D0, D5, and C2.5 systems at 22 and 37^{o}C. The hydrogels were equilibrated in PBS at the set temperature for at least 24 hours and analyzed at respective temperatures.

Thermal diffusivity values were estimated using flash method with a flash light and controller system (FX 60, Balcar).[30] An infrared camera (SC4000, FLIR Systems) was used to record the surface temperatures (1500 frames per second). The nanocomposite discs were imbibed in dark brown ink to make them opaque and ensure efficient light absorption.

7.4.3 Heating in an alternating magnetic field (AMF)

Hydrogel films were cut into circular discs 8.2 mm in diameter and allowed to equilibrate in PBS overnight at 22°C. Heating was then administered remotely via AMF generated by induction power supply (Taylor Winfield, MMF-3-135/400-2) equipped with a solenoid (1.5 cm diameter, 5 turns). The hydrogel disc was covered in Saran wrap in order to limit water evaporation and then placed on top of the solenoid for exposure to the AMF. The hydrogels were exposed to the AMF at about 293 kHz and different AMF amplitudes calculated as 14.8, 19.5, and 25 kA/m. The surface temperature was recorded for first three minutes using infrared camera (AGEMA Thermovision 470). The weight and dimensions of the hydrogel discs were noted before and after heating, and the average of these values were used for calculations.

7.4.4 Statistical analysis

All experiments were performed in triplicates. MYSTAT 12 for Windows (12.02.00) was used for t-tests (paired t-test with unequal variances) to determine any significance in observed data. A p-value of <0.05 was considered statistically significant.

7.5 Results and discussion

7.5.1 Estimation of nanocomposite properties

Figure 7.3 shows the equilibrium volume swelling ratios (Q) of the hydrogels at 22 and 37^{o}C. Q values decreased slightly at 37^{o}C as compared to 22^{o}C ($p<0.05$) suggesting a slight temperature responsive nature of PEG hydrogels. This effect implies that the water content of the hydrogel systems will change slightly when exposed to 37^{o}C during *in vivo* applications. The D systems exhibited less water content than that of the C system, because of a tighter crosslinked network. Thus, the swelling properties of PEG hydrogels can be tailored by changing their composition. For the particle loadings under consideration, the addition of magnetic nanoparticles did not have significant effect ($p>0.05$) on swelling properties for the D systems.

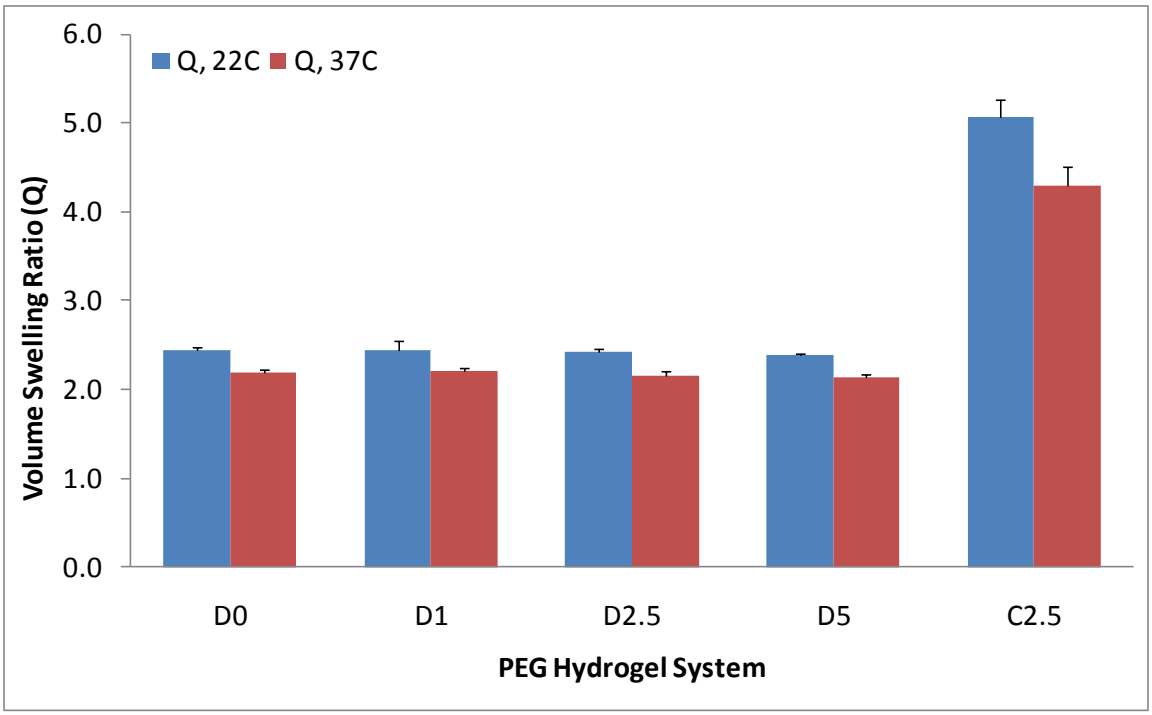

Figure 7.3. Swelling analysis of the PEG hydrogels at 22 and 37^{o}C. N=3±SD

The DSC measurements showed only a slight effect of temperature on the heat capacity (appendix **table B.1**). Additionally, there was negligible effect of particle loadings on $C_{p,h}$ values of PEG D hydrogels. The average of D0 and D5 was used as $C_{p,h}$ for calculations of all the D systems. The thermal diffusivity values were determined by flash analysis method (appendix equation B.2). Thermal conductivity values of the hydrogel nanocomposites were estimated using measured values of density, heat capacity, and thermal diffusivity (appendix equation B.3). Appendix **table B.1** summarizes the thermal conductivity values of some of the hydrogel systems.

In the calculation of heat transfer coefficients from the hydrogel surface to surrounding air, the small geometry of the hydrogel disc and low temperature differentials resulted in low values of Rayleigh numbers (Ra<100). Hence, the correlations derived by Chambers

et al. for simultaneous convection from top and bottom surfaces of a heated plate were used (appendix equations B.4, B.5).[31]

The IR camera recorded only the surface temperatures, while the temperature at the center of the disc could be significantly different. Hence, one of the key steps in the heat transfer analysis was to determine if temperature gradients exist in the disc. Since $t_h << d$, the radial temperature gradients were neglected, and the half thickness of the disc was used as the characteristic length. Using the values of convective heat transfer coefficient, thermal conductivity of hydrogel, and characteristic length, the Biot number (Bi) was calculated to be $4.1x10^{-3}$(appendix equation B.6). Thus, lumped parameter analysis (when Bi <0.1) was applied in this case and temperature gradients in the disc were neglected.

7.5.2 Heating in an alternating magnetic field (AMF)

The recorded rise in temperatures starting around 25^oC is plotted in **figure 7.4(a-c)**. Heating of magnetic particles when exposed to AMF is attributed to Neel and Brownian relaxations.[32] As expected, increasing the amount of magnetic particles resulted in higher equilibrium temperatures at the same AMF amplitude. Similarly, increasing AMF amplitude led to more heating and higher equilibrium temperatures. There was some resistive heating in the case of gels with no magnetic particles.

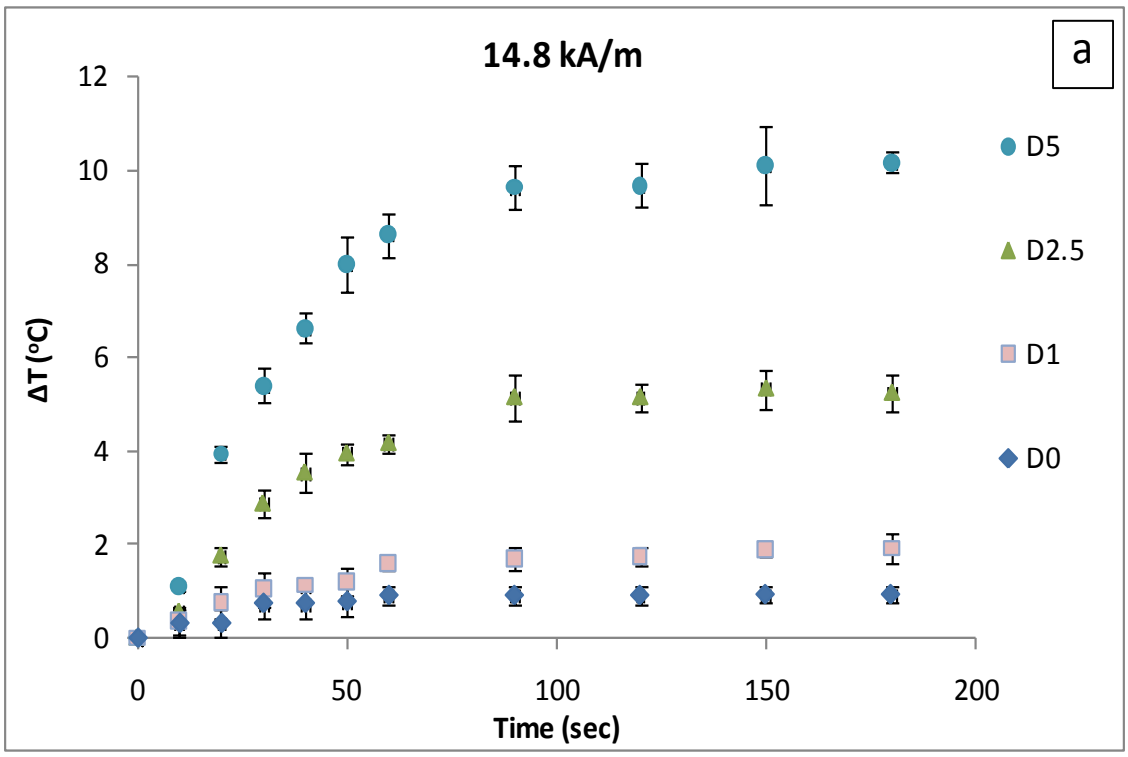
14.8 kA/m
a
ΔT (°C)
Time (sec)
D5
D2.5
D1
D0
0
2
4
6
8
10
12
0
50
100
150
200

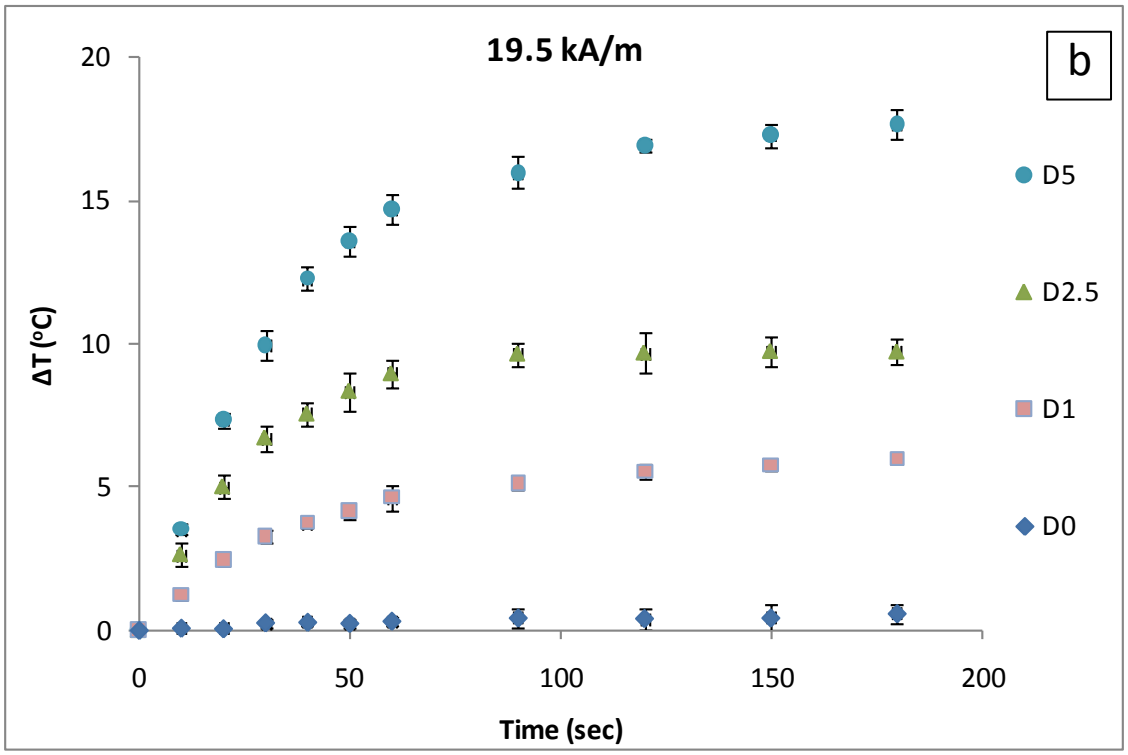
19.5 kA/m
b
ΔT (°C)
Time (sec)
D5
D2.5
D1
D0
0
5
10
15
20
0
50
100
150
200

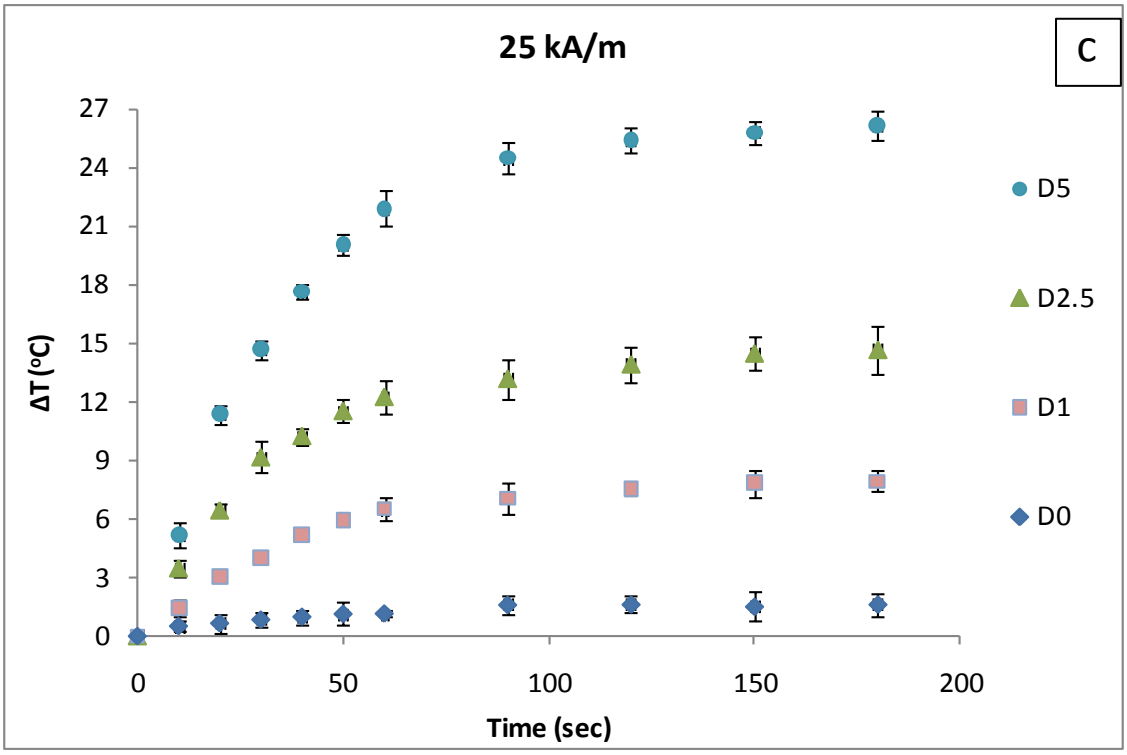

Figure 7.4(a-c). Rise in temperature of D nanocomposites for different particle loadings and AMF amplitudes, N=3±SD.

7.5.3 Comparison of experimental and predicted temperatures

Using equation (7.4) and the steady state temperature values of the D hydrogel nanocomposites (figure 7.4), $\dot{q}$ values at different particle loadings and AMF amplitudes were obtained. The $\dot{q}$ values were normalized against volume swelling ratio (Q) of the D systems at 25^{o}C, in order to allow extension to another temperature or a different hydrogel system. A linear correlation of $\dot{q}$ was obtained with the particle loadings at different AMF amplitudes.

$$\dot{q} = a\,P + b \qquad (7.7)$$

The coefficients a and b at different AMF amplitudes are summarized in **table 7.2**. It is expected that these correlations will be useful in predicting $\dot{q}$ and, in turn, predicting temperatures of the different hydrogel systems.

Table 7.2. Coefficients for $\dot{q}$ correlations at different AMF amplitudes.

AMF amplitude (kA/m)	a	b	Regression (R^2) values
14.8	0.2914	0.0473	0.987
19.5	0.5144	0.1684	0.991
25	0.6974	0.3474	0.993

A MATLAB program was developed (details presented in appendix B.4) to predict the hydrogel temperatures at different time points using equation (7.3). $\dot{q}$ correlations from equation (7.7) and coefficients in table 7.2 were used along with the measured values of heat capacities and swelling ratios. Heat transfer coefficients were estimated at every time point as the disc temperatures changed. **Figure 7.5(a-c)** shows the comparison of experimental and predicted temperature rise of D hydrogel systems. The plots at different AMF amplitudes demonstrate good fits for the temperature rise. The deviations between the experimental and predicted differentials could be attributed to the loss of water as hydrogel temperatures increased. In order to simplify the model derivation, hydrogel mass was assumed constant with time. In spite of short heating times and use of Saran wrap, weight measurements indicated up to 25% mass loss for the system that was heated the most. Overall, the heat transfer model demonstrated the capability to predict resultant temperatures if the hydrogel properties, AMF amplitude, and heat transfer coefficients are known.

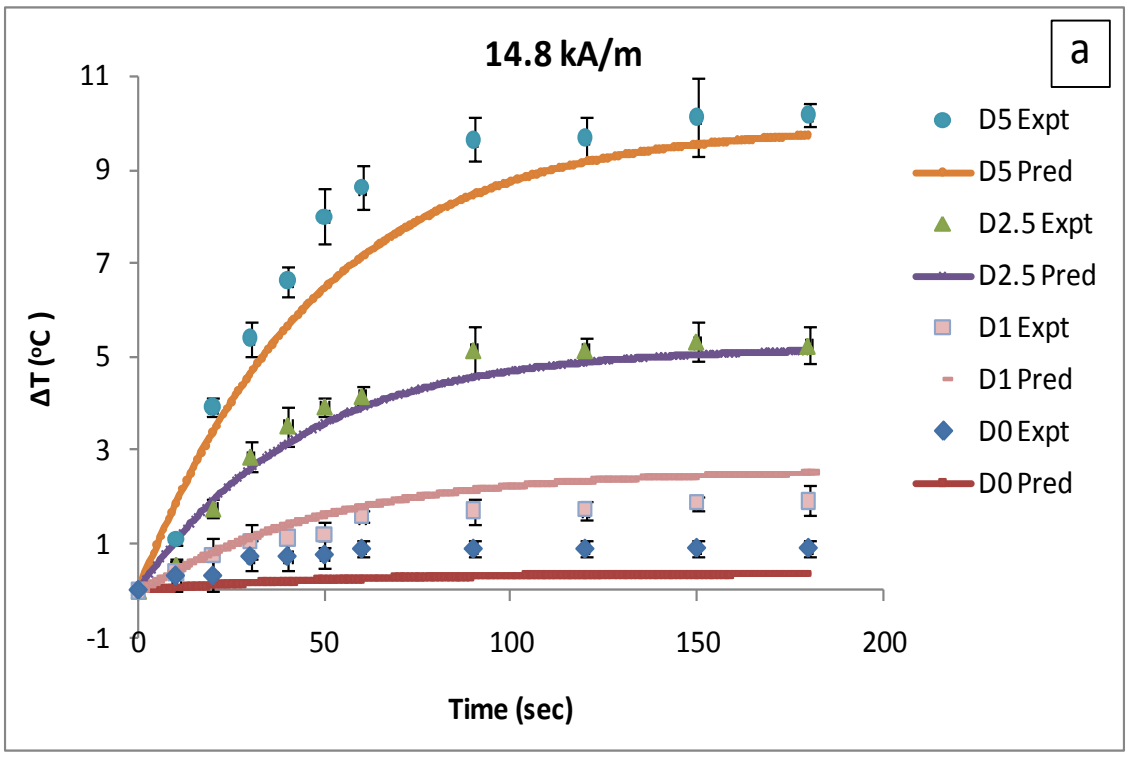
14.8 kA/m
a
ΔT (°C)
Time (sec)
D5 Expt
D5 Pred
D2.5 Expt
D2.5 Pred
D1 Expt
D1 Pred
D0 Expt
D0 Pred

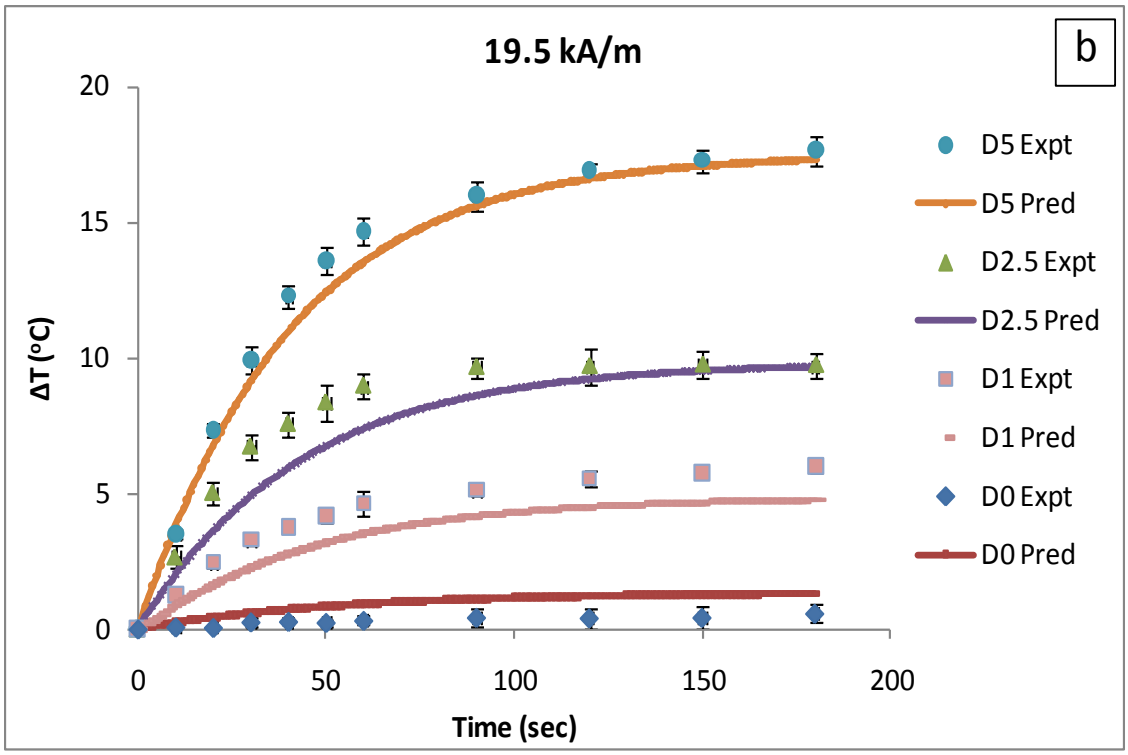
19.5 kA/m
b
ΔT (°C)
Time (sec)
D5 Expt
D5 Pred
D2.5 Expt
D2.5 Pred
D1 Expt
D1 Pred
D0 Expt
D0 Pred

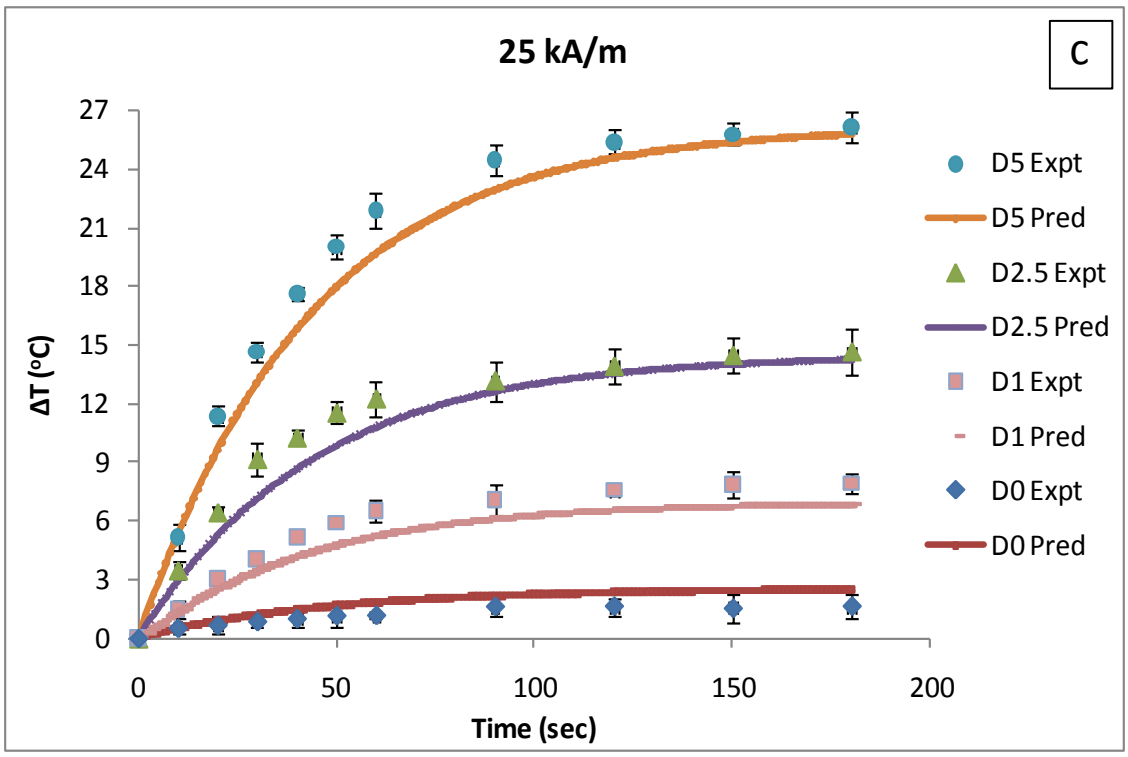

Figure 7.5(a-c). Comparison of experimental and predicted rise in temperature of D nanocomposites for different particle loadings and AMF amplitudes, Expt=Experimental values, Pred= Predicted values.

In order to test the capability of extending the heat transfer model to a different hydrogel system, temperatures of the C2.5 system at different AMF amplitudes were predicted using the model. The C hydrogel system was selected because of significant differences in swelling properties as opposed to the D systems. Higher swelling resulted into lower temperatures due to higher amount of water content. It should be noted that the $\dot{q}$ correlations derived from D hydrogel nanocomposites were used along with the swelling ratios and heat capacity values of C2.5. The predicted temperature differentials are plotted along with observed experimental values in **figure 7.6**. The good agreement between predicted and observed temperature differentials demonstrate that the heat

transfer model can be successfully applied to different hydrogel systems. Furthermore, this model can be applied to different mechanisms of remote heating (near-IR, radiofrequency) provided that the $\dot{q}$ values can be predicted or determined experimentally.

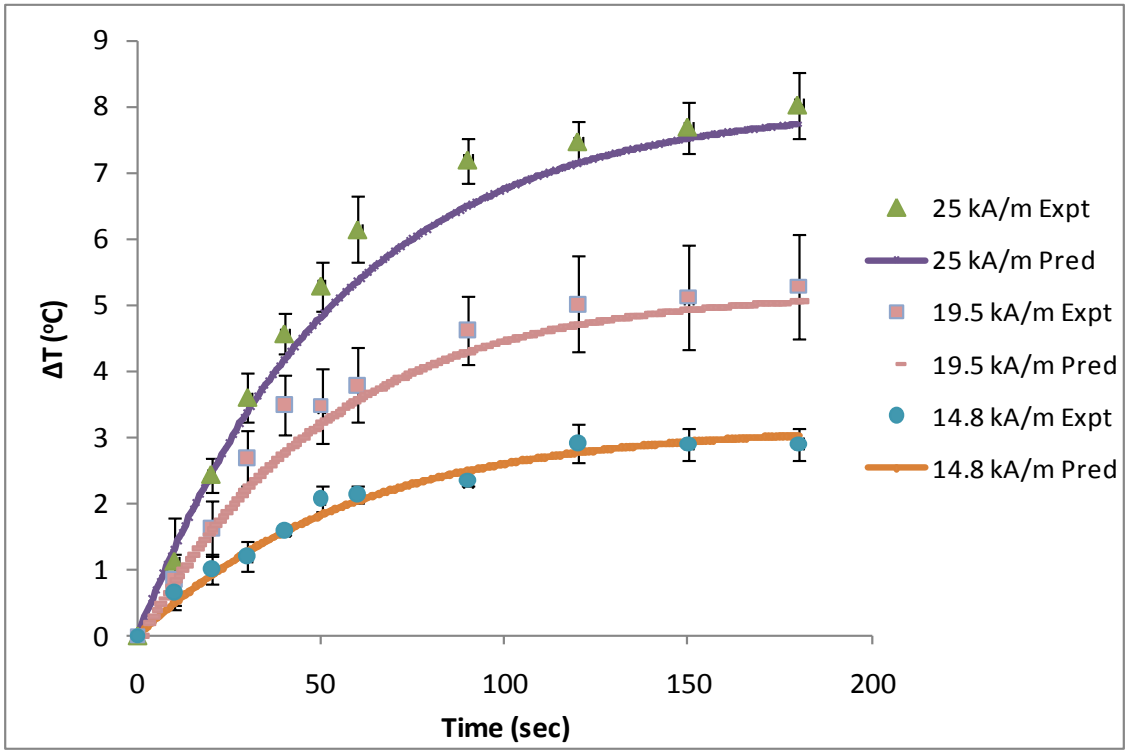

Figure 7.6. Comparison of experimental and predicted rise in temperature of C2.5 nanocomposites for different AMF amplitudes, Expt=Experimental values, Pred= Predicted values

7.5.4 Prediction of *in vivo* temperature profiles

To predict the *in* vivo temperature profiles using COMSOL (details presented in appendix B.5), initial temperature was set to be 37^{o}C in all domains. Initially, the boundaries were set to insulated, and tissue dimensions were chosen large enough to obtain minimum temperature increase at the boundaries (< 2^{o}C). Tissue boundaries were

then set to constant temperature of 37^{o}C, and temperatures of the hydrogel nanocomposites as well as surrounding tissue were predicted. After referring to a number of articles,[23, 33-35] the following values for constants were chosen for COMSOL simulations: k_t = 0.55 W/m/K, ρ_t = 1000 kg/m^3, C_t = 4186 J/kg/K, ρ_b = 1000 kg/m^3, C_b = 4186 J/kg/K, w_b = 0.0005 s^{-1}, T_b = 310.15 K, Q_{met} = 350 W/m^3. The following properties were estimated experimentally for hydrogel D at 37^{o}C: k_h = 0.464 W/m/K, ρ_h = 1112 kg/m^3, C_h= 2.375 J/kg/K. Heat generation values (Q_{ext}) were determined for a particular particle loading and AMF amplitude based on the $\dot{q}$ correlations.

Figure 7.7(a) shows the simulated steady state temperature at the center of hydrogel disc(x=0,y=0,z=0) with radius 4 mm and thickness 0.5 mm placed at the center of tissue with radius 2.5 cm and thickness 4.0 cm. The mesh consisted of 164764 elements. These hydrogel dimensions were identical to the ones used for *in vitro* experiments. The transient analysis showed that the steady state temperatures are reached within the first 5 minutes of AMF exposure. As expected, increasing particle loadings and AMF power increased the ability to heat the nanocomposites. The predicted temperature increased to 40^{o}C for the highest particle loadings at the highest AMF amplitude. This implies that the temperatures at the hydrogel edges could be even lower, causing insufficient tissue heating for hyperthermia.

Nanocomposite temperatures in the tissue environment are lower as compared to temperatures in air due to greater conduction rate in tissue than in air. Flowrate of blood in tissue(w_b) also plays an important role in the heat transfer process. Simulations in this study were carried out with blood flowrate value of 0.0005 s^{-1}. The factors that can influence blood flow include tumor type, size, stage, and site of growth.[21, 35]

Additionally, perfusion in tumors is quite heterogeneous. Researchers have reported that blood perfusion rates in tumor can vary in the range of 0.0001- 0.01 s^{-1}.[36, 37] Hence, more information about the site of implant is necessary for accurate prediction of temperatures in specific applications.

Heating can be enhanced by increasing particle loadings, AMF amplitude, or hydrogel dimensions. The derived $\dot{q}$ correlations are for a fixed AMF amplitude and different particle loadings and, hence, they can be extrapolated for higher particle loadings. Furthermore, we have looked at the effect of hydrogel dimensions on resultant temperatures. Temperatures were predicted for a disc of radius 5 mm and thickness 2 mm placed at the center of tissue of radius 2.5 cm and thickness 4 cm. The mesh consisted of 129000 elements. **Figure 7.7(b)** shows that the steady-state temperature at the center of hydrogel reached approximately 50^{o}C, for 5 weight% particle loadings and 25 kA/m AMF. When hydrogel thickness is increased, the surface area per unit volume decreases, resuting in higher temperatures at the center. The simulations can be extended to different types of polymeric systems as potential implants. For example, this temperature rise can be sufficient to cause volume transition in the case of temperature-responsive hydrogels,[11] or affect the rate of degradation in the case of degradable polymers.[14]

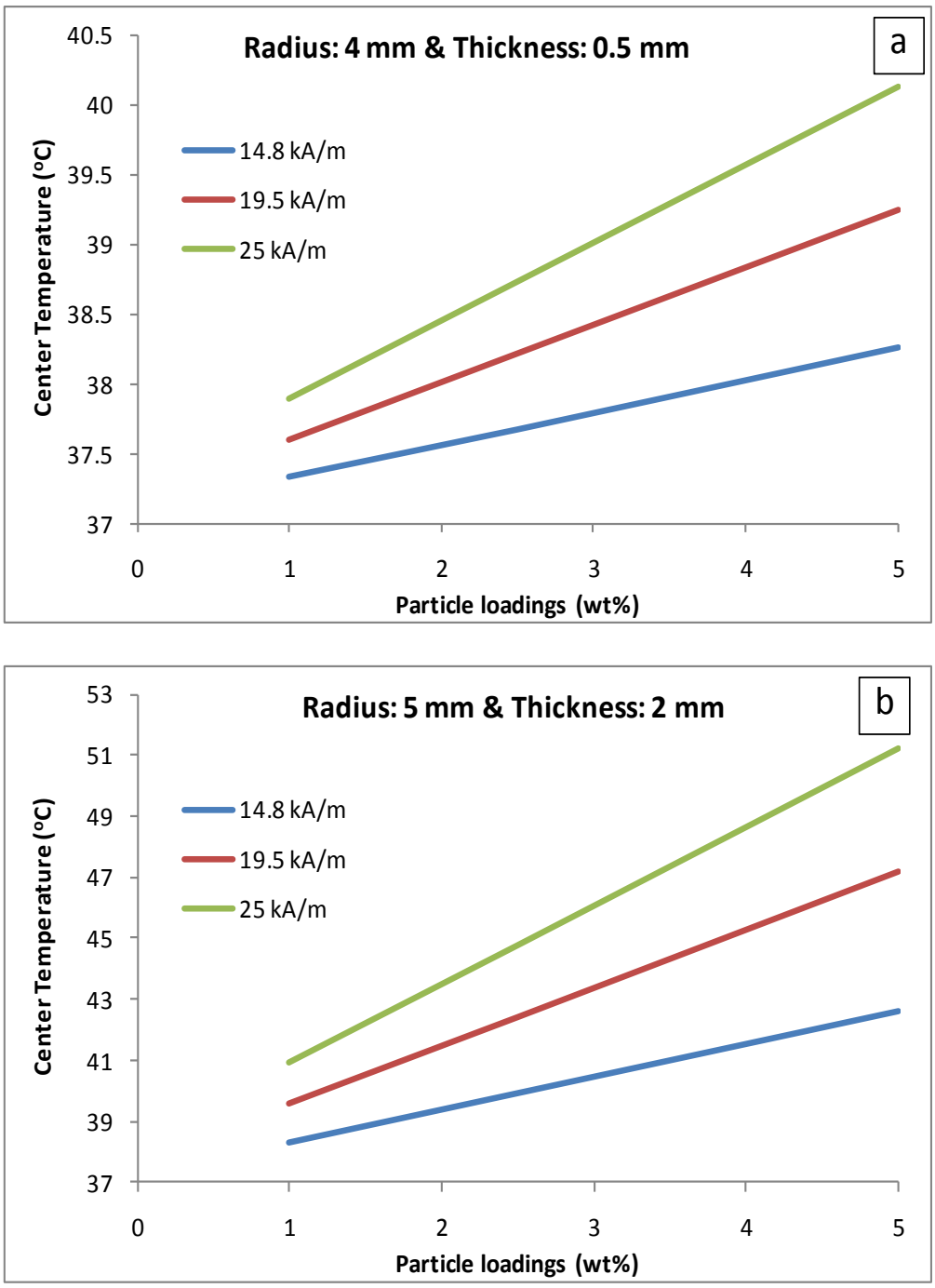

Figure 7.7. Simulated steady state temperatures at the center of hydrogel disc(x=0,y=0,z=0) placed at the center of tissue with radius 2.5 cm and thickness 4.0 cm. For (a) Disc radius 4 mm and thickness 0.5 mm, For (b) Disc radius 5 mm and thickness 2 mm.

Figures 7.8, 7.9(a), and 7.9(b) show simulated steady state temperature profiles of a hydrogel disc (radius 5 mm, thickness 2 mm) with 5 weight% particles and surrounding tissue (radius 2.5 cm and thickness 4 cm) exposed to AMF at a amplitude of 25 kA/m. The temperature profile in an x-z plane along y=0 is plotted in figure 7.8. Nanocomposite heating leads to a symmetrical temperature profile in the surrounding tissue. Tissue temperatures are highest at the hydrogel interface and then gradually reduce to that of the body temperature (37^{o}C). Hyperthermia cancer treatment would require heating the tissue in the range of 41-44^{o}C.[25] Figures 7.9(a) and 7.9(b) are the temperature profiles in x-y plane (2cm x 2cm) at z=1 and z=6 mm respectively. The model insets highlight z position of the x-y plane. The tissue temperature profile at the hydrogel surface shows that tissue temperatures can reach up to 49^{o}C for these specific conditions (7.9(a)). On the other hand, the temperature profile at 5 mm from the hydrogel surface shows that the tissue can heat up to 41^{o}C (7.9(b)). The tissue temperatures in x-y plane are higher in the region closer to the center of the disc. This implies that the hydrogel can effectively heat a significant amount of tissue to hyperthermia temperatures. The temperature profiles can be effectively modulated by changing hydrogel geometry or use of multiple hydrogel discs. AMF amplitude and particle loadings can also be changed to achieve desired temperatures.

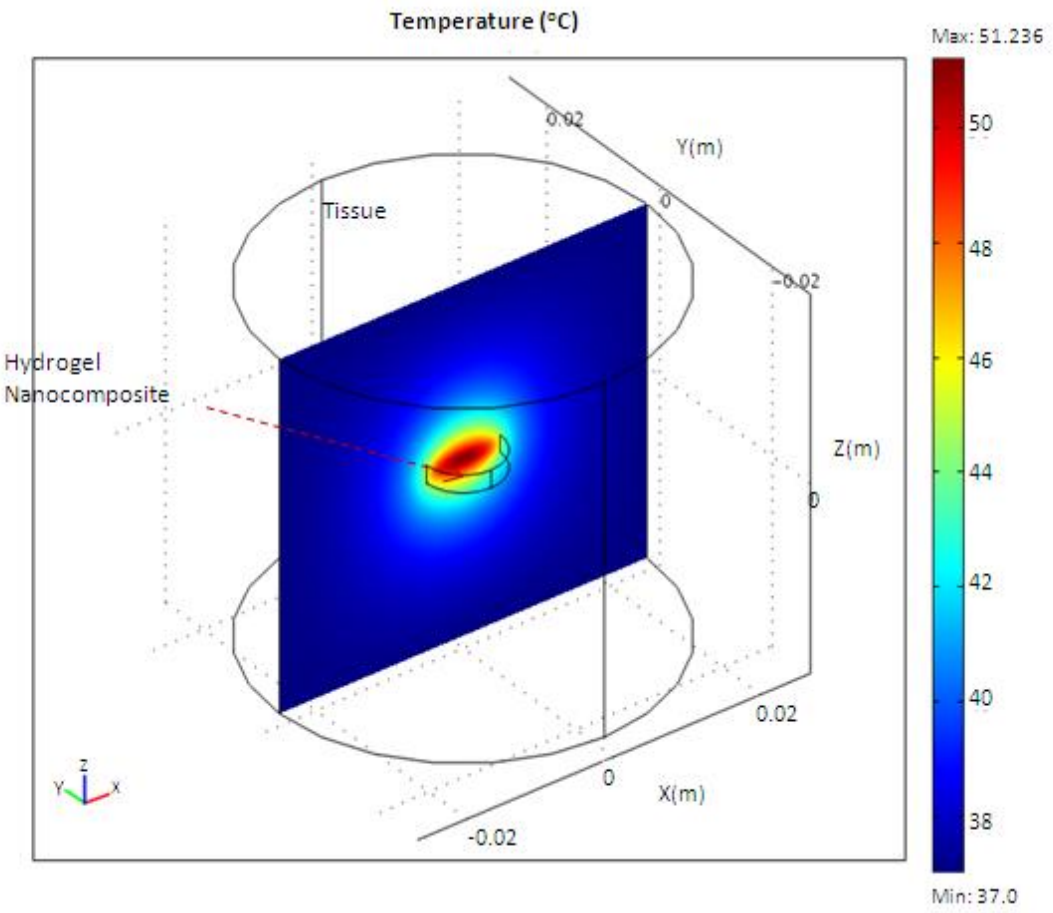

Figure 7.8. Temperature profile at steady state for hydrogel disc (radius 5 mm, thickness 2 mm, particles 5 wt%, AMF 25 kA/m) and surrounding tissue in x-z plane along y=0.

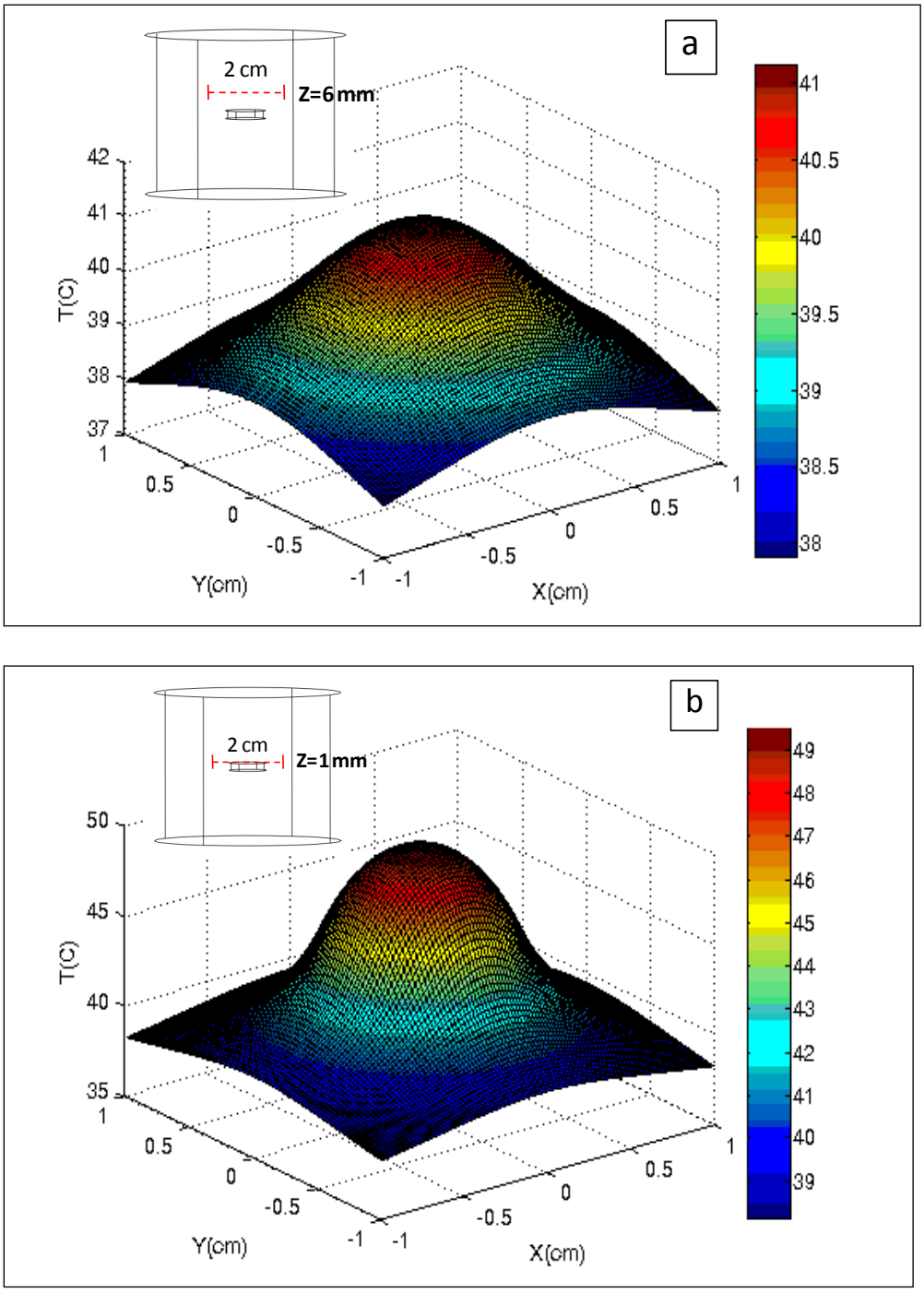

Figure 7.9. Temperature profile at steady state for hydrogel disc (radius 5 mm, thickness 2 mm, particles 5 wt%, AMF 25 kA/m) and surrounding tissue (a) In x-y plane along z=1mm, and (b) In x-y plane along z=6 mm. The model insets highlight z position of the x-y plane.

7.6 Conclusions

Magnetic nanocomposites of PEG hydrogels were synthesized with iron oxide particle loadings (between 0-5 weight %) and remotely heated in an AMF at approximately 293 kHz. A heat transfer model was proposed for predicting temperature profiles of the hydrogel disc heated with AMF in air environment. Nanocomposite temperatures were collected for AMF amplitudes of 14.8, 19.5, and 25 kA/m, and correlations were established for heat generation ($\dot{q}$) dependence on particle loadings. The temperatures predicted using the model and the $\dot{q}$ correlations were found to be in good agreement with experimentally observed values. The model successfully predicted temperatures of a PEG hydrogel system with different swelling characteristics. For *in vivo* predictions, temperature profiles of a hydrogel disc and surrounding tissue were simulated using COMSOL, for evaluation as an implant. Although *in vivo* conditions result in lower hydrogel temperatures, heating profiles can be influenced by hydrogel geometry, particle loadings, and AMF amplitude. Simulations indicated that the nanocomposite heating can raise the surrounding tissue to and above hyperthermia temperatures. It is expected that this study would be helpful for the design of polymer systems heated by various mechanisms (e.g., AMF, near-IR, radiofrequency) and placed in a variety of heat transfer environments.

7.7 Notation

A = heat transfer area of the hydrogel disc, m^2

Bi = Biot number

$C_{p,b}$ = heat capacity of blood, J kg^{-1} K^{-1}

$C_{p,h}$ = heat capacity of hydrogel, J kg^{-1} K^{-1}

$C_{p,t}$ = heat capacity of tissue, J kg^{-1} K^{-1}

h = heat transfer coefficient for convection from hydrogel to air, W m^{-2} K^{-1}

k_h = thermal conductivity of hydrogel, W m^{-1} K^{-1}

k_t = thermal conductivity of tissue, W m^{-1} K^{-1}

l = characteristic length

M = mass of the hydrogel disc, kg

Nu = Nusselt number

P = magnetic particle loadings in hydrogel, wt%

Q_{ext} = heat generation from external sources, W m^{-3}

Q_{met} = metabolic heat generation term, W m^{-3}

$\dot{q}$ = rate of heat generation per unit mass of hydrogel, W kg^{-1}

R = radius of the hydrogel disc, m

Ra = Rayleigh number

T = temperature, K

T_{air} = temperature of surrounding air (22^{o}C)

T_{ss} = temperature of the hydrogel disc at steady state, K

$t_{1/2}$ = time required for back surface to reach half of maximum temperature rise, s

t_h = thickness of the hydrogel disc, m

V_d = volume of hydrogel in dry state, m^3

V_s = volume of hydrogel in swollen state, m^3

w_b = blood perfusion rate in tissue, s^{-1}

α = thermal diffusivity of hydrogel, m^2 s^{-1}

ρ_b = density of blood, kg m^{-3}

ρ_h = density of hydrogel, kg m^{-3}

ρ_t = density of tissue, kg m^{-3}

7.8 References

[1] A.O. Govorov, H.H. Richardson, Generating heat with metal nanoparticles. Nanotoday 2(1) (2007) 30-38.

[2] P. Schexnailder, G. Schmidt, Nanocomposite polymer hydrogels. Colloid & Polymer Science 287(1) (2009) 1-11.

[3] G. Filipcsei, I. Csetneki, A. Szilagyi, M. Zrinyi, Magnetic field-responsive smart polymer composites Adv. Polym. Sci. 206 (2007) 137-189.

[4] R. Benítez, A. Fuentes, K. Lozano, Effects of microwave assisted heating of carbon nanofiber reinforced high density polyethylene. Journal of Materials Processing Technology 190(1-3) (2007) 324-331.

[5] R. Mohr, K. Kratz, T. Weigel, M. Lucka-Gabor, M. Moneke, A. Lendlein, Initiation of shape-memory effect by inductive heating of magnetic nanoparticles in thermoplastic polymers. Proc. Natl. Acad. Sci. U. S. A. 103(10) (2006) 3540-3545.

[6] X. Zeng, H. Jiang, Tunable liquid microlens actuated by infrared light-responsive hydrogel. Appl. Phys. Lett. 93(15) (2008) 151101.

[7] L. Yang, K. Setyowati, A. Li, S. Gong, J. Chen, Reversible infrared actuation of carbon nanotube-liquid crystalline elastomer nanocomposites. Adv. Mater. 20(12) (2008) 2271-2275.

[8] C.M. Yakacki, N.S. Satarkar, K. Gall, R. Likos, J.Z. Hilt, Shape-memory polymer networks with Fe3O4 nanoparticles for remote activation. J. Appl. Polym. Sci. 112(5) (2009) 3166-3176.

[9] S.R. Sershen, G.A. Mensing, M. Ng, N.J. Halas, D.J. Beebe, J.L. West, Independent optical control of microfluidic valves formed from optomechanically responsive nanocomposite hydrogels. Adv. Mater. 17(11) (2005) 1366-1368.

[10] N.S. Satarkar, W. Zhang, R.E. Eitel, J.Z. Hilt, Magnetic hydrogel nanocomposites as remote controlled microfluidic valves. Lab Chip 9(12) (2009) 1773-1779.

[11] N.S. Satarkar, J.Z. Hilt, Magnetic hydrogel nanocomposites for remote controlled pulsatile drug release. J. Control. Rel. 130 (2008) 246-251.

[12] M. Bikram, A.M. Gobin, R.E. Whitmire, J.L. West, Temperature-sensitive hydrogels with SiO2-Au nanoshells for controlled drug delivery. J. Control. Rel. 123(3) (2007) 219-227.

[13] E. Miyako, H. Nagata, K. Hirano, T. Hirotsu, Photodynamic thermoresponsive nanocarbon-polymer gel hybrids. Small 4(10) (2008) 1711-1715.

[14] A. Hawkins, N. Satarkar, J. Hilt, Nanocomposite degradable hydrogels: demonstration of remote controlled degradation and drug release. Pharm. Res. 26(3) (2009) 667-673.

[15] M. Babincova, J. Novotny, J. Rosenecker, P. Babinec, Remote radio-control of siRNA release from magnetite-hydrogel composite. Optoelectronics and Advanced Materials – Rapid Communications 1(11) (2007) 644-647.

[16] M. Babincová, D. Leszczynska, P. Sourivong, P. Cicmanec, P. Babinec, Superparamagnetic gel as a novel material for electromagnetically induced hyperthermia. J. Magn. Magn. Mater. 225(1-2) (2001) 109-112.

[17] R. Ramanujan, K. Ang, S. Venkatraman, Magnet–PNIPA hydrogels for bioengineering applications. J. Mater. Sci. 44(5) (2009) 1381-1387.

[18] S.A. Meenach, A.A. Anderson, M. Suthar, K.W. Anderson, J.Z. Hilt, Biocompatibility analysis of magnetic hydrogel nanocomposites based on poly(N-isopropylacrylamide) and iron oxide. Journal of Biomedical Materials Research Part A 91A(3) (2009) 903-909.

[19] T.-W. Wang, H.-C. Wu, W.-R. Wang, F.-H. Lin, P.-J. Lou, M.-J. Shieh, T.-H. Young, The development of magnetic degradable DP-Bioglass for hyperthermia cancer therapy. Journal of Biomedical Materials Research Part A 83A(3) (2007) 828-837.

[20] S.A. Meenach, J.Z. Hilt, K.W. Anderson, Poly(ethylene glycol)-based magnetic hydrogel nanocomposites for hyperthermia cancer therapy. Acta Biomater. In Press (2009).

[21] B. Hildebrandt, P. Wust, O. Ahlers, A. Dieing, G. Sreenivasa, T. Kerner, R. Felix, H. Riess, The cellular and molecular basis of hyperthermia. Critical Reviews in Oncology/Hematology 43(1) (2002) 33-56.

[22] M.H. Falk, R.D. Issels, Hyperthermia in oncology. International Journal of Hyperthermia 17(1) (2001) 1-18.

[23] H.G. Bagaria, D.T. Johnson, Transient solution to the bioheat equation and optimization for magnetic fluid hyperthermia treatment. International Journal of Hyperthermia, Vol. 21, Taylor & Francis Ltd, 2005, pp. 57-75.

[24] A. Candeo, F. Dughiero, Numerical FEM models for the planning of magnetic induction hyperthermia treatments with nanoparticles. IEEE Trans. Magn. 45(3) (2009) 1658-1661.

[25] M.R. Horsman, J. Overgaard, Hyperthermia: a potent enhancer of radiotherapy. Clinical Oncology 19(6) (2007) 418-426.

[26] J.J. Schmidt, J. Rowley, H.J. Kong, Hydrogels used for cell-based drug delivery. Journal of Biomedical Materials Research Part A 87A(4) (2008) 1113-1122.

[27] J.-F. Lutz, Polymerization of oligo(ethylene glycol) (meth)acrylates: Toward new generations of smart biocompatible materials. Journal of Polymer Science Part A: Polymer Chemistry 46(11) (2008) 3459-3470.

[28] H. Arkin, L.X. Xu, K.R. Holmes, Recent developments in modeling heat transfer in blood perfused tissues. IEEE Transactions on Biomedical Engineering 41(2) (1994) 97-107.

[29] H.H. Pennes, Analysis of tissue and arterial blood temperatures in the resting human forearm. J. Appl. Physiol. 1(2) (1948) 93-122.

[30] W.J. Parker, R.J. Jenkins, C.P. Butler, G.L. Abbott, Flash method of determining thermal diffusivity, heat capacity, and thermal conductivity. J. Appl. Phys. 32(9) (1961) 1679-1684.

[31] B. Chambers, T.-Y.T. Lee, A numerical study of local and average natural convection Nusselt numbers for simultaneous convection above and below a uniformly heated horizontal thin plate. J. Heat Transfer 119(1) (1997) 102-108.

[32] P.P. Vaishnava, R. Tackett, A. Dixit, C. Sudakar, R. Naik, G. Lawes, Magnetic relaxation and dissipative heating in ferrofluids. J. Appl. Phys. 102 (2007) 063914.

[33] E.H. Wissler, Pennes' 1948 paper revisited. J. Appl. Physiol. 85(1) (1998) 35-41.

[34] J.W. Hand, R.W. Lau, J.J.W. Lagendijk, J. Ling, M. Burl, I.R. Young, Electromagnetic and thermal modeling of SAR and temperature fields in tissue due to an RF decoupling coil. Magnetic Resonance in Medicine 42(1) (1999) 183-192.

[35] C.W. Song, Effect of local hyperthermia on blood flow and microenvironment: A review. Cancer Res. 44(10_Supplement) (1984) 4721s-4730.

[36] P. Vaupel, F. Kallinowski, P. Okunieff, Blood flow, oxygen and nutrient supply, and metabolic microenvironment of human tumors: A review. Cancer Res. 49(23) (1989) 6449-6465.

[37] P. Wust, B. Hildebrandt, G. Sreenivasa, B. Rau, J. Gellermann, H. Riess, R. Felix, P.M. Schlag, Hyperthermia in combined treatment of cancer. The Lancet Oncology 3(8) (2002) 487-497.

CHAPTER 8

CONCLUSIONS

This dissertation was focused on development of hydrogel nanocomposites, with the primary objective of achieving remote actuation. The primary nanocomposite systems studied were based on superparamagnetic iron oxide (Fe_3O_4) nanoparticles added to N-isopropylacrylamide (NIPAAm), a negative temperature responsive hydrogel. Poly (ethylene glycol) dimethacrylate crosslinkers with different molecular weights and ratios were used to tailor the temperature responsive swelling response. An alternating magnetic field (AMF) around 300 kHz was applied to heat the nanocomposites, and the control on the heating abilities was achieved by variation of nanoparticle loadings. This method of heating the nanocomposites is unique because the RF stimulus can be applied from a distance, resulting into remote actuation.

The AMF caused fast and uniform heating throughout the nanocomposite, resulting into accelerated collapse as the temperatures increased above lower critical solution temperature (LCST). The nanoparticle loadings and hydrogel composition were tailored to obtain a nanocomposite system that exhibited significant change in volume when exposed to AMF. The mechanism behind this phenomenon and effect of various parameters on the rate of heating, collapse, and recovery was also studied. The nanocomposites were subjected to AMF for several cycles, and the reversibility of the swelling response was observed. A platform for remotely triggering nanocomposite volume change was successfully established for a variety of applications. The key

applications targeted with remote actuation capabilities include matrix drug delivery systems, microfluidic valves, and hyperthermia cancer treatment.

The nanocomposites were loaded with model drugs, and AMF controlled pulsatile drug release was demonstrated. The collapse of the hydrogel discs expelled large amounts of imbibed water, resulting in drug release at an increased rate. Drug release was characterized to understand the effect of different AMF ON-OFF durations as well as drug molecular weights. The release profiles showed that magnetic nanocomposites can give pulsed release when needed in addition to continuous Fickian release profile. RC drug release has promise as a matrix drug delivery system because it can give a unique benefit of controlling drug release rate after the polymer is implanted *in vivo*. Furthermore, this approach can be applied to deep tissue implants and, hence, is advantageous over light actuated gold-NIPAAm nanocomposites.

In another application, the ability to remotely collapse nanocomposites was utilized for microfluidic flow control. A microfluidic device was fabricated using low temperature co-fired ceramic (LTCC) processing technique. A Y-shaped microfluidic channel was obtained, and the hydrogel nanocomposite was placed as a valve in one of the channels. The application of an AMF resulted in the selective heating of the nanocomposite followed by collapse and hence opening of the hydrogel valve, leading to flow of liquid. When AMF was turned off, swelling of hydrogel valve stopped the flow through the channel. The application of multiple ON-OFF AMF cycles to the valve along with analysis of pressure at the inlet demonstrated that the valve can work for multiple cycles with good reproducibility. The collapse and recovery analysis of nanocomposites with different thicknesses showed that response of the hydrogel system can be made faster by

using a smaller geometry. The ON-OFF response of the valve can thus be precisely controlled by nanocomposite composition and geometry. Hydrogel valves are an attractive alternative to pneumatic valves because they can eliminate the need for complex off-chip controls. Furthermore, the mechanism of AMF control utilizes selective remote heating and, hence, eliminates the need to heat the solution around the valve. In addition to lab on chip applications, the valve can also be potentially useful in an implantable reservoir device.

Apart from magnetic nanoparticles, the addition of multi-walled carbon nanotubes (MWCNTs) was also explored. NIPAAm-MWCNT nanocomposites were synthesized with varying amounts of MWCNTs. The effect of varying the amount of acrylamide (AAm) and MWCNTs on temperature responsive swelling properties of NIPAAm hydrogels was characterized. The addition of AAm to the hydrogels shifted the LCST to higher temperatures, which is critical for physiological applications. The incorporation of MWCNTs in the hydrogels decreased the extent of swelling due to hydrophobic nature of MWCNTs. MWCNTs enhanced the mechanical properties of hydrogels and the enhancement can be tailored by the concentration of MWCNTs. The application of a RF field of 13.56 MHz significantly heated the nanocomposites, and the resultant heating was dependent on MWCNT loadings. This is the first report on the use of radiofrequency to remotely heat MWCNT-hydrogel nanocomposites.

In order to design the nanocomposite system for a specific application, it is very important to understand the RC heating and the resultant changes in the nanocomposite properties. Magnetic nanocomposites of poly (ethylene glycol) hydrogels were synthesized with iron oxide nanoparticle loadings (between 0-5 weight%) and remotely

heated in an AMF. A semi-empirical heat transfer model was proposed for predicting temperature profiles of the hydrogel disc heated with an AMF in air environment. A MATLAB program was developed to predict the nanocomposite temperatures. The temperature rise as well as equilibrium temperatures predicted by the model were found to be in good agreement with experimentally observed values for different hydrogel dimensions, swelling properties, nanoparticles loadings, and AMF amplitudes. COMSOL was used to simulate temperature rise of hydrogel nanocomposite and the surrounding tissue for hyperthermia cancer treatment application. Although *in vivo* conditions result in lower hydrogel temperatures, heating profile can be influenced by hydrogel geometry, particle loadings, and AMF amplitude. Simulations indicated that the nanocomposite heating can raise the surrounding tissue to and above hyperthermia temperatures. It is expected that the modeling approach can be applied to RC hydrogel heating with other mechanisms (e.g., light), as well as when placed in different environments.

This dissertation discussed hydrogel nanocomposite systems containing magnetic nanoparticles and carbon nanotubes. The nanocomposites present a unique platform with the ability to tune their temperature responsive swelling, mechanical properties, and RC heating. The phenomenon of RC actuation was used to obtain RC pulsatile drug release and RC microvalves for microfluidics. Furthermore, modeling and simulations indicated that the RC nanocomposites can be an effective tool for hyperthermia cancer treatment. Thus, the nanocomposites promise a variety of high interest biomedical applications.

APPENDIX A

FABRICATION AND ASSEMBLY OF THE MICROFLUIDIC DEVICE FOR RC VALVE APPLICATIONS

This section is based on work published as:

N.S. Satarkar, W. Zhang, R. Eitel, J.Z. Hilt, Magnetic hydrogel nanocomposites as remote controlled microfluidic valves, Lab Chip 9 (2009) 1773-1779.

A.1 Introduction

The LTCC manufacturing process which was used to fabricate the fluidic chips in this study, is a multilayer electronic packaging technology commercially used for applications requiring high packaging density and high reliability interconnects, including personal electronics and wireless communication devices.[1] LTCC is currently being developed for highly integrated microsystems and microfluidic devices for chemical analysis, materials synthesis, and polymerase chain reaction (PCR).[2-5] LTCC utilizes a layered assembly process and is compatible with a wide range of metallic and ceramic materials, making a logical choice for the integration of complex truly three dimensional structures and multifunctional materials. Since LTCC is a true packaging technology, LTCC modules are more durable than polymeric substrates and there is no need for additional protective envelope as when utilizing Si-based MEMS devices. Finally the layer manufacturing process utilized for LTCC means that design changes can be

performed on a single layer and rapidly incorporated into the final device leading to short development time and lower cost production.[6, 7]

The commercial LTCC process begins w/ flexible "green tapes" composed of ceramic particles, glass frit, and organic binders as shown in **figure A.1**. LTCC tapes can be easily patterned in "green" state (before firing) and become rigid once fired. Electronic components and circuitry are patterned on each layer of the "green" tape either by screen printing or photolithography. Electrical interconnects between tape layers are made by punching through holes (vias) and backfilling with a conductive ink. The individual layers are then aligned, stacked, and laminated at moderate pressure and temperature. A final high temperature sintering (co-firing) treatment yields a robust monolithic ceramic package. Additional components can be printed, glued, or soldered to the surface based on the desired application. Minor modifications to the above LTCC process provide the possibility to integrate complex 3D structures and microchannels in the final device.

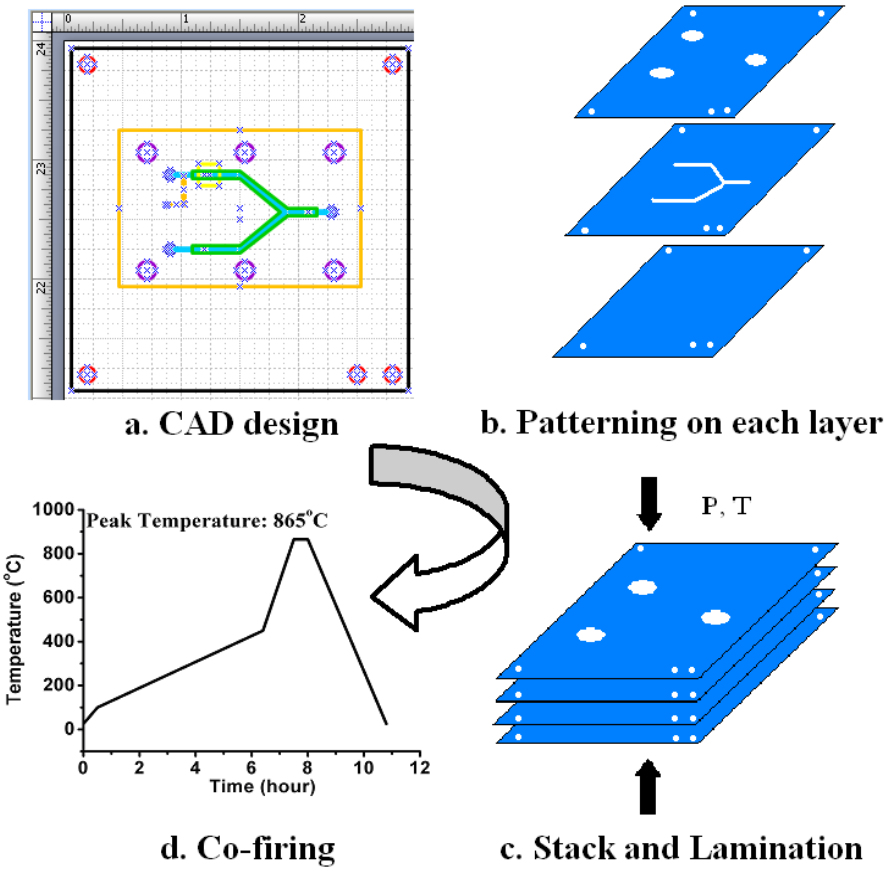

Figure A.1. Three dimensional microfluidic structures were fabricated by incorporating an additional physical patterning step (b) into the traditional LTCC process

A.2 Fabrication of the LTCC microfluidic device

The LTCC microfluidic chips were fabricated using a modified LTCC process, as shown in **figure A.1**. Starting from the initial CAD design, physical features such as channels and cavities are patterned on each layer by CNC micromachining or laser ablation. Individual layers are then aligned and stacked in the correct sequence, laminated and finally co-fired to form the desired 3D structure.

The flow system consisted of two straight channels of width 600 μm and depth 650 μm with a Y-shape junction. The final 3D structure of microchannel was designed in a CAD

program. A square cavity in the middle of one channel was used to anchor the hydrogel valve. Additionally, a side branch between the inlet and hydrogel valve was used for pressure release once the channel is blocked by closed hydrogel valve. Since a Heralock ® is a "zero shrink" LTCC system no compensation for firing shrinkage (typically ~10% in the plane of the tape) was required in the design and patterning process.

In this study, the test device was assembled from two individually sintered ceramic substrates, and a transparent sandwich gasket as illustrated in **figure A.2**. The cover layer (LTCC) was patterned from a single four-layer green tape stack (A.2(a). The transparent polymer (HDPE) gasket was used for channel sealing and optical imaging of valve operation (A.2(b)). The micro-channel (A.2(c)), valve cavity (A.2(d)), and bottom layer (A.2(e)) were each patterned from three-layer thick green tape stacks, which were laminated together and sintered to form the main structure of the microchannel-valve assembly (LTCC).

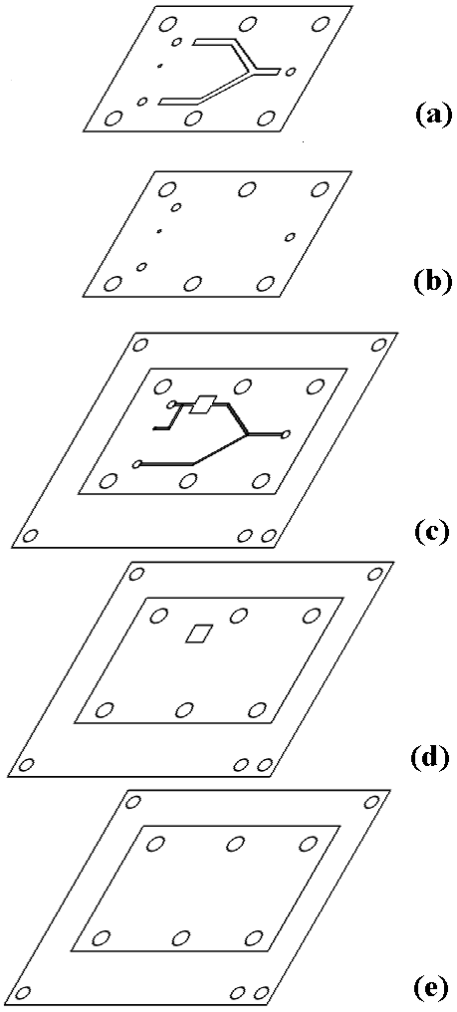

Figure A.2. Five individual layers were used in the final microfluidic chip design; (a) a ceramic cover (LTCC); (b) transparent polymer gasket (HDPE); (c) micro-channel,(d) valve cavity and (e) bottom layer (all LTCC). The cover layer (a) was patterned from a single four-layer green tape stack. Layers (c), (d) and (e) were each patterned from three-layer thick green tape stacks, which were laminated together and sintered to form the main structure of the microchannel-valve assembly.

A CO_2 laser (VersaLaser S 3.50, Universal Laser Systems) was used to pattern the design features, alignment holes, and fiducial marks to the green tapes simultaneously. Laser parameters were adjusted to achieve uniform features and minimize scalloping of channel

edges (HDPO optics, speed 30 mm/sec, power 15 Watts). By adjusting laser parameters and focus it is possible to pattern features as small as 100 μm across with depth control of ~50 μm. Alignment of individual layers was implemented using a fixture with five registration pins and corresponding holes in the corner of each patterned layer. A uniaxial hydraulic press (3851-0, CARVER®) with heated platens was used for the lamination process, 200psi for 3 minutes and then 1000psi for 10 minutes at 75°C. Finally, the laminate was sintered (cofired) at 865°C for 30 minutes on a flat alumina setter in a box furnace (Isotemp® Programmable Muffle Furnace, Fisher Scientific) in air following the manufacturer's recommended firing profile.

A.3 Assembly of the microfluidic device

The patterned gasket was inserted between the ceramic cover and microchannel laminate. Six sets of nylon screws and nuts (Micro Plastic®) were used to seal the channel. To complete the assembly of microdevice, luer connectors were attached to the inlet and outlet ports with cyanoacrylate adhesive.

The final width and depth of the fabricated microchannel were 600 μm and 650 μm respectively, as shown in **figure A.3(a)**. The LTCC fabrication process yielded good control of device design with crisp fluidic features. **Figure A.3(b)** shows a picture of the assembled microdevice containing the hydrogel composite valve in upper channel.

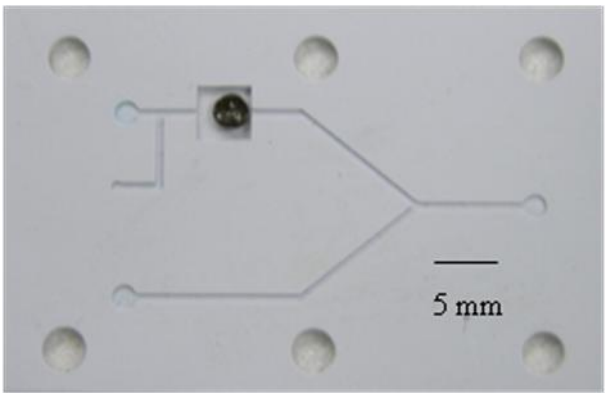

(a)

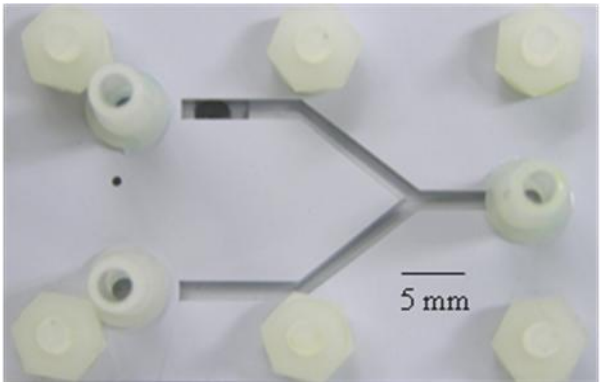

(b)

Figure A.3. Picture of microfluidic device with hydrogel composite as a valve in the upper channel, (a) Bottom part of device and (b) Assembled device

A.4 References

[1] L.J. Golonka, Technology and applications of low temperature cofired ceramic (LTCC) based sensors and microsystems. Bulletin of the Polish Academy of Sciences, Technical Sciences 54(2) (2006) 221-231.

[2] N. Ibañez-Garcia, R.D.M. Gonçalves, Z.M. da Rocha, M.R. Góngora-Rubio, A.C. Seabra, J.A. Chamarro, LTCC meso-analytical system for chloride ion determination in drinking waters. Sensors and Actuators B: Chemical 118(1-2) (2006) 67-72.

[3] G.A. Groß, T. Thelemann, S. Schneider, D. Boskovic, J.M. Köhler, Fabrication and fluidic characterization of static micromixers made of low temperature cofired ceramic (LTCC). Chem. Eng. Sci. 63(10) (2008) 2773-2784.

[4] N. Ibanez-Garcia, M. Puyol, C.M. Azevedo, C.S. Martinez-Cisneros, F. Villuendas, M.R. Gongora-Rubio, A.C. Seabra, J. Alonso, Vortex configuration flow cell based on low-temperature cofired ceramics as a compact chemiluminescence microsystem. Anal. Chem. 80(14) (2008) 5320-5324.

[5] K. Moeller, J. Besecker, G. Hampikian, A. Moll, D. Plumlee, J. Youngsman, J.M. Hampikian, A prototype continuous flow polymerase chain reaction LTCC device. THERMEC '2006 Conference, Minerals, Metals and Materials Society, Vancouver, Canada, July 2006.

[6] M.R. Gongora-Rubio, P. Espinoza-Vallejos, L. Sola-Laguna, J.J. Santiago-Avilés, Overview of low temperature co-fired ceramics tape technology for meso-system technology (MsST). Sensors and Actuators A: Physical 89(3) (2001) 222-241.

[7] T. Thelemann, H. Thust, M. Hintz, Using LTCC for microsystems. Microelectronics International 19 (2002) 19-23.

APPENDIX B

SUPPORTING INFORMATION FOR MODELING AND SIMULATIONS OF NANOCOMPOSITE HEATING

This section is based on work published as:

N.S. Satarkar, S.A. Meenach, K. Anderson, J.Z. Hilt, Remote actuation of hydrogel nanocomposites: Heating analysis, modeling, and simulations, AIChE J, Accepted.

B.1 Additional equations for determination of model parameters

Volume swelling ratio (Q) is given by

$$Q = \frac{V_s}{V_d} \tag{B.1}$$

Thermal diffusivity(α) was estimated by flash method[1]

$$\propto = 1.38 \frac{{t_h}^2}{\pi^2 t_{1/2}} \tag{B.2}$$

Thermal diffusivity was in turn used to determine thermal conductivity(k_h)[1]

$$k_h = \propto \rho_h C_{p,h} \tag{B.3}$$

Heat transfer coefficients for convection from hydrogel disc to air were determined using following correlations[2]:

For upper surface,

$$Nu = 0.653 Ra^{0.143} \tag{B.4}$$

For lower surface,

$$\mathrm{Nu} = 0.979\mathrm{Ra}^{0.137} \qquad (B.5)$$

Biot number (Bi) calculations were performed using following equation:

$$\mathrm{Bi} = \frac{\mathrm{hl}}{\mathrm{k_h}} \qquad (B.6)$$

B.2 Thermal properties of hydrogel systems

Table B.1. Heat capacity and thermal conductivity values of the hydrogel systems

System	Heat capacity (J kg^{-1} K^{-1}) x 10^3		Thermal conductivity (W m^{-1} K^{-1})
	25°C	**37°C**	**25°C**
D0	2.78±0.12	2.34±0.18	0.423±0.03
D5	2.71±0.25	2.41±0.10	0.505±0.12
C2.5	2.86±0.10	3.10±0.27	0.497±0.08

B.3 References

[1] W.J. Parker, R.J. Jenkins, C.P. Butler, G.L. Abbott, Flash method of determining thermal diffusivity, heat capacity, and thermal conductivity. J. Appl. Phys. 32(9) (1961) 1679-1684.

[2] B. Chambers, T.-Y.T. Lee, A numerical study of local and average natural convection Nusselt numbers for simultaneous convection above and below a uniformly heated horizontal thin plate. J. Heat Transfer 119(1) (1997) 102-108.

B.4 MATLAB program for nanocomposite temperature prediction

```
function [T] = heat_q_eqn(part,pwr,Tini,m,A)
Q=2.4;
Cp=2.745;
T(1)=Tini;
%Tinf is bulk air temperature for h calculations
Tinf=22;
%for PEG system diameter 7.5 mm, so L=D/4
L=1.875*10^(-3);
g=9.81;
if ((pwr<16) && (pwr>14))
   q=0.2914*part+0.0473;
end
if((pwr<26) && (pwr>24))
   q=0.5144*part+0.1684;
end
if((pwr<41) && (pwr>39))
   q=0.6974*part+0.3474;
end

for t = 2:181
        %Tav is calculated to get h; and is based on T at t-1
        Tav(t)=(Tinf+T(t-1))/2+273;
        Time(t) = t;
        beta(t)=1/(Tav(t));
        v(t)=8.4*10^(-8)*(Tav(t))-8.462*10^(-6);
        Gr(t)=g*beta(t)*(T(t-1)-Tinf)*(L^3)/((v(t))^2);
        Pr(t)=(-0.133333*Tav(t)+746.53)/1000;
        Ra(t)=Gr(t)*Pr(t);
        Nuu(t)=0.653*(Ra(t))^0.143;
        Nul(t)=0.979*(Ra(t))^0.137;
        Nu(t)=(Nuu(t)+Nul(t))/2;
        k(t)=7.05*10^(-5)*Tav(t)+0.0054038;
```

```
        hu(t)=Nuu(t)*k(t)/L;
        hl(t)=Nul(t)*k(t)/L;
        h(t)=(hu(t)+hl(t))/2;
        T(t) = Tini + q/Q*m/(h(t)*A)*(1-exp(-(h(t)*A)/(m*Cp)*t));
end
%d =[Time' Tav' beta' v' Gr' Ra' Nuu' Nul' Nu' hu' hl' h' T'];
d =[T'];
Time;
T;
xlswrite('Heating Data 7-23-09.xlsx',d,'T pred w q eqn','AG5');
%plot(Time, T)
```

B.5 COMSOL report for a nanocomposite placed in tissue and subjected to AMF

1. Model Properties

Property	Value
Model name	Simulations of Nanocomposite Heating *In Vivo*
Author	Nitin Satarkar
Company	University of Kentucky
Department	Chemical and Materials Engineering
Reference	
URL	
Saved date	Sep 17, 2009 2:38:06 PM
Creation date	Aug 22, 2009 1:16:42 PM
COMSOL version	COMSOL 3.5.0.608

File name: /home/hastingslab/Desktop/nitin satarkar/d1_t0.2_d5_t4_SS_insu_bc_5_40.mph

1.1. Application modes and modules used in this model:

- Geom1 (3D)
- Bioheat Equation (Heat Transfer Module)

2. Geometry

Number of geometries: 1

2.1. Geom1

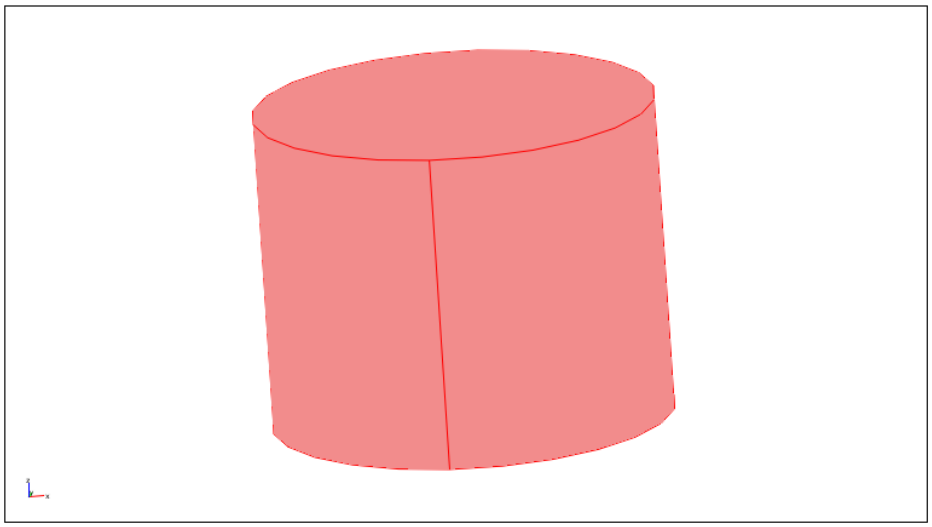

2.1.1. Subdomain mode

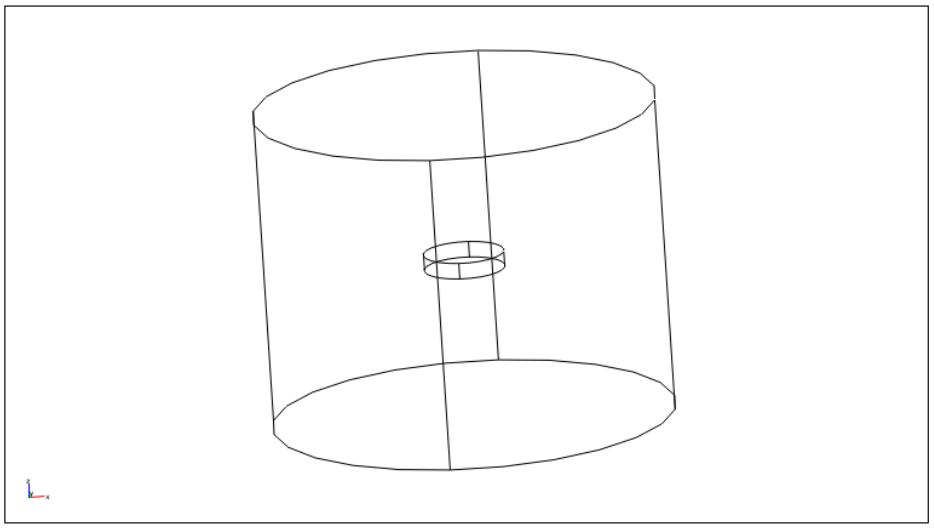

3. Geom1

Space dimensions: 3D

Independent variables: x, y, z

3.1. Mesh

3.1.1. Mesh Statistics

Number of degrees of freedom	181092
Number of mesh points	24698
Number of elements	128874
Tetrahedral	128874
Prism	0
Hexahedral	0
Number of boundary elements	6000
Triangular	6000
Quadrilateral	0
Number of edge elements	247
Number of vertex elements	16
Minimum element quality	0.234
Element volume ratio	0.006

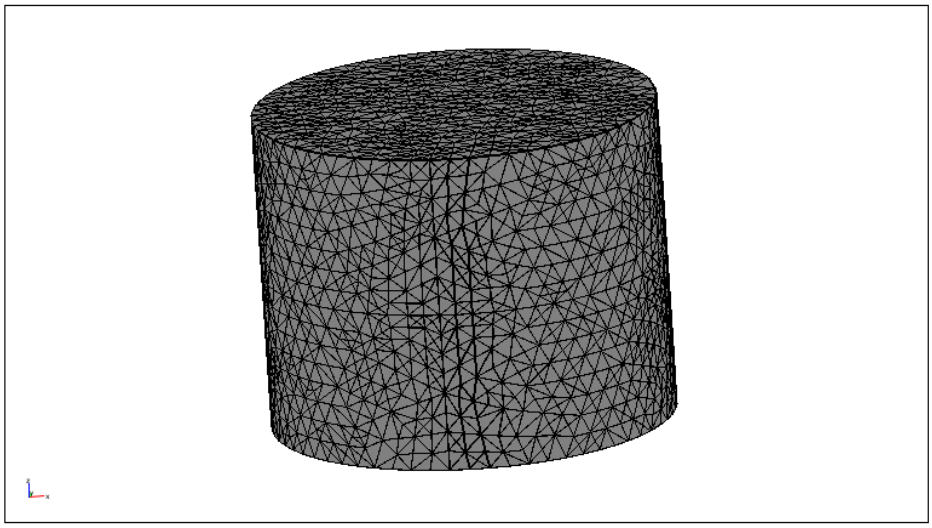

3.2. Application Mode: Bioheat Equation (htbh)

Application mode type: Bioheat Equation (Heat Transfer Module)

Application mode name: htbh

3.2.1. Application Mode Properties

Property	Value
Default element type	Lagrange - Quadratic
Analysis type	Stationary
Frame	Frame (ref)
Weak constraints	Off
Constraint type	Ideal

3.2.2. Variables

Dependent variables: T

Shape functions: shlag(2,'T')

Interior boundaries not active

3.2.3. Boundary Settings

Boundary		1-4, 9, 12
Type		Temperature

3.2.4. Subdomain Settings

Subdomain		1	2
Thermal conductivity of tissue (k)	W/(m·K)	**0.55**	**0.464**
Density of blood (rhob)	kg/m^3	**1000**	0
Specific heat of blood (Cb)	J/(kg·K)	**4186**	0
Blood perfusion rate (wb)	1/s	**0.0005**	0
Metabolic heat source (Qmet)	W/m^3	**350**	0
Spatial heat source (Qext)	W/m^3	0	**1974805**

Subdomain initial value		1	2
Temperature (T)	K	310.15	310.15

4. Solver Settings

Solve using a script: off

Analysis type	Stationary
Auto select solver	On
Solver	Stationary
Solution form	Automatic
Symmetric	auto
Adaptive mesh refinement	Off
Optimization/Sensitivity	Off
Plot while solving	Off

4.1. Conjugate gradients

Solver type: Linear system solver

Parameter	**Value**
Relative tolerance	1.0E-6
Factor in error estimate	400.0
Maximum number of iterations	10000
Preconditioning	Left

4.1.1. Algebraic multigrid

Solver type: Preconditioner

Parameter	**Value**
Number of iterations	2
Multigrid cycle	V-cycle
Maximum number of levels	6
Max DOFs at coarsest level	5000
Quality of multigrid hierarchy	3

4.1.1.1. SOR

Solver type: Presmoother

Parameter	Value
Number of iterations	2
Relaxation factor (omega)	1.0
Blocked version	Off

4.1.1.2. SORU

Solver type: Postsmoother

Parameter	Value
Number of iterations	2
Relaxation factor (omega)	1.0
Blocked version	Off

4.1.1.3. UMFPACK

Solver type: Coarse solver

Parameter	Value
Drop tolerance	0.0
Pivot threshold	0.1
Memory allocation factor	0.7

4.2. Stationary

Parameter	Value
Linearity	Automatic
Relative tolerance	1.0E-6
Maximum number of iterations	25
Manual tuning of damping parameters	Off
Highly nonlinear problem	Off
Initial damping factor	1.0
Minimum damping factor	1.0E-4
Restriction for step size update	10.0

4.3. Advanced

Parameter	Value
Constraint handling method	Elimination
Null-space function	Automatic
Automatic assembly block size	On
Assembly block size	5000
Use Hermitian transpose of constraint matrix and in symmetry detection	Off
Use complex functions with real input	Off
Stop if error due to undefined operation	On
Store solution on file	Off
Type of scaling	Automatic
Manual scaling	
Row equilibration	On
Manual control of reassembly	Off
Load constant	On
Constraint constant	On
Mass constant	On
Damping (mass) constant	On
Jacobian constant	On
Constraint Jacobian constant	On

5. Postprocessing

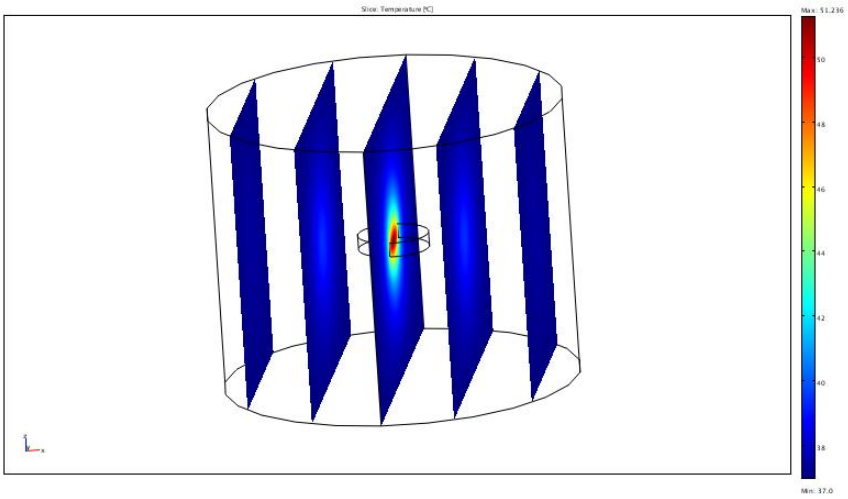

6. Variables

6.1. Boundary

Name	Description	Unit	Expression
nflux_htbh	Normal heat flux	W/m^2	nx_htbh * fluxx_htbh+ny_htbh * fluxy_htbh+nz_htbh * fluxz_htbh

6.2. Subdomain

Name	Description	Unit	Expression
fluxx_htbh	Heat flux, x component	W/m^2	-kxx_htbh * Tx-kxy_htbh * Ty-kxz_htbh * Tz
fluxy_htbh	Heat flux, y component	W/m^2	-kyx_htbh * Tx-kyy_htbh * Ty-kyz_htbh * Tz
fluxz_htbh	Heat flux, z component	W/m^2	-kzx_htbh * Tx-kzy_htbh * Ty-kzz_htbh * Tz
gradT_htbh	Temperature gradient	K/m	sqrt(Tx^2+Ty^2+Tz^2)
flux_htbh	Heat flux	W/m^2	sqrt(fluxx_htbh^2+fluxy_htbh^2+fluxz_htbh^2)
Qb_htbh	Blood perfusion heat source	W/m^3	rhob_htbh * Cb_htbh * wb_htbh * (Tb_htbh-T)
Hb_htbh	Blood perfusion heat transfer		

APPENDIX C

SYNTHESIS AND CHARACTERIZATION OF MAGNETIC SHAPE MEMORY POLYMER NANOCOMPOSITES

This section is based on work published as:

C. Yakacki, N.S. Satarkar, K. Gall, R. Likos, J.Z. Hilt, Shape-memory polymer networks with Fe_3O_4 nanoparticles for inductive heating, J Appl Polymer Sci 112 5(2009) 3166-3176.

C.1 Summary

Shape-memory polymers (SMPs) have recently shown the capacity to actuate by remote heating via the incorporation of magnetic nanoparticles into the polymer matrix and exposure to an alternating magnetic field (AMF). In this study, methacrylate-based thermoset SMP networks were synthesized through free-radical polymerization with varying amounts of Fe_3O_4 magnetite (0, 1, and 2.5 wt%). The remote heating of the networks was shown to be a direct function of the nanoparticle concentration and independent of the polymer chemistry.

C.2 Introduction

Shape memory polymers (SMPs) are a class of polymers with the ability to go from temporary shape to permanent shape on application of an external stimulus.[1, 2] Heat is the most widely studied stimulus to actuate shape memory polymers.[3-5] SMPs are

being pursued for a variety of applications including minimally invasive surgery,[6-11] sensors, and actuators.[5, 12]

The shape in which SMPs are synthesized is called their permanent shape. A typical shape memory cycle begins by heating the SMP above its glass transition temperature (T_g). A force is then applied in its rubbery state to allow for deformation. The sample is cooled below its T_g to lock the polymer in the temporary shape. Ideally, it is possible for the polymer to remain in the temporary shape for long periods of time. Reheating the polymer through glass transition would lead to recovery to its permanent shape.[13]

In the case of biomedical applications, it may not be possible to deliver heat directly at the site of implant. One of the ways to achieve remote controlled (RC) SMP heating is through actuation of embedded nanoparticulate material. In particular, magnetic nanoparticles can generate heat when exposed to alternating magnetic field (AMF).[14-16] The goal of this study is to develop a magnetic SMP nanocomposite and achieve remote shape actuation through application AMF. **Figure C.1** is an example of a remotely heated shape-memory polymer recovering from a flattened strip to a helix shape.

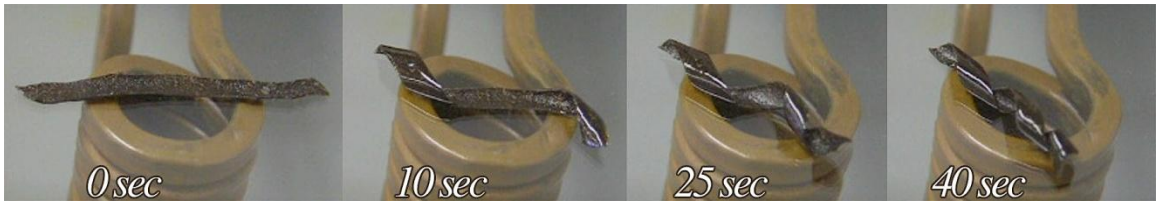

Figure C.1. Fe_3O_4 reinforced shape-memory polymer recovering from a flattened sheet to a helix using remote heating for activation.

The following sections describe synthesis, conversion analysis, characterization of dispersion, and remote heating of magnetic SMP nanocomposites. The details of thermomechanical characterization are not presented here and can be found in the published article.

C.3 Materials and methods

C.3.1 Materials

Methyl methacrylate (MMA), poly(ethylene glycol)$_n$ dimethacrylate (PEGDMA) with a typical M_n of 550, 750, and 1000 g/mol, photoinitiator 2,2-dimethoxy-2-phenylacetophenone (DMPA), and thermal initiator 2,2'-Azobisisobutyronitrile were ordered from Sigma-Aldrich and used as received. Spherical iron-oxide nanoparticles (Fe_3O_4 magnetite) with a mean diameter of 20-30 nm were purchased from Nanostructured and Amorphous Materials Inc.

C.3.2 Nanocomposite synthesis

Monomer solutions were created using MMA crosslinked with PEGDMA. The amount and M_n of the PEGDMA was varied to create three polymer networks with similar glass transition temperatures and varying rubbery modulus values. The networks were designated 9006, 9011, and 9016 and contain 29.2, 36.2, and 47.0 wt% of PEGDMA crosslinking monomer, respectively. Ethanol was added 50% by weight and nanoparticles were added at loadings of 0, 1, and 2.5 wt% of the monomer mixture (0, 0.227, 0.565 vol%, respectively). The particles were dispersed uniformly in the solution by probe sonication (Fisher Scientific, Sonic Dismembrator Model 500) for 5 minutes followed by sonication in an ultrasonic bath for 30 minutes. The photoinitiator and thermal initiator

were added at 1 wt% each of the total monomer mixture and their complete dissolution was insured by bath sonication. The solutions were then pipetted into a mold of two 15 x 15 cm^2 glass plates separated by a 500 μm Teflon spacer. The mold was then transferred to a UV source (LESCO, FEM 1011) with a wavelength 365 nm and intensity 17.5 mW/cm^2. Polymerization was carried out for 5 minutes. Uniform intensity on both sides of the film was ensured during polymerization. The mold was then immediately removed and placed in an oven at 55^oC for 24 hours to increase overall conversion. The polymer film was then removed from the mold and placed in deionized water. Each nanocomposite film was washed daily by changing its water until no significant monomers were observed in wash water. The films were then dried in air followed by vacuum oven for 24 hours.

C.3.3 Conversion analysis

The conversion of the nanocomposite synthesis was analyzed using attenuated total reflectance Fourier transformed infrared spectroscopy (FTIR-ATR). First, the IR spectrum of the monomer solution was collected. After polymerization was complete, the IR spectrum of the nanocomposite surface was collected on both sides of the nanocomposite film. The conversion of the monomers were determined by standard baseline techniques using the peak area of the 1636 cm^{-1} for C=C vibration and the area of 1716 cm^{-1} for C=O stretching as reference. The conversion of the double bond was determined from the following formula:

$$\varepsilon = 1 - \frac{C}{U} \qquad (C.1)$$

Where *C* is the ratio of peak area of the C=C to the reference peak area of C=O after polymerization, and *U* is the ratio of same peak area of the pre-polymer solution.

C.3.4 SEM analysis

The morphology of nanocomposites and nanoparticle dispersion was analyzed using scanning electron microscopy (Hitachi, S4300). The samples were freeze-fractured and cross-sectional images were taken for 0, 1, and 2.5% particle loaded 9016 systems.

C.3.5 Remote heating on exposure to alternating magnetic field(AMF)

The heating response of nanocomposites exposed to an alternating magnetic field (AMF) was characterized using an induction power supply (Taylor Winfield, MMF-3-135/400-2). Polymer discs were cut in to 15 mm diameters and placed in a glass Petri dish on top of the solenoid (15 mm diameter, 5 turns) to get AMF strength of 33×10^{-4} T and frequency 297 kHz. An IR camera (AGEMA, Thermovision 470) was used to record surface temperatures of the discs. The field heating was continued for 5 minutes and results were averaged over three samples.

C.4 Results and discussion

C.4.1 Conversion analysis

The method for calculating the conversion is shown in **figure C.2(a)**, which shows the reduction in absorbance at 1636 cm^{-1} for C=C vibrations in the acrylic double bonds. For high conversions, the polymerizations showed approximately a complete disappearance of the absorbance peak at 1636 cm^{-1}. The conversions of the polymer networks are shown

in **figure C.2(b)**. Near complete conversion is reached for the virgin networks containing no Fe_3O_4 nanoparticles. The 9006 networks showed near complete conversion for both nanoparticle concentrations. The 9011 network dropped to 93 and 91% conversion for the 1 and 2.5 wt% compositions, respectively. In the 9016 networks, a slight drop in conversion to 92% was seen for the 1 wt% composition, though near complete conversion was seen in the 2.5 wt% composition. The decrease in conversions can lead to decrease in the thermomechanical properties of the material.

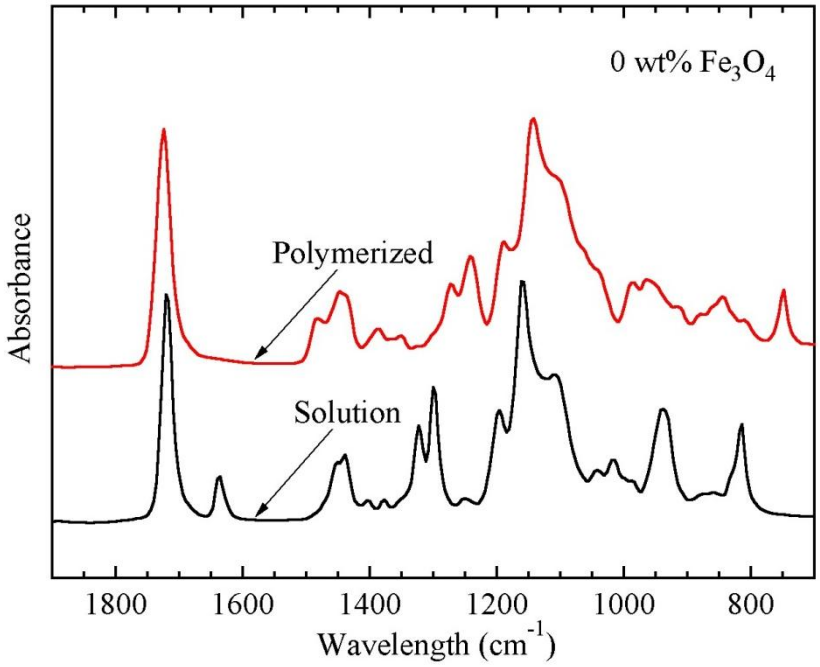

(a)

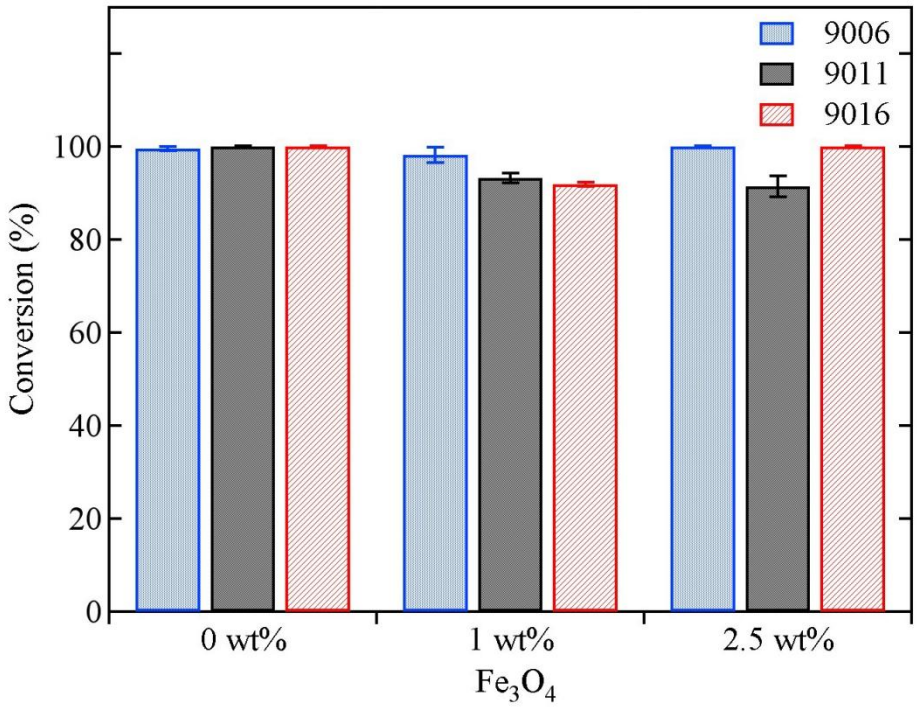

(b)

Figure C.2. (a) FTIR analysis of the starting monomer solution and final polymer. (b) Conversion of all 9 polymer networks.

C.4.2 SEM analysis

SEM analysis of the cross-sectional view of the virgin and reinforced polymers are shown in **figure C.3**. The bottom set of photographs shows the samples at 10x more magnification than the top set. The virgin networks containing no Fe_3O_4 nanoparticles show smoother fracture planes as compared to the reinforced networks. The lower magnification images show the regions with significant particle agglomerations.

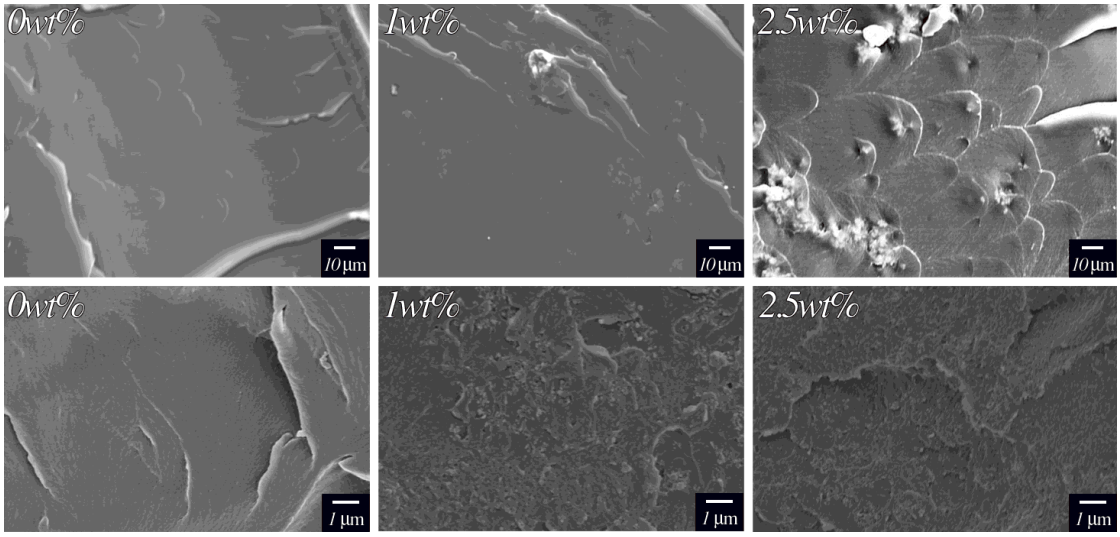

Figure C.3. SEM analysis of 0, 1, and 2.5 wt% Fe_3O_4 networks at low (top) and high (bottom) magnifications.

C.4.3 Remote heating on exposure to alternating magnetic field(AMF)

The heating was assessed via infrared imaging. **Figure C.4(a)** shows the infrared images of the 9006 network with 2.5 wt% Fe_3O_4 being heated over a 5 minute period. The heating profiles of the networks over time are summarized in **figure C.4(b)**. In general, all of the networks started at room temperature and experienced heating over 5 minutes. The networks with 2.5 wt% Fe_3O_4 experienced the greatest heating and all reached 51.7°C after 5 minutes while the networks with 1.0 wt% Fe_3O_4 reached tempearatures between 38 and 41°C. As a baseline for comparison, the networks with 0 wt% were measured and experienced an increase of approximately 7°C above room temperature to 30°C.

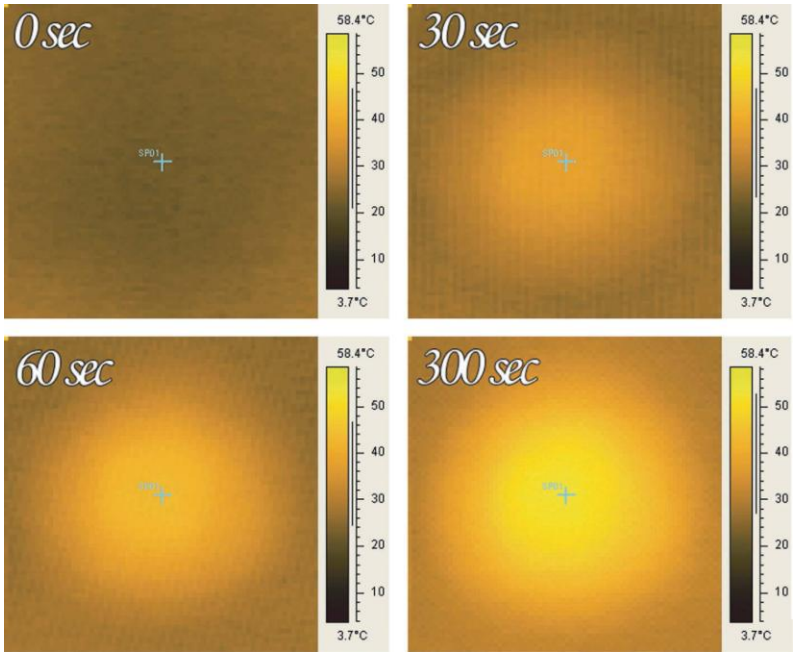

(a)

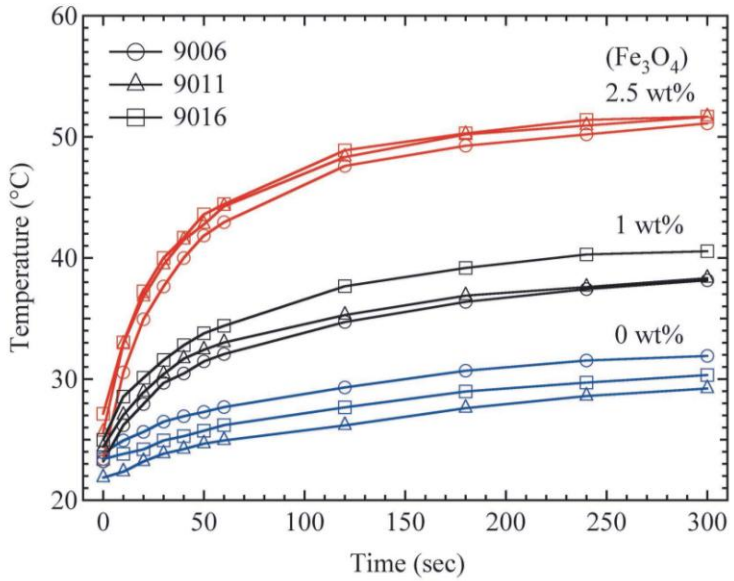

(b)

Figure C.4. **(**a) Image analysis of heating a 2.5 wt% Fe_3O_4 sample. (b) Heating profiles of the 9 networks over time.

C.5 Conclusions

Methacrylate-based SMP networks were synthesized through free-radical polymerization with varying amounts of Fe_3O_4 nanoparticles (0, 1, and 2.5 wt%). The analysis of conversion and particle dispersion was conducted. The heating of the Fe_3O_4 filled SMPs was directly influenced by the concentration of magnetite and not by the crosslink density of the networks. Additionally, remotely activated polymer recovery was demonstrated.

C.6 References

[1] Z.G. Wei, R. Sandstrom, S. Miyazaki, Shape-memory materials and hybrid composites for smart systems - Part I Shape-memory materials. Journal of Materials Science 33(15) (1998) 3743-3762.

[2] D. Ratna, J. Karger-Kocsis, Recent advances in shape memory polymers and composites: a review. Journal of Materials Science 43(1) (2008) 254-269.

[3] C.M. Yakacki, S. Willis, C. Luders, K. Gall, Deformation Limits in Shape-Memory Polymers. Advanced Engineering Materials 10(1-2) (2008) 112-119.

[4] M. Behl, A. Lendlein, Shape-memory polymers. Materials Today 10(4) (2007) 20-28.

[5] J. Kunzelman, T. Chung, P.T. Mather, C. Weder, Shape memory polymers with built-in threshold temperature sensors. Journal of Materials Chemistry 18(10) (2008) 1082-1086.

[6] G. Baer, T.S. Wilson, D.L. Matthews, D.J. Maitland, Shape-memory behavior of thermally stimulated polyurethane for medical applications. Journal of Applied Polymer Science 103(6) (2007) 3882-3892.

[7] C.M. Yakacki, R. Shandas, C. Lanning, B. Rech, A. Eckstein, K. Gall, Unconstrained recovery characterization of shape-memory polymer networks for cardiovascular applications. Biomaterials 28(14) (2007) 2255-2263.

[8] F. El Feninat, G. Laroche, M. Fiset, D. Mantovani, Shape memory materials for biomedical applications. Advanced Engineering Materials 4(3) (2002) 91-104.

[9] W. Sokolowski, A. Metcalfe, S. Hayashi, L. Yahia, J. Raymond, Medical applications of shape memory polymers. Biomed. Mater. 2(1) (2007) S23-S27.

[10] H.M. Wache, D.J. Tartakowska, A. Hentrich, M.H. Wagner, Development of a polymer stent with shape memory effect as a drug delivery system. Journal of Materials Science-Materials in Medicine 14(2) (2003) 109-112.

[11] A. Lendlein, S. Kelch, Shape-memory polymers as stimuli-sensitive implant materials. Clinical Hemorheology and Microcirculation 32(2) (2005) 105-116.

[12] K. Gall, P. Kreiner, D. Turner, M. Hulse, Shape-memory polymers for microelectromechanical systems. Journal of Microelectromechanical Systems 13(3) (2004) 472-483.

[13] K. Gall, C.M. Yakacki, Y.P. Liu, R. Shandas, N. Willett, K.S. Anseth, Thermomechanics of the shape memory effect in polymers for biomedical applications. Journal of Biomedical Materials Research Part A 73A(3) (2005) 339-348.

[14] P.R. Buckley, G.H. McKinley, T.S. Wilson, W. Small, W.J. Benett, J.P. Bearinger, M.W. McElfresh, D.J. Maitland, Inductively heated shape memory polymer for the magnetic actuation of medical devices. IEEE Trans Biomed Eng 53(10) (2006) 2075-2083.

[15] R. Mohr, K. Kratz, T. Weigel, M. Lucka-Gabor, M. Moneke, A. Lendlein, Initiation of shape-memory effect by inductive heating of magnetic nanoparticles in thermoplastic polymers. Proc. Natl. Acad. Sci. U. S. A. 103(10) (2006) 3540-3545.

[16] M.Y. Razzaq, M. Anhalt, L. Frormann, B. Weidenfeller, Thermal, electrical and magnetic studies of magnetite filled polyurethane shape memory polymers. Materials Science and Engineering: A 444(1-2) (2007) 227-235.

APPENDIX D

SUPPORTING INFORMATION FOR DIFFERENT CHARACTERIZATION TECHNIQUES

D.1 Buoyancy measurements

Swelling studies were performed by weight measurements of the hydrogel disc in air (W_a) and in n-Heptane (W_h). Based on the Archimedes' principle,

$$W_a - W_h = V\rho g \qquad (D.1)$$

where V is the volume of the hydrogel disc, ρ is density of n-Heptane, and g is acceleration due to gravity.

Volume swelling ratio is the ratio of hydrogel volume in swollen state (V_s) to the volume in dry state (V_d)

$$Q = \frac{V_s}{V_d} \qquad (D.2)$$

Using equations (D.1) and (D.2), the volume swelling ratio can be expressed as

$$Q = \frac{W_a^s - W_h^s}{W_a^d - W_h^d} \qquad (D.3)$$

D.2Calculation of AMF amplitude

Consider a solenoid of certain length (l) and radius (r) carrying given current (i) (**Figure D.1)**.

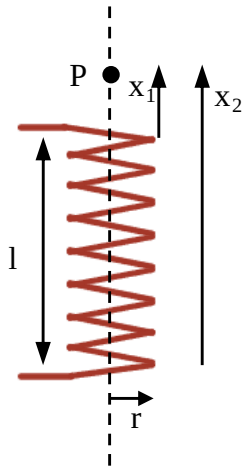

Figure D.1. Schematic of a solenoid generating AMF.

The amplitude of the resultant magnetic field varies with the position. Flux density at point P along axis of the solenoid is given by[1]

$$B = \frac{\mu_0 iN}{2l}\left[\frac{x_2}{\sqrt{x_2^2 + r^2}} - \frac{x_1}{\sqrt{x_1^2 + r^2}}\right] \qquad (D.4)$$

where μ_0 is permeability constant of air (1.25 x 10^{-6} T.m/A), N is the number of turns, x_1 and x_2 is the distance of point P from the ends of solenoid. The amplitude at the center of solenoid is given by

$$B = \frac{\mu_0 iN}{\sqrt{l^2 + r^2}} \qquad (D.5)$$

AMF amplitude (H) is given by

$$H = \frac{B}{\mu_0} \qquad (D.6)$$

D.3 Heating of magnetic nanoparticles in alternating magnetic fields (AMF)

Fe_3O_4 particles at very small size (<30 nm) can be superparamagnetic in nature. Superparamagnetism is a magnetization reversal mechanism driven by thermal energy. When superparamagnetic nanoparticles are exposed to AMF, the resultant heating is attributed to Neel and Brownian relaxation processes.[2] Relaxation processes are the gradual alignment of magnetic moments during magnetization process. The Brownian relaxation time is given by following equation

$$\tau_B = \frac{3\eta V_H}{\kappa T} \qquad (D.7)$$

where η is the viscosity of the liquid surrounding particle, V_H is hydrodynamic volume of the particle, κ is a constant, and T is absolute temperature

The Neel relaxation time is given by

$$\tau_N = \tau_0 \exp \frac{KV}{K_b T} \qquad (D.8)$$

where τ_0 is time constant, K_b is Boltzmann constant, K is anisotropy constant, and V is the volume of particle core.

The power loss due to Neel and Brownian relaxations is approximately given by

$$P = \pi \mu_0 \chi_0 H_0^2 f \frac{2\pi f\tau}{1 + (2\pi f\tau)^2} \qquad (D.9)$$

where μ_0 is permeability of vacuum (1.25 x 10^{-6} T.m/A), χ_0 is the equilibrium susceptibility, H_0 is the amplitude and *f* is the frequency of AMF. Both the relaxations

simultaneously occur in AMF and the fastest process (shortest time) dominates the resultant relaxation time (τ).

Fe_3O_4 nanoparticles at a bigger size (>20 nm) can be ferromagnetic in nature. The heat generation on the application of AMF can result from hysteresis losses, in addition to the relaxation processes. Hysteresis loops for the Fe_3O_4 nanoparticles used in synthesis of magnetic hydrogel nanocomposites are presented in **figure D.2**. Heat generated due to hysteresis losses is proportional to the area of hysteresis loop and the frequency of AMF.[3]

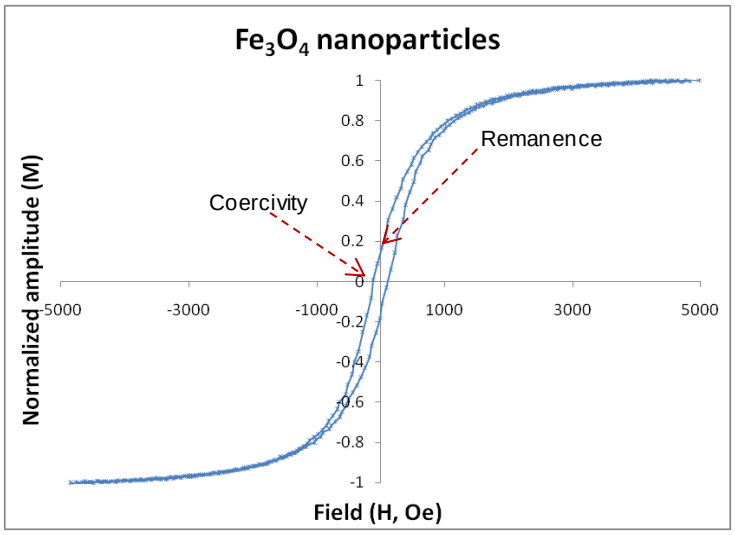

Figure D.2. Hysteresis loops for magnetic nanoparticles obtained using vibrating sample magnetometry.

D.4Analysis of drug release

Drug release from polymeric systems can be described by the power law model[4]

$$\frac{M_t}{M_\infty} = kt^n \qquad (D.10)$$

where M_t and M_∞ are the absolute cumulative amounts of drug released at time t and infinite time, respectively; k is a constant incorporating geometric and structural characteristics of the device; n is the release exponent, indicating mechanism of release. In case of the slab geometry, n=0.5 indicates diffusion controlled (Case I) transport, while n=1 indicates swelling controlled (Case II) transport[5].

For a matrix system with drug uniformly dispersed throughout the system, unsteady state drug diffusion in slab geometry (**figure D.3**) is given by Fick's second law of diffusion

$$\frac{dC_A}{dt} = D\frac{d^2C_A}{dx^2} \qquad (D.11)$$

where C_A is the concentration and D is diffusivity of the drug molecule.

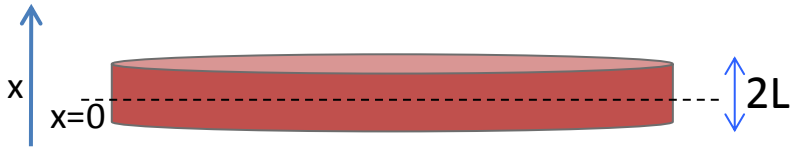

Figure D.3. Schematic of a slab geometry with drug uniformly dispersed throughout the matrix.

For constant diffusivity, infinite sink conditions around the slab, and neglecting edge effects (aspect ratio>10), the solution of above equation is given by[6]

$$\frac{M_t}{M_\infty} = 1 - \sum_{n=0}^{\infty} \frac{8}{(2n+1)^2\pi^2} \exp\left[\frac{-(2n+1)^2\pi^2 D}{L^2}t\right] \qquad (D.12)$$

where L is the half thickness of the slab. For short time intervals ($0< M_t/M_\infty <0.6$), equation (D.12) can be approximated as

$$\frac{M_t}{M_\infty} = 4\left(\frac{Dt}{\pi L^2}\right)^{1/2} \qquad (D.13)$$

D.5 References

[1] P.A. Tipler, G.P. Mosca, Physics for scientists and engineers, W.H.Freeman, 2008.

[2] X. Wang, H. Gu, Z. Yang, The heating effect of magnetic fluids in an alternating magnetic field. J. Magn. Magn. Mater. 293 (2005) 334-340.

[3] M. Ma, Y. Wu, J. Zhou, Y. Sun, Y. Zhang, N. Gu, Size dependence of specific power absorption of Fe3O4 particles in AC magnetic field. J. Magn. Magn. Mater. 268(1-2) (2004) 33-39.

[4] J. Siepmann, N.A. Peppas, Modeling of drug release from delivery systems based on hydroxypropyl methylcellulose (HPMC). Adv. Drug Deliver. Rev. 48(2-3) (2001) 139-157.

[5] C.-C. Lin, A.T. Metters, Hydrogels in controlled release formulations: Network design and mathematical modeling. Adv. Drug Deliver. Rev. 58(12-13) (2006) 1379-1408.

[6] J.Z. Hilt, M.E. Byrne, N.A. Peppas, Microfabrication of intelligent biomimetic networks for recognition of d-glucose. Chem. Mater. 18(25) (2006) 5869-5875.

BIBLIOGRAPHY

Adriane K., Jian H., Guowei D., Jie C., Yinfeng L., Self assembled magnetic PVP/PVA hydrogel microspheres; magnetic drug targeting of VX2 auricular tumours using pingyangmycin. J. Drug Targeting 14(4) (2006) 243-253.

Agarwal A.K., Dong L., Beebe D.J., Jiang H., Autonomously-triggered microfluidic cooling using thermo-responsive hydrogels. Lab Chip 7(3) (2007) 310-315.

Andra W., in: W. Andra and H. Nowak (Eds.), Magnetism in medicine, Wiley-VCH, Berlin, 1998, pp. 455-470.

Arkin H., Xu L.X., Holmes K.R., Recent developments in modeling heat transfer in blood perfused tissues. IEEE Transactions on Biomedical Engineering 41(2) (1994) 97-107.

Babincová M., Leszczynska D., Sourivong P., Cicmanec P., Babinec P., Superparamagnetic gel as a novel material for electromagnetically induced hyperthermia. J. Magn. Magn. Mater. 225(1-2) (2001) 109-112.

Babincova M., Novotny J., Rosenecker J., Babinec P., Remote radio-control of siRNA release from magnetite-hydrogel composite. Optoelectronics and Advanced Materials – Rapid Communications 1(11) (2007) 644-647.

Baer G., Wilson T.S., Matthews D.L., Maitland D.J., Shape-memory behavior of thermally stimulated polyurethane for medical applications. Journal of Applied Polymer Science 103(6) (2007) 3882-3892.

Bagaria H.G., Johnson D.T., Transient solution to the bioheat equation and optimization for magnetic fluid hyperthermia treatment. International Journal of Hyperthermia, Vol. 21, Taylor & Francis Ltd, 2005, pp. 57-75.

Baldi A., Yuandong G., Loftness P.E., Siegel R.A., Ziaie B., A hydrogel-actuated environmentally sensitive microvalve for active flow control. Journal of Microelectromechanical Systems 12(5) (2003) 613-621.

Bashir R., Hilt J.Z., Elibol O., Gupta A., Peppas N.A., Micromechanical cantilever as an ultrasensitive pH microsensor. Appl. Phys. Lett. 81(16) (2002) 3091-3093.

Baughman R.H., Zakhidov A.A., De Heer W.A., Carbon nanotubes--The route toward applications. Science 297(5582) (2002) 787-792.

Beebe D.J., Moore J.S., Bauer J.M., Yu Q., Liu R.H., Devadoss C., Jo B.-H., Functional hydrogel structures for autonomous flow control inside microfluidic channels. Nature 404(6778) (2000) 588-590.

Behl M., Lendlein A., Shape-memory polymers. Materials Today 10(4) (2007) 20-28.

Benítez R., Fuentes A., Lozano K., Effects of microwave assisted heating of carbon nanofiber reinforced high density polyethylene. Journal of Materials Processing Technology 190(1-3) (2007) 324-331.

Bhattacharyya S., Guillot S., Dabboue H., Tranchant J.-F., Salvetat J.-P., Carbon nanotubes as structural nanofibers for hyaluronic acid hydrogel scaffolds. Biomacromolecules 9(2) (2008) 505-509.

Bianco A., Kostarelos K., Partidos C.D., Prato M., Biomedical applications of functionalised carbon nanotubes. Chemical Communications(5) (2005) 571-577.

Bikram M., Gobin A.M., Whitmire R.E., West J.L., Temperature-sensitive hydrogels with SiO2-Au nanoshells for controlled drug delivery. J. Control. Rel. 123(3) (2007) 219-227.

Boldor D., Gerbo N.M., Monroe W.T., Palmer J.H., Li Z., Biris A.S., Temperature measurement of carbon nanotubes using infrared thermography. Chem. Mater. 20(12) (2008) 4011-4016.

Buckley P.R., Mckinley G.H., Wilson T.S., Small W., Benett W.J., Bearinger J.P., Mcelfresh M.W., Maitland D.J., Inductively heated shape memory polymer for the magnetic actuation of medical devices. IEEE Trans Biomed Eng 53(10) (2006) 2075-2083.

Budhlall B.M., Marquez M., Velev O.D., Microwave, photo- and thermally responsive PNIPAAm gold nanoparticle microgels. Langmuir 24(20) (2008) 11959-11966.

Bussemer T., Otto I., Bodmeier R., Pulsatile drug-delivery systems. Crit. Rev. Ther. Drug. 18(5) (2001) 433-458.

Candeo A., Dughiero F., Numerical FEM models for the planning of magnetic induction hyperthermia treatments with nanoparticles. IEEE Trans. Magn. 45(3) (2009) 1658-1661.

Chakraborty S., Raj C.R., Mediated electrocatalytic oxidation of bioanalytes and biosensing of glutamate using functionalized multiwall carbon nanotubes-biopolymer nanocomposite. J. Electroanal. Chem. 609(2) (2007) 155-162.

Chakravarty P., Marches R., Zimmerman N.S., Swafford A.D.-E., Bajaj P., Musselman I.H., Pantano P., Draper R.K., Vitetta E.S., Thermal ablation of tumor cells with antibody-functionalized single-walled carbon nanotubes. Proceedings of the National Academy of Sciences 105(25) (2008) 8697-8702.

Chambers B., Lee T.-Y.T., A numerical study of local and average natural convection Nusselt numbers for simultaneous convection above and below a uniformly heated horizontal thin plate. J. Heat Transfer 119(1) (1997) 102-108.

Chaterji S., Kwon I.K., Park K., Smart polymeric gels: Redefining the limits of biomedical devices. Prog. Polym. Sci. 32(8-9) (2007) 1083-1122.

Chen G., Svec F., Knapp D.R., Light-actuated high pressure-resisting microvalve for on-chip flow control based on thermo-responsive nanostructured polymer. Lab Chip 8(7) (2008) 1198-1204.

Chen J., Yang L., Liu Y., Ding G., Pei Y., Li J., Hua G., Huang J., Preparation and characterization of magnetic targeted drug controlled-release hydrogel microspheres. Macromol. Symp. 225(1) (2005) 71-80.

Chirra H., Biswal D., Hilt J.Z., in: D. T. Pathak (Ed.), Nanoparticulate Drug Delivery Systems (NPDDS) II: Formulation and Characterization, Informa Healthcare, New York, 2009, in press, pp. 90-114.

Coffey D.S., Getzenberg R.H., Deweese T.L., Hyperthermic biology and cancer therapies: A hypothesis for the "Lance Armstrong Effect". JAMA: The Journal of the American Medical Association 296(4) (2006) 445-448.

Coleman J.N., Khan U., Gun-Ko Y.K., Mechanical reinforcement of polymers using carbon nanotubes. Adv. Mater. 18 (2006) 689-706.

Das M., Sanson N., Fava D., Kumacheva E., Microgels loaded with gold nanorods: Photothermally triggered volume transitions under physiological conditions Langmuir 23(1) (2006) 196-201.

Derfus A.M., Maltzahn G.V., Harris T.J., Duza T., Vecchio K.S., Ruoslahti E., Bhatia S.N., Remotely triggered release from magnetic nanoparticles. Adv. Mater. 19 (2007) 3932-3936.

Dong L., Jiang H., Autonomous microfluidics with stimuli-responsive hydrogels. Soft Matter 3(10) (2007) 1223-1230.

Dresco P.A., Zaitsev V.S., Gambino R.J., Chu B., Preparation and Properties of Magnetite and Polymer Magnetite Nanoparticles. Langmuir 15(6) (1999) 1945-1951.

Eddington D.T., Beebe D.J., Flow control with hydrogels. Adv. Drug Deliver. Rev. 56(2) (2004) 199-210.

Eddington D.T., Beebe D.J., A valved responsive hydrogel microdispensing device with integrated pressure source. Journal of Microelectromechanical Systems 13(4) (2004) 586-593.

Eddington D.T., Liu R.H., Moore J.S., Beebe D.J., An organic self-regulating microfluidic system. Lab Chip 1(2) (2001) 96-99.

Edelman E.R., Kost J., Bobeck H., Langer R., Regulation of drug release from polymer matrices by oscillating magnetic fields. J. Biomed. Mater. Res. 19(1) (1985) 67-83.

El Feninat F., Laroche G., Fiset M., Mantovani D., Shape memory materials for biomedical applications. Advanced Engineering Materials 4(3) (2002) 91-104.

Falk M.H., Issels R.D., Hyperthermia in oncology. International Journal of Hyperthermia 17(1) (2001) 1-18.

Filipcsei G., Csetneki I., Szilagyi A., Zrinyi M., Magnetic field-responsive smart polymer composites Adv. Polym. Sci. 206 (2007) 137-189.

Frimpong R.A., Fraser S., Hilt J.Z., Synthesis and temperature response analysis of magnetic-hydrogel nanocomposites. J. Biomed. Mater. Res. A 80A(1) (2007) 1-6.

Frimpong R.A., Hilt J.Z., in: N. A. Peppas, J. Z. Hilt and J. B. Thomas (Eds.), Nanotechnology in Therapeutics: Current Technology and Applications, Horizon Scientific Press, Norfolk, 2007, pp. 241-256.

Frimpong R.A., Hilt J.Z., Magnetic nanoparticles in biomedicine: Properties, synthesis, and functionalization. Nanomedicine (Under review).

Frimpong R.A., Hilt J.Z., Poly(n-isopropylacrylamide)-based hydrogel coatings on magnetite nanoparticles via atom transfer radical polymerization. Nanotechnology 19(Issue 17) (2008) 175101-175107.

Fuhrer R., Athanassiou E.K., Luechinger N.A., Stark W.J., Crosslinking metal nanoparticles into the polymer backbone of hydrogels enables preparation of soft, magnetic field-driven actuators with muscle-like flexibility. Small 5(3) (2009) 383-388.

Fujigaya T., Morimoto T., Niidome Y., Nakashima N., NIR laser-driven reversible volume phase transition of single-walled carbon nanotube/poly(N-isopropylacrylamide) composite gels. Adv. Mater. 20(19) (2008) 3610-3614.

Gall K., Kreiner P., Turner D., Hulse M., Shape-memory polymers for microelectromechanical systems. Journal of Microelectromechanical Systems 13(3) (2004) 472-483.

Gall K., Yakacki C.M., Liu Y.P., Shandas R., Willett N., Anseth K.S., Thermomechanics of the shape memory effect in polymers for biomedical applications. Journal of Biomedical Materials Research Part A 73A(3) (2005) 339-348.

Gannon C.J., Cherukuri P., Yakobson B.I., Cognet L., Kanzius J.S., Kittrell C., Weisman R.B., Pasquali M., Schmidt H.K., Smalley R.E., Curley S.A., Carbon nanotube-enhanced thermal destruction of cancer cells in a noninvasive radiofrequency field. Cancer 110(12) (2007) 2654-2665.

Gattas-Asfura K.M., Zheng Y., Micic M., Snedaker M.J., Ji X., Sui G., Orbulescu J., Andreopoulos F.M., Pham S.M., Wang C., Leblanc R.M., Immobilization of quantum dots in the photo-cross-linked poly(ethylene glycol)-based hydrogel. J. Phys. Chem. B 107(38) (2003) 10464-10469.

Ghosh S., Yang C., Cai T., Hu Z., Neogi A., Oscillating magnetic field-actuated microvalves for micro- and nanofluidics. J. Phys. D: Appl. Phys. 42(13) (2009) 135501.

Gil E.S., Hudson S.M., Stimuli-reponsive polymers and their bioconjugates. Prog. Polym. Sci. 29(12) (2004) 1173-1222.

Golonka L.J., Technology and applications of low temperature cofired ceramic (LTCC) based sensors and microsystems. Bulletin of the Polish Academy of Sciences, Technical Sciences 54(2) (2006) 221-231.

Gong P., Yu J., Sun H., Hong J., Zhao S., Xu D., Yao S., Preparation and characterization of OH-functionalized magnetic nanogels under UV irradiation. Journal of Applied Polymer Science 101(3) (2006) 1283-1290.

Gongora-Rubio M.R., Espinoza-Vallejos P., Sola-Laguna L., Santiago-Avilés J.J., Overview of low temperature co-fired ceramics tape technology for meso-system technology (MsST). Sensors and Actuators A: Physical 89(3) (2001) 222-241.

Govorov A.O., Richardson H.H., Generating heat with metal nanoparticles. Nanotoday 2(1) (2007) 30-38.

Grayson A.C.R., Choi I.S., Tyler B.M., Wang P.P., Brem H., Cima M.J., Langer R., Multi-pulse drug delivery from a resorbable polymeric microchip device. Nat. Mater. 2 (2003) 767 - 772.

Groß G.A., Thelemann T., Schneider S., Boskovic D., Köhler J.M., Fabrication and fluidic characterization of static micromixers made of low temperature cofired ceramic (LTCC). Chem. Eng. Sci. 63(10) (2008) 2773-2784.

Hahn R., Krumbholz S., Reichl H., Low profile power inductors based on ferromagnetic LTCC technology. Electronic Components and Technology Conference, 2006. Proceedings. 56th, 2006, p. 6 pp.

Haider S., Park S.-Y., Saeed K., Farmer B.L., Swelling and electroresponsive characteristics of gelatin immobilized onto multi-walled carbon nanotubes. Sensors and Actuators B: Chemical 124(2) (2007) 517-528.

Hand J.W., Lau R.W., Lagendijk J.J.W., Ling J., Burl M., Young I.R., Electromagnetic and thermal modeling of SAR and temperature fields in tissue due to an RF decoupling coil. Magnetic Resonance in Medicine 42(1) (1999) 183-192.

Haraguchi K., Nanocomposite hydrogels. Current Opinion in Solid State and Materials Science 11(3-4) 47-54.

Haraguchi K., Li H.-J., Control of the coil-to-globule transition and ultrahigh mechanical properties of PNIPA in nanocomposite hydrogels. Angew. Chem. 117(40) (2005) 6658-6662.

Haraguchi K., Li H.J., Matsuda K., Takehisa T., Elliott E., Mechanism of forming organic/inorganic network structures during in-situ free-radical polymerization in PNIPA-clay nanocomposite hydrogels. Macromolecules 38(8) (2005) 3482-3490.

Haraguchi K., Takehisa T., Nanocomposite hydrogels: A unique organic-inorganic network structure with extraordinary mechanical, optical, and swelling/de-swelling properties. Adv. Mater. 14(16) (2002) 1120-1124.

Harmon M.E., Tang M., Frank C.W., A microfluidic actuator based on thermoresponsive hydrogels. Polymer 44(16) (2003) 4547-4556.

Hawkins A., Satarkar N., Hilt J., Nanocomposite degradable hydrogels: demonstration of remote controlled degradation and drug release. Pharm. Res. 26(3) (2009) 667-673.

He C., Kim S.W., Lee D.S., In situ gelling stimuli-sensitive block copolymer hydrogels for drug delivery. J. Control. Rel. 127(3) (2008) 189-207.

Hergt R., Andra W., D'ambly C.G., Hilger I., Kaiser W.A., Richter U., Schmidt H.G., Physical limits of hyperthermia using magnetite fine particles. Magnetics, IEEE Transactions on 34(5) (1998) 3745-3754.

Hildebrandt B., Wust P., Ahlers O., Dieing A., Sreenivasa G., Kerner T., Felix R., Riess H., The cellular and molecular basis of hyperthermia. Critical Reviews in Oncology/Hematology 43(1) (2002) 33-56.

Hilt J.Z., Byrne M.E., Peppas N.A., Microfabrication of intelligent biomimetic networks for recognition of d-glucose. Chem. Mater. 18(25) (2006) 5869-5875.

Hilt J.Z., Gupta A.K., Bashir R., Peppas N.A., Ultrasensitive biomems sensors based on microcantilevers patterned with environmentally responsive hydrogels. Biomedical Microdevices 5(3) (2003) 177-184.

Hirotsu S., Hirokawa Y., Tanaka T., Volume-phase transitions of ionized N-isopropylacrylamide gels. The Journal of Chemical Physics 87(2) (1987) 1392-1395.

Hoare T., Santamaria J., Goya G.F., Irusta S., Lin D., Lau S., Padera R., Langer R., Kohane D.S., A magnetically triggered composite membrane for on-demand drug delivery. Nano Lett. 9(10) (2009) 3651-3657.

Hoare T.R., Kohane D.S., Hydrogels in drug delivery: Progress and challenges. Polymer 49(8) (2008) 1993-2007.

Hoffman A.S., Applications of thermally reversible polymers and hydrogels in therapeutics and diagnostics. J. Control. Rel. 6(1) (1987) 297-305.

Hoffman A.S., Hydrogels in biomedical applications. Adv. Drug Deliver. Rev. 43 (2002) 3-12.

Horsman M.R., Overgaard J., Hyperthermia: a potent enhancer of radiotherapy. Clinical Oncology 19(6) (2007) 418-426.

Hou Y., Tang J., Zhang H., Qian C., Feng Y., Liu J., Functionalized few-walled carbon nanotubes for mechanical reinforcement of polymeric composites. ACS Nano 3(5) (2009) 1057-1062.

Hsieh D.S., R L., J F., Magnetic modulation of release of macromolecules from polymers. Proc. Natl. Acad. Sci. U. S. A. 78(3) (1981) 1863-1867.

Hu S.-H., Liu T.-Y., Liu D.-M., Chen S.-Y., Controlled pulsatile drug release from a ferrogel by a high-frequency magnetic field. Macromolecules 40(19) (2007) 6786-6788.

Hu S.-H., Liu T.-Y., Liu D.-M., Chen S.-Y., Nano-ferrosponges for controlled drug release. J. Control. Rel. 121(3) (2007) 181-189.

Ibañez-Garcia N., Gonçalves R.D.M., Da Rocha Z.M., Góngora-Rubio M.R., Seabra A.C., Chamarro J.A., LTCC meso-analytical system for chloride ion determination in drinking waters. Sensors and Actuators B: Chemical 118(1-2) (2006) 67-72.

Ibanez-Garcia N., Puyol M., Azevedo C.M., Martinez-Cisneros C.S., Villuendas F., Gongora-Rubio M.R., Seabra A.C., Alonso J., Vortex configuration flow cell based on low-temperature cofired ceramics as a compact chemiluminescence microsystem. Anal. Chem. 80(14) (2008) 5320-5324.

Jiang X., Xiong D.A., An Y., Zheng P., Zhang W., Shi L., Thermoresponsive hydrogel of poly(glycidyl methacrylate-co-N-isopropylacrylamide) as a nanoreactor of gold nanoparticles. Journal of Polymer Science Part A: Polymer Chemistry 45(13) (2007) 2812-2819.

Kam N.W.S., O'connell M., Wisdom J.A., Dai H., Carbon nanotubes as multifunctional biological transporters and near-infrared agents for selective cancer cell destruction. Proc. Natl. Acad. Sci. U. S. A. 102(33) (2005) 11600-11605.

Kaneko Y., Yoshida R., Sakai K., Sakurai Y., Okano T., Temperature-responsive shrinking kinetics of poly (N-isopropylacrylamide) copolymer gels with hydrophilic and hydrophobic comonomers. J. Membr. Sci. 101(1-2) (1995) 13-22.

Kato N., Takizawa Y., Takahashi F., Magnetically driven chemomechanical device with poly(N-isopropylacrylamide) hydrogel containing gamma-Fe2O3. Journal of Intelligent Material Systems and Structures 8 (7) (1997) 588-595.

Kawano T., Niidome Y., Mori T., Katayama Y., Niidome T., PNIPAM Gel-Coated Gold Nanorods for Targeted Delivery Responding to a Near-Infrared Laser. Bioconjugate Chemistry 20(2) (2009) 209-212.

Kikuchi A., Okano T., Pulsatile drug release control using hydrogels. Adv. Drug Deliver. Rev. 54 (2002) 53-77.

Kim H., Kim Y., Kim J., An integrated LTCC inductor embedding NiZn ferrite. Magnetics Conference, 2006. INTERMAG 2006. IEEE International, 2006, 353-353.

Kim J.-H., Lee T.R., Thermo- and pH-Responsive Hydrogel-Coated Gold Nanoparticles. Chemistry of Materials 16(19) (2004) 3647-3651.

Kim J.-W., Shashkov E.V., Galanzha E.I., Kotagiri N., Zharov V.P., Photothermal antimicrobial nanotherapy and nanodiagnostics with self-assembling carbon nanotube clusters. Lasers in Surgery and Medicine 39(7) (2007) 622-634.

Koerner H., Price G., Pearce N.A., Alexander M., Vaia R.A., Remotely actuated polymer nanocomposites[mdash]stress-recovery of carbon-nanotube-filled thermoplastic elastomers. Nat. Mater. 3(2) (2004) 115-120.

Kokabi M., Sirousazar M., Hassan Z.M., PVA-clay nanocomposite hydrogels for wound dressing. Eur. Polym. J. 43(3) (2007) 773-781.

Kost J., Langer R., Responsive polymeric delivery systems. Adv. Drug Deliver. Rev. 46 (2001) 125-148.

Kost J., Noecker R., Kunica E., Langer R., Magnetically controlled release systems: effect of polymer composition. J. Biomed. Mater. Res. 19 (1985) 935-940.

Kost J., Wolfrum J., Langer R., Magnetically enhanced insulin release in diabetic rats. J. Biomed. Mater. Res. 21 (1987) 1367-1373.

Kunzelman J., Chung T., Mather P.T., Weder C., Shape memory polymers with built-in threshold temperature sensors. Journal of Materials Chemistry 18(10) (2008) 1082-1086.

Langer R., Peppas N.A., Advances in biomaterials, drug delivery, and bionanotechnology. AIChE J. 49(12) (2003) 2990-3006.

Lao L.L., Ramanujan R.V., Magnetic and hydrogel composite materials for hyperthermia applications. J. Mater. Sci.: Mater. Med. 15 (2004) 1061-1064.

Lee W.-F., Chen Y.-C., Effect of hydrotalcite on the physical properties and drug-release behavior of nanocomposite hydrogels based on poly[acrylic acid-co-poly(ethylene glycol) methyl ether acrylate] gels. J. Appl. Polym. Sci. 94(2) (2004) 692-699.

Lee W.-F., Tsao K.-T., Effect of intercalant content of mica on the various properties for the charged nanocomposite poly(N-isopropyl acrylamide) hydrogels. J. Appl. Polym. Sci. 104(4) (2007) 2277-2287.

Lendlein A., Kelch S., Shape-memory polymers as stimuli-sensitive implant materials. Clinical Hemorheology and Microcirculation 32(2) (2005) 105-116.

Lin C.-C., Metters A.T., Hydrogels in controlled release formulations: Network design and mathematical modeling. Adv. Drug Deliver. Rev. 58(12-13) (2006) 1379-1408.

Liu C., Joong Yull P., Xu Y., Lee S., Arrayed pH-responsive microvalves controlled by multiphase laminar flow. Journal of Micromechanics and Microengineering 17 (2007) 1985-1991.

Liu T.-Y., Hu S.-H., Liu K.-H., Liu D.-M., Chen S.-Y., Preparation and characterization of smart magnetic hydrogels and its use for drug release. J. Magn. Magn. Mater. 304 (2006) e397-e399.

Liu T.-Y., Hu S.-H., Liu K.-H., Liu D.-M., Chen S.-Y., Study on controlled drug permeation of magnetic-sensitive ferrogels: Effect of Fe3O4 and PVA. J. Control. Rel. 126(3) (2008) 228-236.

Liu T.Y., Hu S.H., Liu D.M., Chen S.Y., Magnetic-sensitive behavior of intelligent ferrogels for controlled release of drug. Langmuir 22(14) (2006) 5974-5978.

Liu Y.-J., Guo S.-S., Zhang Z.-L., Huang W.-H., Baigl D., Chen Y., Pang D.-W., Integration of minisolenoids in microfluidic device for magnetic bead--based immunoassays. J. Appl. Phys. 102(8) (2007) 084911-084916.

Lowman A.M., Peppas N.A., Hydrogels. in: E. Mathiowitz (Ed.), Encyclopedia of Controlled Drug Delivery, Vol. 1, Wiley, New York, 1999, pp. 397-418.

Lu F., Gu L., Meziani M.J., Wang X., Luo P.G., Veca L.M., Cao L., Sun Y.-P., Advances in bioapplications of carbon nanotubes. Adv. Mater. 21(2) (2009) 139-152.

Lu Z., Prouty M.D., Guo Z., Golub V.O., Kumar C.S.S.R., Lvov Y.M., Magnetic switch of permeability for polyelectrolyte microcapsules embedded with Co@Au nanoparticles. Langmuir 21 (2005) 2042-2050.

Luo Q., Mutlu S., Gianchandani Y.B., Svec F., Fréchet J.M.J., Monolithic valves for microfluidic chips based on thermoresponsive polymer gels. Electrophoresis 24(21) (2003) 3694-3702.

Lutz J.-F., Polymerization of oligo(ethylene glycol) (meth)acrylates: Toward new generations of smart biocompatible materials. Journal of Polymer Science Part A: Polymer Chemistry 46(11) (2008) 3459-3470.

Ma J., Xu Y., Zhang Q., Zha L., Liang B., Preparation and characterization of pH- and temperature-responsive semi-IPN hydrogels of carboxymethyl chitosan with poly (N-isopropyl acrylamide) crosslinked by clay. Colloid & Polymer Science 285(4) (2007) 479-484.

Ma M., Wu Y., Zhou J., Sun Y., Zhang Y., Gu N., Size dependence of specific power absorption of Fe3O4 particles in AC magnetic field. J. Magn. Magn. Mater. 268(1-2) (2004) 33-39.

Meenach S.A., Anderson A.A., Suthar M., Anderson K.W., Hilt J.Z., Biocompatibility analysis of magnetic hydrogel nanocomposites based on poly(N-isopropylacrylamide) and iron oxide. Journal of Biomedical Materials Research Part A 91A(3) (2009) 903-909.

Meenach S.A., Hilt J.Z., Anderson K.W., Poly(ethylene glycol)-based magnetic hydrogel nanocomposites for hyperthermia cancer therapy. Acta Biomater. In Press (2009).

Melin J., Quake S.R., Microfluidic large-scale integration: The evolution of design rules for biological automation. Annu. Rev. Biophys. Biomol. Struct. 36(1) (2007) 213-231.

Meyer D.E., Shin B.C., Kong G.A., Dewhirst M.W., Chilkoti A., Drug targeting using thermally responsive polymers and local hyperthermia. J. Control. Rel. 74(1-3) (2001) 213-224.

Miyako E., Nagata H., Hirano K., Hirotsu T., Photodynamic thermoresponsive nanocarbon-polymer gel hybrids. Small 4(10) (2008) 1711-1715.

Miyata T., Asami N., Uragami T., A reversibly antigen-responsive hydrogel. Nature 399(6738) (1999) 766-769.

Moeller K., Besecker J., Hampikian G., Moll A., Plumlee D., Youngsman J., Hampikian J.M., A prototype continuous flow polymerase chain reaction LTCC device. THERMEC '2006 Conference, Minerals, Metals and Materials Society, Vancouver, Canada, July 2006.

Mohr R., Kratz K., Weigel T., Lucka-Gabor M., Moneke M., Lendlein A., Initiation of shape-memory effect by inductive heating of magnetic nanoparticles in thermoplastic polymers. Proc. Natl. Acad. Sci. U. S. A. 103(10) (2006) 3540-3545.

Müller-Schulte D., Schmitz-Rode T., Thermosensitive magnetic polymer particles as contactless controllable drug carriers. J. Magn. Magn. Mater. 302(1) (2006) 267-271.

Murali Mohan Y., Lee K., Premkumar T., Geckeler K.E., Hydrogel networks as nanoreactors: A novel approach to silver nanoparticles for antibacterial applications. Polymer 48(1) (2007) 158-164.

Murali Mohan Y., Premkumar T., Lee K., Geckeler K.E., Fabrication of silver nanoparticles in hydrogel networks. Macromol. Rapid Commun. 27(16) (2006) 1346-1354.

Murthy P.S.K., Murali Mohan Y., Varaprasad K., Sreedhar B., Mohana Raju K., First successful design of semi-IPN hydrogel-silver nanocomposites: A facile approach for antibacterial application. J. Colloid Interface Sci. 318(2) (2008) 217-224.

Nayak S., Lyon L.A., Soft nanotechnology with soft nanoparticles. Angew. Chem. Int. Ed. 44(47) (2005) 7686-7708.

Omar M.A., Gharaibeh B., Salazar A.J., Saito K., Infrared thermography (IRT) and ultraviolet fluorescence (UVF) for the nondestructive evaluation of ballast tanks' coated surfaces. NDT & E International 40(1) (2007) 62-70.

Ozarkar S., Jassal M., Agrawal A.K., pH and electrical actuation of single walled carbon nanotube/chitosan composite fibers. Smart Materials and Structures 17(5) (2008) 055016.

Pamme N., Magnetism and microfluidics. Lab Chip 6(1) (2006) 24-38.

Pankhurst Q.A., Connolly J., Jones S.K., Dobson J., Applications of magnetic nanoparticles in biomedicine. J. Phys. D: Appl. Phys. 36 (2003) R167-R181.

Paoli V.M.D., Lacerda S.H.D.P., Spinu L., Ingber B., Rosenzweig Z., Rosenzweig N., Effect of an oscillating magnetic field on the release properties of magnetic collagen gels. Langmuir 22 (2006) 5894-5899.

Parker W.J., Jenkins R.J., Butler C.P., Abbott G.L., Flash method of determining thermal diffusivity, heat capacity, and thermal conductivity. J. Appl. Phys. 32(9) (1961) 1679-1684.

Paton K.R., Windle A.H., Efficient microwave energy absorption by carbon nanotubes. Carbon 46(14) (2008) 1935-1941.

Pennes H.H., Analysis of tissue and arterial blood temperatures in the resting human forearm. J. Appl. Physiol. 1(2) (1948) 93-122.

Peppas N.A., in: B. D. Ratner, A. S. Hoffman, F. J. Schoen and J. E. Lemons (Eds.), Biomaterials science, Second Ed.: An introduction to materials in medicine, Academic Press, New York 2004, pp. 100-107.

Peppas N.A., Bures P., Leobandung W., Ichikawa H., Hydrogels in pharmaceutical formulations. European Journal of Pharmceutics and Biopharmaceutics 50 (2000) 27-46.

Peppas N.A., Hilt J.Z., Khademhosseini A., Langer R., Hydrogels in biology and medicine: from molecular principles to bionanotechnology. Adv. Mater. 18 (2006) 1345-1360.

Poland C.A., Duffin R., Kinloch I., Maynard A., Wallace W.A.H., Seaton A., Stone V., Brown S., Macnee W., Donaldson K., Carbon nanotubes introduced into the abdominal cavity of mice show asbestos-like pathogenicity in a pilot study. Nat Nano 3(7) (2008) 423-428.

Qiu Y., Park K., Environment-sensitive hydrogels for drug delivery. Adv. Drug Deliver. Rev. 53(3) (2001) 321-339.

Ramanujan R., Ang K., Venkatraman S., Magnet–PNIPA hydrogels for bioengineering applications. J. Mater. Sci. 44(5) (2009) 1381-1387.

Ramanujan R.V., Lao L.L., The mechanical behavior of smart magnet-hydrogel composites. Smart Materials and Structures 15(4) (2006) 952-956.

Ratna D., Karger-Kocsis J., Recent advances in shape memory polymers and composites: a review. Journal of Materials Science 43(1) (2008) 254-269.

Razzaq M.Y., Anhalt M., Frormann L., Weidenfeller B., Thermal, electrical and magnetic studies of magnetite filled polyurethane shape memory polymers. Materials Science and Engineering: A 444(1-2) (2007) 227-235.

Rebecca A.M., Christopher M.V., Mihalis K., Jan P.S., Carbon nanotubes increase the electrical conductivity of fibroblast-seeded collagen hydrogels. Acta Biomater. 4(6) (2008) 1583-1592.

Richter A., Kuckling D., Howitz S., Thomas G., Arndt K.F., Electronically controllable microvalves based on smart hydrogels: magnitudes and potential applications. Journal of Microelectromechanical Systems 12(5) (2003) 748-753.

Rzaev Z.M.O., Dincer S., Piskin E., Functional copolymers of N-isopropylacrylamide for bioengineering applications. Prog. Polym. Sci. 32(5) (2007) 534-595.

Satarkar N.S., Hilt J.Z., Magnetic hydrogel nanocomposites for remote controlled pulsatile drug release. J. Control. Rel. 130 (2008) 246-251.

Satarkar N.S., Hilt J.Z., Magnetic hydrogel nanocomposites for remote controlled pulsatile drug release. J. Control. Rel. 130(3) (2008) 246-251.

Satarkar N.S., Hilt J.Z., Nanocomposite hydrogels as remote controlled biomaterials. Acta Biomater. 4 (2008) 11-16.

Satarkar N.S., Zhang W., Eitel R.E., Hilt J.Z., Magnetic hydrogel nanocomposites as remote controlled microfluidic valves. Lab Chip 9(12) (2009) 1773-1779.

Satarkar N.S., Zhang W., Eitel R.E., Hilt J.Z., Magnetic hydrogel nanocomposites as remote controlled microfluidic valves. Lab Chip (2009) In Press.

Schexnailder P., Schmidt G., Nanocomposite polymer hydrogels. Colloid & Polymer Science 287(1) (2009) 1-11.

Schild H.G., Poly(N-isopropylacrylamide): experiment, theory, and application. Prog. Polym. Sci. 17 (1992) 163-249.

Schmidt J.J., Rowley J., Kong H.J., Hydrogels used for cell-based drug delivery. Journal of Biomedical Materials Research Part A 87A(4) (2008) 1113-1122.

Sershen S.R., Mensing G.A., Ng M., Halas N.J., Beebe D.J., West J.L., Independent optical control of microfluidic valves formed from optomechanically responsive nanocomposite hydrogels. Adv. Mater. 17(11) (2005) 1366-1368.

Sershen S.R., West J.L., Implantable, polymeric systems for modulated drug delivery. Adv. Drug Deliver. Rev. 54 (2002) 1225-1235.

Sershen S.R., Westcott S.L., Halas N.J., West J.L., Temperature-sensitive polymer-nanoshell composites for photothermally modulated drug delivery. J. Biomed. Mater. Res. 51(3) (2000) 293-298.

Shi J., Guo Z.X., Zhan B., Luo H., Li Y., Zhu D., Actuator based on MWNT/PVA hydrogels. J. Phys. Chem. B 109(31) (2005) 14789-14791.

Shiotani A., Mori T., Niidome T., Niidome Y., Katayama Y., Stable incorporation of gold nanorods into N-Isopropylacrylamide hydrogels and their rapid shrinkage induced by near-infrared laser irradiation. Langmuir 23(7) (2007) 4012-4018.

Siegel A.C., Shevkoplyas S.S., Weibel D.B., Bruzewicz D.A., Martinez A.W., Whitesides G.M., Cofabrication of electromagnets and microfluidic systems in poly(dimethylsiloxane). Angew. Chem. 118(41) (2006) 7031-7036.

Siepmann J., Peppas N.A., Modeling of drug release from delivery systems based on hydroxypropyl methylcellulose (HPMC). Adv. Drug Deliver. Rev. 48(2-3) (2001) 139-157.

Sokolowski W., Metcalfe A., Hayashi S., Yahia L., Raymond J., Medical applications of shape memory polymers. Biomed. Mater. 2(1) (2007) S23-S27.

Sondi I., Salopek-Sondi B., Silver nanoparticles as antimicrobial agent: a case study on E. coli as a model for Gram-negative bacteria. J. Colloid Interface Sci. 275(1) (2004) 177-182.

Song C.W., Effect of local hyperthermia on blood flow and microenvironment: A review. Cancer Res. 44(10_Supplement) (1984) 4721s-4730.

Stubbe B.G., Smedt S.C.D., Demeester J., "Programmed Polymeric Devices" for pulsed drug delivery. Pharm. Res. 21(10) (2004) 1732-1740.

Sugiura S., Sumaru K., Ohi K., Hiroki K., Takagi T., Kanamori T., Photoresponsive polymer gel microvalves controlled by local light irradiation. Sensors and Actuators A: Physical 140(2) (2007) 176-184.

Sun H., Zhang L., Zhang X., Zhang C., Wei Z., Yao S., 188Re-labeled MPEG-modified superparamagnetic nanogels: preparation and targeting application in rabbits. Biomedical Microdevices 10(2) (2008) 281-287.

Suzuki A., Tanaka T., Phase transition in polymer gels induced by visible light. Nature 346(6282) (1990) 345-347.

Tae Gwan Park A.S.H., Deswelling characteristics of poly(N-isopropylacrylamide) hydrogel. J. Appl. Polym. Sci. 52(1) (1994) 85-89.

Thelemann T., Thust H., Hintz M., Using LTCC for microsystems. Microelectronics International 19 (2002) 19-23.

Thomas V., Namdeo M., Mohan Y.M., Bajpai S.K., Bajpai M., Review on polymer, hydrogel and microgel metal nanocomposites: A facile nanotechnological approach. J. Macromol. Sci., Part A: Pure Appl. Chem. 45(1) (2008) 107-119.

Thomas V., Yallapu M.M., Sreedhar B., Bajpai S.K., A versatile strategy to fabricate hydrogel-silver nanocomposites and investigation of their antimicrobial activity. J. Colloid Interface Sci. 315(1) (2007) 389-395.

Tipler P.A., Mosca G.P., Physics for scientists and engineers, W.H.Freeman, 2008.

Tsai Y.-C., Huang J.-D., Chiu C.-C., Amperometric ethanol biosensor based on poly(vinyl alcohol)-multiwalled carbon nanotube-alcohol dehydrogenase biocomposite. Biosensors and Bioelectronics 22(12) (2007) 3051-3056.

Tzu-Wei Wang, Hsi-Chin Wu, Wei-Ren Wang, Feng-Huei Lin, Pei-Jen Lou, Ming-Jium Shieh, Tai-Horng Young, The development of magnetic degradable DP-Bioglass for hyperthermia cancer therapy. Journal of Biomedical Materials Research Part A 83A(3) (2007) 828-837.

Ulijn R.V., Bibi N., Jayawarna V., Thornton P.D., Todd S.J., Mart R.J., Smith A.M., Gough J.E., Bioresponsive hydrogels. Materials Today 10(4) (2007) 40-48.

Vaishnava P.P., Tackett R., Dixit A., Sudakar C., Naik R., Lawes G., Magnetic relaxation and dissipative heating in ferrofluids. J. Appl. Phys. 102 (2007) 063914.

Vaupel P., Kallinowski F., Okunieff P., Blood flow, oxygen and nutrient supply, and metabolic microenvironment of human tumors: A review. Cancer Res. 49(23) (1989) 6449-6465.

Wache H.M., Tartakowska D.J., Hentrich A., Wagner M.H., Development of a polymer stent with shape memory effect as a drug delivery system. Journal of Materials Science-Materials in Medicine 14(2) (2003) 109-112.

Wang J., Chen Z., Mauk M., Hong K.-S., Li M., Yang S., Bau H.H., Self-Actuated, Thermo-Responsive Hydrogel Valves for Lab on a Chip. Biomedical Microdevices 7(4) (2005) 313-322.

Wang M.B., Li Y.B., Wu J.Q., Xu F.L., Zuo Y., Jansen J.A., In vitro and in vivo study to the biocompatibility and biodegradation of hydroxyapatite/poly(vinyl alcohol)/gelatin composite. Journal of Biomedical Materials Research Part A 85A(2) (2008) 418-426.

Wang S.-F., Shen L., Zhang W.-D., Tong Y.-J., Preparation and mechanical properties of chitosan/carbon nanotubes composites. Biomacromolecules 6(6) (2005) 3067-3072.

Wang T.-W., Wu H.-C., Wang W.-R., Lin F.-H., Lou P.-J., Shieh M.-J., Young T.-H., The development of magnetic degradable DP-Bioglass for hyperthermia cancer therapy. Journal of Biomedical Materials Research Part A 83A(3) (2007) 828-837.

Wang X., Gu H., Yang Z., The heating effect of magnetic fluids in an alternating magnetic field. J. Magn. Magn. Mater. 293 (2005) 334-340.

Wei Z.G., Sandstrom R., Miyazaki S., Shape-memory materials and hybrid composites for smart systems - Part I Shape-memory materials. Journal of Materials Science 33(15) (1998) 3743-3762.

Whitesides G.M., The origins and the future of microfluidics. Nature 442(7101) (2006) 368-373.

Wissler E.H., Pennes' 1948 paper revisited. J. Appl. Physiol. 85(1) (1998) 35-41.

Wust P., Hildebrandt B., Sreenivasa G., Rau B., Gellermann J., Riess H., Felix R., Schlag P.M., Hyperthermia in combined treatment of cancer. The Lancet Oncology 3(8) (2002) 487-497.

Xiang Y., Peng Z., Chen D., A new polymer/clay nano-composite hydrogel with improved response rate and tensile mechanical properties. Eur. Polym. J. 42(9) (2006) 2125-2132.

Xu H., Wang Y.J., Zheng Y.D., Chen X.F., Ren L., Wu G., Huang X.S., Preparation and characterization of bioglass/polyvinyl alcohol composite hydrogel. Biomedical Materials 2(2) (2007) 62-66.

Xu Z.Z., Wang C.C., Yang W.L., Deng Y.H., Fu S.K., Encapsulation of nanosized magnetic iron oxide by polyacrylamide via inverse miniemulsion polymerization. Journal of Magnetism and Magnetic Materials 277(1-2) (2004) 136-143.

Xulu P.M., Filipcsei G., Zrinyi M., Preparation and response properties of magnetically soft poly(N-isopropylacrylamide) gels. Macromolecules 33 (2000) 1716-1719.

Yakacki C.M., Satarkar N.S., Gall K., Likos R., Hilt J.Z., Shape-memory polymer networks with Fe3O4 nanoparticles for remote activation. J. Appl. Polym. Sci. 112(5) (2009) 3166-3176.

Yakacki C.M., Shandas R., Lanning C., Rech B., Eckstein A., Gall K., Unconstrained recovery characterization of shape-memory polymer networks for cardiovascular applications. Biomaterials 28(14) (2007) 2255-2263.

Yakacki C.M., Willis S., Luders C., Gall K., Deformation Limits in Shape-Memory Polymers. Advanced Engineering Materials 10(1-2) (2008) 112-119.

Yang L., Setyowati K., Li A., Gong S., Chen J., Reversible infrared actuation of carbon nanotube-liquid crystalline elastomer nanocomposites. Adv. Mater. 20(12) (2008) 2271-2275.

Yang Z., Cao Z., Sun H., Li Y., Composite films based on aligned carbon nanotube arrays and a poly(N-isopropyl acrylamide) hydrogel. Adv. Mater. 20(11) (2008) 2201-2205.

Yoshida R., Sakai K., Okano T., Sakurai Y., Modulating the phase transition temperature and thermosensitivity in N-isopropylacrylamide copolymer gels. J. Biomater. Sci., Polym. Ed. 6 (1994) 585-598.

Yoshida R., Sakai K., Okano T., Sakurai Y., Modulating the phase transition temperature and thermosensitivity in N-isopropylacrylamide copolymer gels. J. Biomater. Sci., Polym. Ed. 6 (1995) 585-598.

Yoshida R., Sakai K., Okano T., Sakurai Y., Pulsatile drug delivery systems using hydrogels. Adv. Drug Deliver. Rev. 11(1-2) (1993) 85-108.

Youan B.-B.C., Chronopharmaceutics: gimmick or clinically relevent approach to drug delivery? J. Control. Rel. 98 (2004) 337-353.

Yu C., Mutlu S., Selvaganapathy P., Mastrangelo C.H., Svec F., Frechet J.M.J., Flow control valves for analytical microfluidic chips without mechanical parts based on thermally responsive monolithic polymers. Anal. Chem. 75(8) (2003) 1958-1961.

Yu Q., Bauer J.M., Moore J.S., Beebe D.J., Responsive biomimetic hydrogel valve for microfluidics. Appl. Phys. Lett. 78(17) (2001) 2589-2591.

Zeng X., Jiang H., Tunable liquid microlens actuated by infrared light-responsive hydrogel. Appl. Phys. Lett. 93(15) (2008) 151101.

Zhao X., Ding X., Deng Z., Zheng Z., Peng Y., Long X., Thermoswitchable electronic properties of a gold nanoparticle/hydrogel composite. Macromol. Rapid Commun. 26(22) (2005) 1784-1787.

Zhao X., Ding X., Deng Z., Zheng Z., Peng Y., Tian C., Long X., A kind of smart gold nanoparticle-hydrogel composite with tunable thermo-switchable electrical properties. New J. Chem. 30(6) (2006) 915-920.

Zrínyi M., Intelligent polymer gels controlled by magnetic fields. Colloid & Polymer Science 278(2) (2000) 98-103.

Zrinyi M., Barsi L., Buki A., Deformation of ferrogels induced by nonuniform magnetic fields. The Journal of Chemical Physics 104(21) (1996) 8750-8756.

Zrinyi M., Szabo D., Kilian H.-G., Kinetics of the shape change of magnetic field sensitive polymer gels. Polymer Gels and Networks 6 (1998) 441-454.

VITA

Nitin Suresh Satarkar was born on November 9, 1983 in Aurangabad, Maharashtra, India. He completed Bachelors in Chemical Engineering with First Class from the Institute of Chemical Technology (formerly known as UDCT), Mumbai, India, in May 2005. He joined Department of Chemical and Materials Engineering at the University of Kentucky in August 2005 as a PhD candidate.

HONORS AND AWARDS

- Recipient of Society for Biomaterials (SFB) Student Travel Achievement Recognition (STAR) Award, 2009
- 2^{nd} prize at the University of Kentucky Chemical and Materials Engineering poster competition, 2009
- Honorable Mention at Bionanotechnology Graduate Student Award Session, American Institute of Chemical Engineers (AIChE) Annual Meeting, Nashville, 2009
- Recipient of AIChE Division 15 Travel Award for AIChE Annual Meeting, Philadelphia, 2008
- Recipient of University of Kentucky Research Challenge Trust Fund Fellowship, 2006-2007
- Recipient of J. R. D. Tata Scholarship for meritorious performance in engineering, 2002-2004
- Recipient of DTE Government of India Scholarship for engineering students, 2001-2004

PUBLICATIONS

- N.S. Satarkar, S.A. Meenach, K. Anderson, J.Z. Hilt, Remote actuation of hydrogel nanocomposites: Heating analysis, modeling, and simulations, AIChE J, Accepted.
- N.S. Satarkar, D. Biswal, J.Z. Hilt, Hydrogel nanocomposites: A review of applications as remote controlled biomaterials, Soft Matter, In Press.

- N.S. Satarkar, D. Johnson, B. Marrs, R. Andrews et al, Synthesis and characterization of temperature responsive hydrogel-MWCNT nanocomposites, J Appl Polymer Sci, In Press.
- N.S. Satarkar, W. Zhang, R. Eitel, J.Z. Hilt, Magnetic hydrogel nanocomposites as remote controlled microfluidic valves, Lab Chip 9 (2009) 1773-1779.
- N.S. Satarkar, J.Z. Hilt, Hydrogel nanocomposites as remote-controlled biomaterials, Acta Biomater 4 1(2008) 11-16.
- N.S. Satarkar, A.M. Hawkins, J.Z. Hilt, Hydrogel nanocomposites in biology and medicine: Applications and interactions, In: R. Bizios and D. Puleo, eds. Biological interactions on materials surfaces, Springer, 2009.
- N.S. Satarkar, J.Z. Hilt, Magnetic hydrogel nanocomposites for remote controlled pulsatile drug release, J Control Rel 130 3(2008) 246-251.
- C. Yakacki, N.S. Satarkar, K. Gall, R. Likos et al, Shape-memory polymer networks with Fe_3O_4 nanoparticles for inductive heating, J Appl Polymer Sci 112 5(2009) 3166-3176.
- A.M. Hawkins, N.S. Satarkar, J.Z. Hilt, Demonstration of remote-controlled drug release from degradable nanocomposite hydrogels, Pharm Res 26 3(2009) 667-673.

CONFERENCE PRESENTATIONS

Nitin has presented papers and posters at several national and regional meetings including AIChE Annual Meetings (San Francisco, 2006; Salt Lake City, 2007; Philadelphia, 2008; Nashville, 2009), and SFB Annual Meetings (Chicago, 2007; San Antonio, 2009)